TECHNISCHE UNIVERSITÄT MÜNCHEN

Fakultät für Chemie

Copper-Paddlewheel-Based Surface Mounted Metal-Organic Framework Thin Films

Zheng Wang

Vollständiger Abdruck der von der Fakultät für Chemie der Technischen Universität München zur Erlangung des akademischen Grades eines Doktors der Naturwissenschaften (Dr. rer. nat.) genehmigten Dissertation.

Vorsitzender:	Prof. Dr. Klaus Köhler
Prüfende der Dissertation:	1. Prof. Dr. Roland A. Fischer
	2. Jun.-Prof. Dr. Sebastian Henke

Die Dissertation wurde am 09.07.2019 bei der Technischen Universität München eingereicht und durch die Fakultät für Chemie am 31.07.2019 angenommen.

Copper-Paddlewheel-Based Surface Mounted Metal-Organic Framework Thin Films

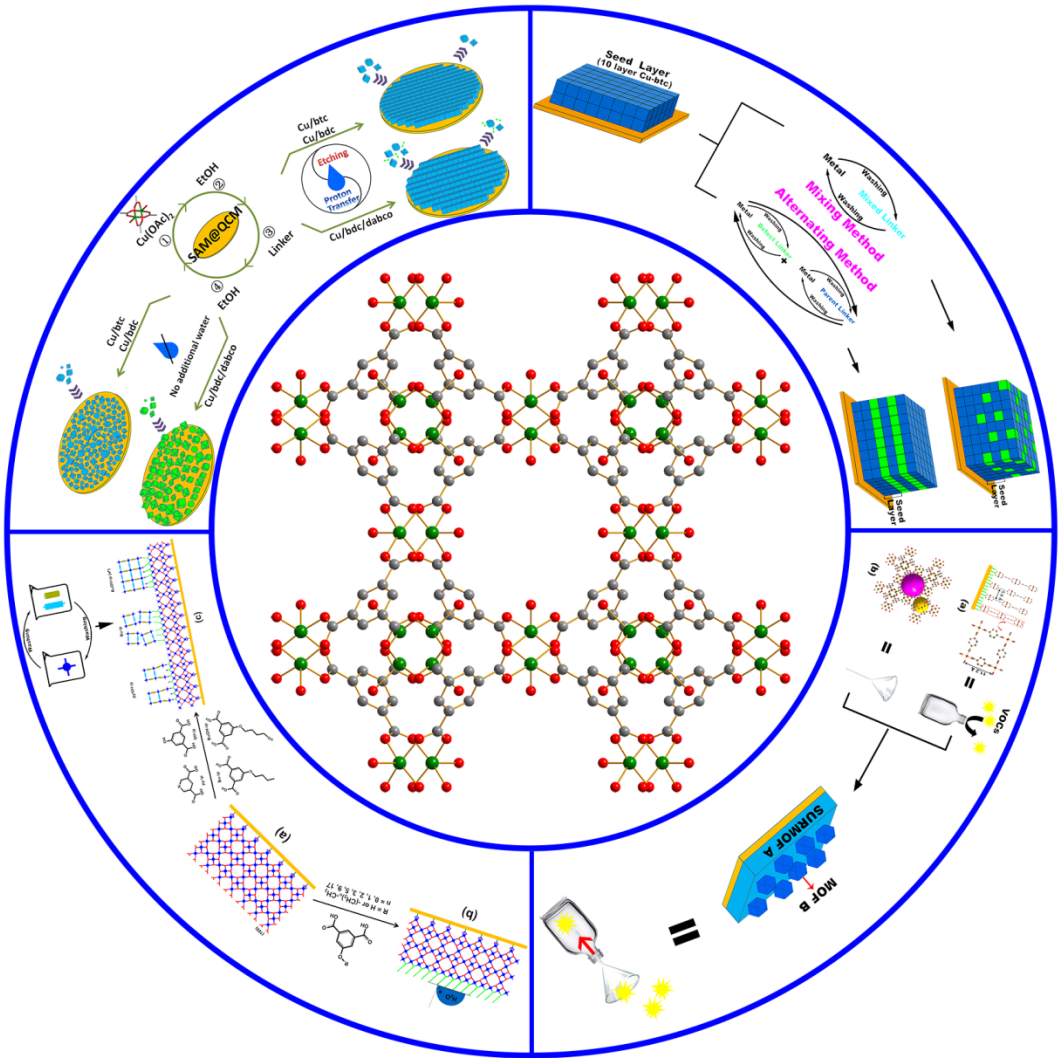

DISSERTATION

Submitted by

Zheng Wang

July 2019

Anhang I

Eidesstattliche Erklärung

Ich erkläre an Eides statt, dass ich die bei der Fakultät für Chemie der TUM zur Promotionsprüfung vorgelegte Arbeit mit dem Titel:

Copper-Paddlewheel-Based Surface Mounted Metal-Organic Framework Thin Films

in der Fakultät für Chemie, Lehrstuhl für Anorganische und Metallorganische Chemie

unter der Anleitung und Betreuung durch Prof. Dr. Roland A. Fischer ohne sonstige Hilfe erstellt und bei der Abfassung nur die gemäß § 6 Ab. 6 und 7 Satz 2 angebotenen Hilfsmittel benutzt habe.

× Ich habe keine Organisation eingeschaltet, die gegen Entgelt Betreuerinnen und Betreuer für die Anfertigung von Dissertationen sucht, oder die mir obliegenden Pflichten hinsichtlich der Prüfungsleistungen für mich ganz oder teilweise erledigt.

× Ich habe die Dissertation in dieser oder ähnlicher Form in keinem anderen Prüfungsverfahren als Prüfungsleistung vorgelegt.

× Ich habe den angestrebten Doktorgrad noch nicht erworben und bin nicht in einem früheren Promotionsverfahren für den angestrebten Doktorgrad endgültig gescheitert.

Die öffentlich zugängliche Promotionsordnung der TUM ist mir bekannt, insbesondere habe ich die Bedeutung von § 28 (Nichtigkeit der Promotion) und § 29 (Entzug des Doktorgrades) zur Kenntnis genommen. Ich bin mir der Konsequenzen einer falschen Eidesstattlichen Erklärung bewusst.

Mit der Aufnahme meiner personenbezogenen Daten in die Alumni-Datei bei der TUM bin ich einverstanden,

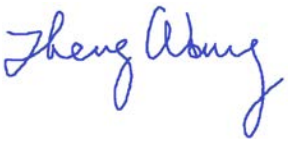

Zheng Wang

Garching, 04.07.2019

Acknowledgement

It is an unforgettable experience to do a doctorate in Germany. During the time of PhD study I have met a lot of challenges, which frustrated me especially at the beginning. Finally, I overcame these challenges with the help from my colleagues and family. In the four years' study, I learnt a lot of lessons that are precious treasure in my life and will continue benefiting my rest life.

First of all, I would like to address my special thanks and appreciation to my PhD supervisor, **Prof. Dr. Roland A. Fischer**, for recruiting me in the Chair of Inorganic and Metal-Organic Chemistry (AMC) to work on this interesting topic. I am very grateful for his continuous instruction, support, suggestion and encouragement during my PhD study, as well as for his numerous of effort put in my work. His valuable guidance always inspires me a lot and helps me enrich my knowledge and improves my scientific skills. I am also grateful for his generosity to supply the opportunities of attendance international conference and research stay in other groups from which I met a lot of professional people and broadened my horizon.

I acknowledge to China Scholarship Council (CSC) for providing the full scholarship to support my living and studying in Germany. I also want to thank the Chair of Inorganic chemistry II in Ruhr University Bochum and the Chair of Inorganic and Metal-Organic Chemistry in Technical University of Munich for the laboratory facilities and chemicals which I can access for my PhD study. I am grateful for the financial support to international conference in USA by Graduate School of Technical University of Munich.

I would like to address my special thanks to **Prof. Dr. Klaus Köhler** for accepting to be the chairperson of my doctoral dissertation defence. I would like to express my special thanks and appreciation to **Prof. Dr. Roland A.**

Fischer and **JProf. Dr. Sebastian Henke** for accepting to be the examiners of my doctoral dissertation defence.

I would like to express my special thanks to **Dr. Yuemin Wang** for his kindness as my mentor.

Special thanks to **Prof Dr. Christof Wöll**, **Dr. Hartmut Gliemann**, **Priv.-Doz. Dr. Lars Heinke**, and **Dr. Carsten Natzeck** for their warmly welcome and fruitful discussions during my research stay at Karlsruhe Institute of Technology.

I would like to address my special thanks to **Dr. Min Tu** and **Dr. Suttipong Wannapaiboon**, for introducing me into the fields of MOFs and SURMOFs. Thanks for **Dr. Suttipong Wannapaiboon** for his patience, guidance and help on my work and paper revision.

I would also like to thank **Katia Rodewald** for the SEM measurements, **Dr. Eliza Gemel** for the instruction of BET measurement, **Jürgen Kudermann** for training the operation of IR and GC-FID, **Olaf Ackermann** for the HPLC measurements. Special thanks to **JProf. Dr. Sebastian Henke** and **Dr. Michael Paulus** for the measurements of 2D-GIXRD in DELTA synchrotron, Dortmund, Germany. Also I would like to thank my colleagues **Dr. Suttipong Wannapaiboon**, **Dr. Hung Banh**, **Dr. Konstantin Epp**, **Dr. Stefano Dissegna**, **Christian Schneider**, **Werner Heinz**, **Michael Ehrenreich**, **David Mayer, Lena Staiger**, **Rodica Dumitrescu** and **Maria Matthews** for their help and support in my work.

I am grateful to **Martin Schellerer** for his help in dealing with German-documentation affairs. And special thanks to **Dr. Christian Gemel**, **Dr. Alexander Pöthig**, **Dr. Gregor Kieslich**, **Dr. Markus Drees**, **Dr. Gabriele**

Raudaschl-Sieber and **Prof. Dr. Richard Fischer** for their suggestion, support and help in my project.

Also I am very grateful to all members of AMC for such a good working atmosphere, kind help and everything that we have done together. I have spent an unforgettable time in this group. You have made my life in Germany happy and memorable. Particularly, I want to thank to **Dr. Hung Banh**, **Dr. Suttipong Wannapaiboon**, **Dr. Konstantin Epp**, **Dr. Andreas Schneemann**, **Dr. Raghavender Medishetty**, **Zhiying Fan** and **Shengyang Guan** for numerous suggestions, supports and helps. Special thanks to **Zhiying Fan** and **Shengyang Guan**, it is really a nice time to stay with you.

I am deeply grateful to my parents (王其龙，张如琴) and my brother (王帅) for your continuous support and encouragements over the past time. May you live happily everafter.

Last but not least, I would like to address my deepest appreciation to my beloved wife (谢倩杰) for her trust and encouragements. I am lucky to have you being on my side and understanding me. Wish you happy every day!

To my dear wife (谢倩杰)

路漫漫其修远兮 吾将上下而求索

屈原《离骚》

Table of Content

Abbreviations

2D	2-Dimensional
2D-GIXRD	2-dimensional grazing incidence X-ray diffraction
ALD	Atomic layer deposition
APTES	3-aminopropyltriethoxysilane
bdc	Terephthalate
btc	Benzene-1,3,5-tricarboxylate
Bu	Butoxy
BuOH	4-Hydroxybutoxy
CNT	Carbon nanotube
CP	Coordination polymer
CPM	Crystalline porous material
CPO-27-M	M(2,5-dihydroxyterephthalate), M = Ni, Co, Mg, Zn and Mn
$Cu(OAc)_2$	Copper acetate
CVD	Chemical vapor deposition
dabco	1,4-Diazabicyclo[2.2.2]octane
De	Decyloxy
DE	Defect engineered
EH	Environmental humidity
Et	Ethoxy
FTO/ITO	Fluorine doped/indium tin oxide
fu-ip	functionalized isophthalate
GB	Gentle beam
GIXRD	Grazing incidence X-ray diffraction
H_2ip	Isophthalic acid
H_2OH-ip	5-hydroxyisophthalic acid

H_2pydc	3,5-pyridinecarboxylic acid
He	Hexyloxy
HKUST-1	Cu_3btc_2
IRMOF-3	Zn(2-amino-terephthalate)
IRRAS	Infrared reflection absorption spectroscopy
IUPAC	International Union of Pure and Applied Chemistry
LbL	Layer-by-Layer
LB	Langmuir–Blodgett
LMCT	Ligand-metal-charge-transfer
LPE	Liquid phase epitaxy
Me	Methoxy
MFC	Mass flow controller
MHDA	16-mercaptohexadecanoic acid
MIL-47	VO(bdc)
MIL-53	Al(OH)(bdc)
MOF	Metal-organic frameworks
MOF-2	Cubdc
MOF-5	$Zn_4O(BDC)_3$
MTV-MOF	Multivariate metal-organic framework
MUD	11-mercaptoundecanol
ndc	1,4-Naphthalenedicarboxylic
NMR	Nuclear magnetic resonance
NP	Nanoparticles
Od	Octadecyloxy
OH	Hydroxy
PCP	Porous coordination polymer
POM	Polyoxometalate
PPMT	(4,(4-pyridyl)phenyl)-methanethiol

Pr	Propoxy
PSM	Post-synthetical modification
py	Pyridine
QCM	Quartz crystal microbalance
QD	Quantum dot
SALE	Solvent assisted linker exchange
SAM	Self-assembly monolayer
SBU	Secondary building unit
SEM	Scanning electron microscope
SIM-1	Zn(4-methyl-5-imidazolecarboxaldehyde)$_2$
SPR	Surface plasmon resonance
SURMOF	Surface mounted metal-organic framework
SURMOF-2	Cubdc thin film
TCNQ	7,7,8,8-tetracyanoquinododimethane
TF-bdc	Tetrafluoroterephthalate
ToF-SIMS	Time-of-flight secondary ion mass spectroscopy
UIO-66	$Zr_6O_4(OH)_4(bdc)_6$
UV-Vis	Ultraviolet-visible
VOC	Volatile organic compound
WCA	Water contact angle
XRD	X-ray diffraction
ZIF	Zeolite imidazole frameworks
ZIF-22	Zn(5-azabenzimidazole)$_2$

Chapter 1

General introduction and motivations

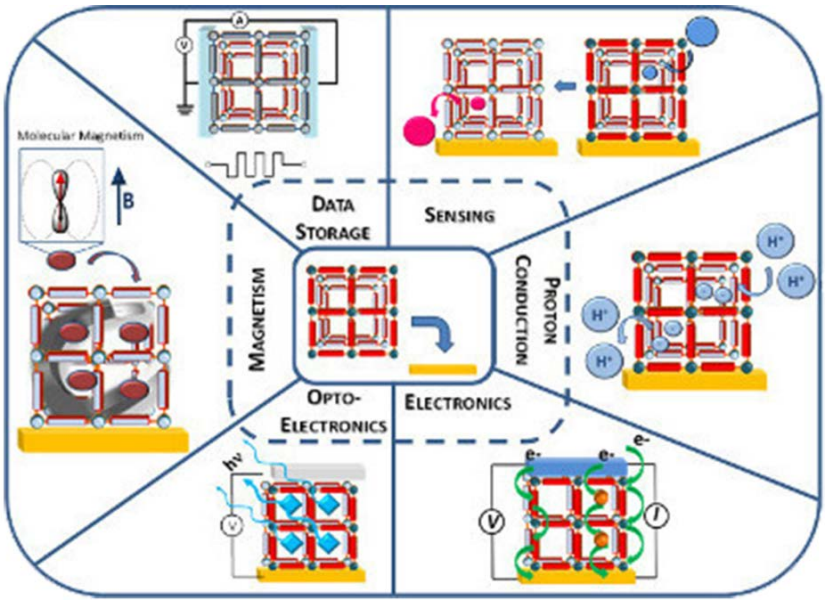

1.1 Metal-Organic Frameworks (MOFs): an emerging class of crystalline porous materials

1.1.1 Porous materials and applications

The efforts of design and synthesis of materials with multiple properties and advanced functionalities have never been ceased to fulfill the rising demands from the real world. Porous materials, which are defined as solids containing empty voids,[1] are one of the most intensively researched fields from fundamental research to large-scale industrial process. The porous materials with empty voids have been widely used in storage and separation, purification, sensing, volatile organic compounds (VOCs) capturing, heterogeneous catalysis, energy storage and biomedicine, *etc*. According to the definition from International Union of Pure and Applied Chemistry (IUPAC), porous materials can be classified into three main catalogues based on the size of contained pores: micro-pore material (<2 nm), meso-pore material (2–50 nm) and macro-pore material (>50 nm).[2] Moreover, the shape of pore in porous materials also has non-negligible impacts to achieve particular functionalities. Regarding to this, amorphous porous materials and crystalline porous materials (CPMs) are sorted according to the uniformity of contained pores. Amorphous porous materials, such as activated carbons, porous polymers, metal foams and so on, normally show disordered pore structure in which many of the pores are isolated and blind (Figure 1.1).[3] The presence of such kinds of pores would severely affects many processes happened in porous materials like sorption and mass transfer. The isolated and blind pores reduce the volume of valid pores (through pores and open pores) in amorphous porous materials. Differing from amorphous porous materials, all of the pores of CPMs are active for related processes. CPMs (e.g., zeolites[4] and open-framework aluminophosphates[5]) crystallize with defined pore size and

shape, which have attracted lots of research interest. CPMs with defined pore structure are an ideal platform for fundamental research and practical applications. For example, zeolites, constructed from [SiO_4] and [AlO_4] tetrahedra and shown rigid structure, well-defined channels or cavities, and high pH- and thermo-stability, have made the largest contribution to industrial applications as catalysts, adsorbents and ion-exchangers.[4]

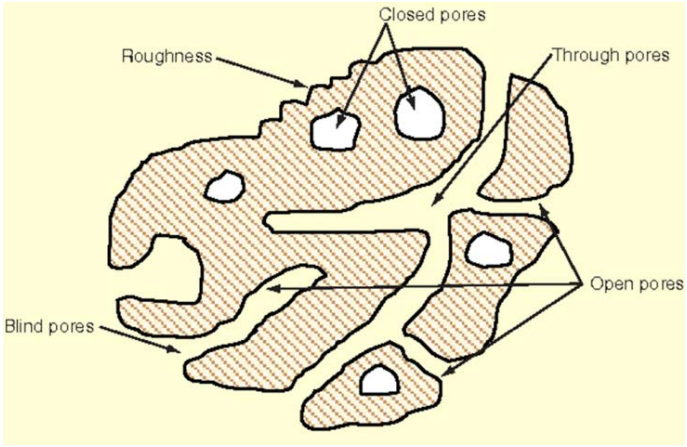

Figure 1.1. Schematic cross-section of amorphous porous materials.

Over the past decades, more and more practical applications require the CPMs owning tunable properties and multiple functions. Especially under the pressure of global energy shortage and environmental pollution, designing new CPMs with fascinating properties and functionalities is more urgent. However, it is a great challenge to multifunctionalize traditional zeolites and aluminophosphates as desired because their networks are established by rigid and with limited elements [TO_4] (T = Si and Al) tetrahedra. However, considering the flexibility and versatility of the organic-based moieties, introducing organic ligands into the networks of CPMs could drastically enhance the controllability and tunability of obtained structures. Directed by this idea, a new potential class of CPMs so-called metal–organic frameworks (MOFs) was emerged.

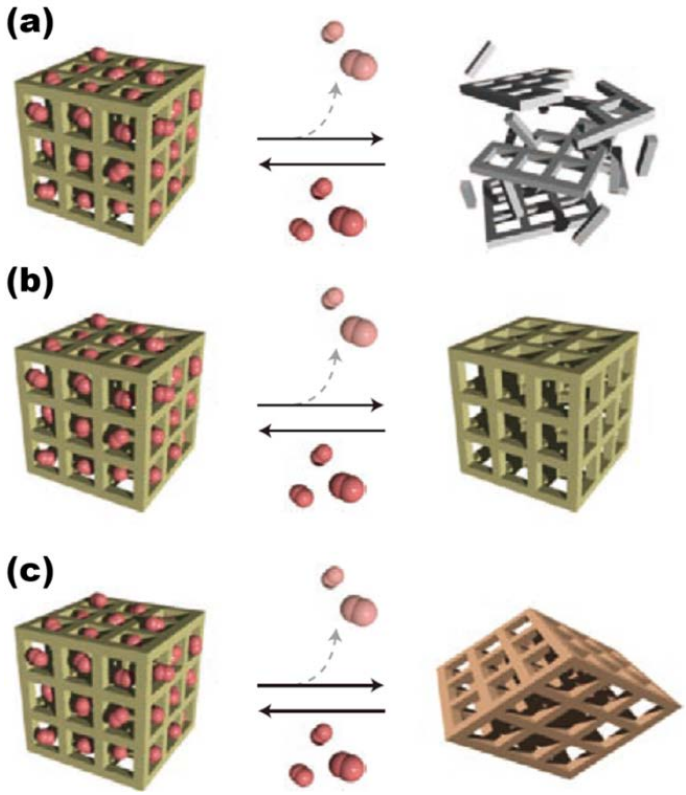

Figure 1.2. Three kinds of MOFs depending on properties of the networks e.g. upon guest sorption process. [Adapted with permission from ref. 11. Copyright 2009 Macmillan Publishers Limited]

1.1.2 Structure diversity and functionality of MOFs

MOFs, also known as porous coordination polymers (PCPs), are composed of metal nodes (including single metal ions and second building units (SBUs)) and multitopic organic spacing linkers to form infinite frameworks with defined voids.[6-7] Actually, MOFs or, more generally speaking, coordination polymers (CPs) have been reported since the late 1950s and the early 1960s.[8-9] However, the frameworks of these MOF materials collapse irreversibly after the removal of guest molecules, which means that there is no permanent porosity (Figure 1.2a).[10-11] Until the middle of 1990s the situation was improved by the pioneering works of Yaghi et al.,[7, 12] Kitagawa and coworkers,[13] and Ferey et al.[14] The emergence of stable and robust MOFs,

in which porous structure remains after removing guest molecules (Figure 1.2b), results in a long-lasting impact in the fields of chemistry, biology, physics, and materials science. Furthermore, MOFs with flexible or dynamic frameworks (also called soft porous crystals), which reversibly respond to external stimuli, were developed as well (Figure 1.2c).[10, 15] Note that, according to the suggestion from IUPAC in 2013, MOF is defined as "*a coordination network repeating coordination entities extending in 1, 2, or 3 dimensions.*"[16]

SBUs play an important role in the design of directionality for the construction of MOFs and to achieve robust frameworks (Figure 1.3).[17-18] SBUs allow the MOF structures to serve as rigid, directional, and stable building units in the design of robust crystalline materials with predetermined structures and properties. Under the solvothermal conditions, SBUs are assembled from metal ions and bridging oxygen or nitrogen atoms with different topologies. To date, hundreds of SBUs have been reported in existing MOF structures, from which it is not difficult to imagine how diversity the structure of MOFs could be.[19-20] Moreover, many properties, such as adsorption, catalysis, magnetism and so on, are also influenced or even determined by the SBUs employed in MOFs. For example, MOFs constructed by the SBUs with open sites, like Cu/Zn paddlewheel and $M_3(\mu_3\text{-O})$ (M = Fe and Cr), show high affinity to CO_2 due to the chemical bonding between guest CO_2 molecules and these open sites.[21-22] Furthermore, the SBUs with open sites are Lewis acids, which are catalytically active for lots of organic reactions such as cyanosilylation,[23] ring opening reaction,[24] Mukaiyama-aldol reaction[25], Knoevenagel condensation[26] and redox reaction[27]. Interestingly, the stability of MOFs is influenced by the SBUs as well.[28] According to previous studies, MOFs, which contain SBUs coordinated by high-valence metal ions and/or N-donor ligands, normally show relative high stability. For

instance, UIO-66, in which SBUs are composed of Zr^{4+}, displays high thermal stability (up to 500 °C which is comparable to that of zeolites) and high resistance to acid and base.[29-30]

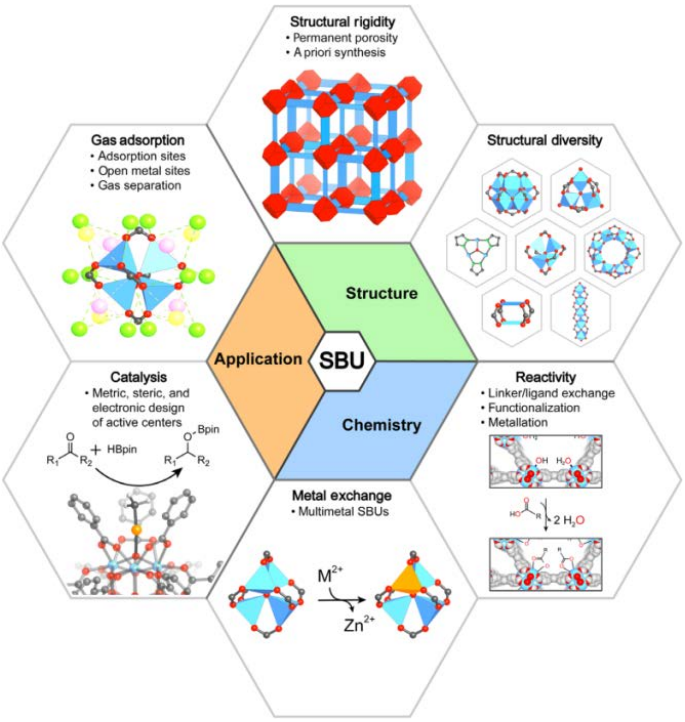

Figure 1.3. The impact of the SBUs on the structure, chemistry, and applications of MOFs. [Reprinted with permission from ref. 18. Copyright 2018 The Authors, some rights reserved; exclusive licensee American Association for the Advancement of Science]

In MOF structures, organic linkers act as spacers to connect SBUs via the coordination bonds to form reticular frameworks. The flexibility and versatility of organic linkers has profound impacts on the design and synthesis of MOFs with tunable structural features and properties. By employing linkers with different length, the pores of obtained MOFs could be rationally tuned varying from several to 98 Å (Figure 1.4a).[31] With such large pore opening and high porosity, MOFs are promising candidates for gas adsorption/separation[32] and encapsulating active species[33]. Moreover, decorating the linkers with

functional pendant groups, such as -X (X = F, Cl, Br), -NH_2, -NO_2 and alkoxy groups, various new or enhanced properties can be generated in MOFs as well.[34] Particularly, multivariate MOFs (MTV-MOFs), which are assembled by incorporating distinct linker functionalities within one pure phase, exhibit the properties that do not arise from linear combinations of the pure constituents (Figure 1.4b).[35-36]

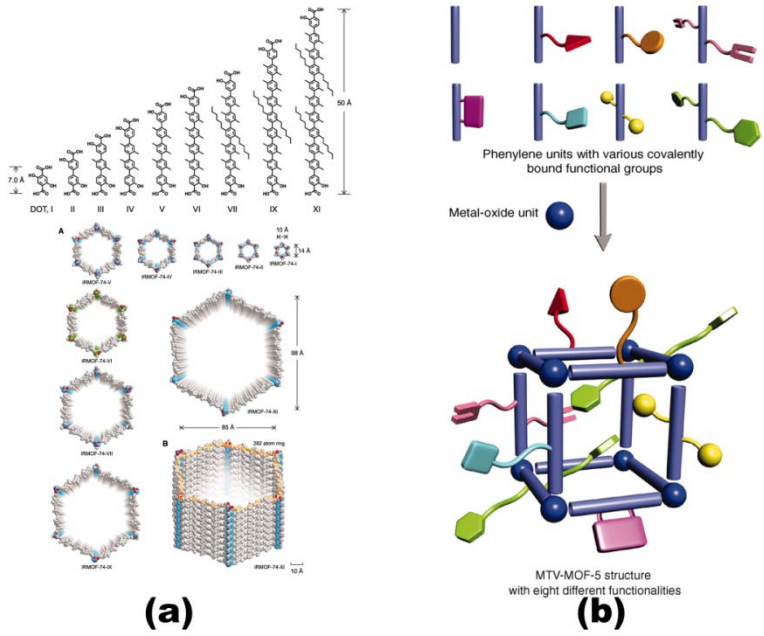

Figure 1.4. (a) Linker length-dependent pore size of MOFs, and (b) MTV-MOF-5 with eight distinct functionalities in one pure phase. [Reprinted with permission from ref. 31 (a) and 35 (b). Copyright 2012 and 2010 American Association for the Advancement of Science, respectively]

Plenty of synthetic methods have been developed to synthesize MOFs so far, such as hydrothermal and solvothermal methods, electrochemistry, microwave-assisted heating, mechanochemistry, sonochemistry *etc*.[37] However, how to control the synthesis process of MOFs to achieve desired quality is still a significant challenge. Recently, some valuable synthetic strategies have been proposed to improve the quality controllability of MOF

crystals. The introduction of coordination modulator into synthesis processes is one of the most used strategies, through which we can enhance the crystallinity,[38] control the morphology of MOFs[39], and even induce new MOF structures[40]. Another practical strategy for controlling the morphology and size of obtained MOF crystals is using mixed solvent as the synthetic medium. The size of ZIF-71 crystals can be controlled ranging from below 100 nm to several micrometers by adjusting the solvent with different ratio of methanol and DMF.[41-42] Recently, solvent assisted linker exchange (SALE) has emerged for synthesizing those MOFs cannot be obtained by direct synthetical methods.[43] Till now, many new types of MOFs have been prepared by SALE. Meanwhile, the functionalities and application scope can be also extended by exchanging the fixed linkers in MOF frameworks with pre-functionalized ones. Despite many synthetic efforts have been developed, it is still not easy to control the quality of MOFs as desired.

The tremendous diversity of SBUs and organic linkers provides the possibilities to subtly design the structure of frameworks and feasibly tune the chemical and physical properties of the pore surfaces.[20, 44] The structural diversity enables MOFs a variety of interesting properties, such as high porosity, chirality, large surface area, magnetism, luminescence, spin-crossover and electron/proton conductivity,[45] which make them as promising candidates in many application fields such as storage,[46] separation,[32] sensing[47] and catalysis.[48]

1.2 Strategies for further improving the performance of MOF materials

One of primary challenges facing the practical applications of MOFs is how to improve the synthesis processes that allow MOFs to be compatibly in

real-working conditions, meanwhile obtain enhanced performance. In terms of this issue, many strategies have been developed to improve the performance of MOF materials and broaden their application scope. Except selecting different SBUs and pre-functionalizing linkers, research efforts are also devoted from two aspects in general to further functionalize MOFs: one is incorporating alien species into MOFs to form MOF composites; the other one is improving the synthetic skills to enhance or create intrinsic properties in MOFs, which includes post-synthetical modification (PSM), defect engineering, heterostructured MOFs and MOF thin films.

1.2.1 MOF composites

The ultrahigh and uniform porosity of MOFs can be used as matrix for hosting alien functional species, through which MOF composite materials are obtained. Controllable integration of MOFs and alien functional species leads to the generation of new properties in MOF composites which are superior to those of the individual components through the collective behavior of the functional units. A lot of species with various functionalities, such as noble metal nanoparticles (NPs), oxides, quantum dots (QDs), polyoxometalates (POMs), polymers, graphene, carbon nanotubes (CNTs), biomolecules and so on (Figure 1.5), have been incorporated in MOFs.[49] By selecting functional species for incorporation, the application scope of MOF composites has broadened from life science to industrial fields. Among them, the composite of noble metal NPs encapsulated in MOFs (M-NPs@MOF) is the most intensively studied and shows great potentials in catalysis and hydrogen storage.[50-53] Moreover, POMs loaded Cu_3btc_2 (also known as HKUST-1, btc = benzene-1,3,5-tricarboxylate) composites (POM@Cu_3btc_2) show not only advanced catalytic properties but also enhanced stability which can exist in acid solution up to 0.02 M.[54-55] The parent Cu_3btc_2, however, shows poor tolerance to acid. The strategy of incorporating functional species in MOFs

provides a feasible method to improve the performance and broaden the application of MOF materials.

Figure 1.5. The composites of MOFs and functional materials. [Reprinted with permission from ref. 49. Copyright 2014 The Royal Society of Chemistry]

1.2.2 Enhancing/creating intrinsic properties in MOFs

1.2.2.1 Post-synthetical modification (PSM)

PSM is an efficient synthetic strategy to functionalize MOF materials with desired properties, especially for those cannot be achieved by direct synthesis.[34, 56] In this method, the linkers of pre-assembled MOFs are modified by chemicals through amide couplings, isocyanate condensations, 'click' chemistry, or other suitable reactions with preservation of the lattice structure. Various functional groups have been successfully immobilized on the fixed linkers by PSM so far, through which the functionalities of MOFs are greatly enhanced and more controllable than the parent one. For example, the gas adsorption property of MOFs can be subtly tuned by grafting side chains with different length on the linkers using PSM approach.[57]

1.2.2.2 Defect engineering

Defect engineering, which is artificially controlling the defect concentration in materials to alter their intrinsic properties, has been a powerful tool to tailor

the properties of MOFs.[58-59] The control of defect density in MOFs is implemented by the incorporation of missing linker and/or missing node defects into MOFs during the fabrication processes. The defect engineering opens up novel opportunities to tailor the properties of MOFs not only in controlling physical characteristics such as band gap as well as magnetic and electrical/conductive properties, but also in sorption and catalysis within MOF materials. Metal and linker vacancies created by the incorporation of defect-generating linkers into MOFs might induce disturbed electronic coupling states compare to that of parent MOFs, which have huge impacts on electronic, magnetic, and optical properties.[60] Moreover, defects in MOFs could affect mass-transport pathways within the pores, combining with the increased active sites on prearranged SBUs by defect-generating linkers, shown great potential in catalysis application.[61-62]

1.2.2.3 Heterostructured MOFs

Integrating different MOF types into one structure is another efficient strategy to improve the performance of MOF materials, which shows hybrid properties from the single phases of MOF components as well as new functions generated from the synergistic effects of heterostructure (Figure 1.6). The as-synthesized MOF materials are so-called composite MOFs (or MOF-on-MOF or core-shell MOFs or MOF@MOF). This synthetic strategy is promising to synthesize MOF materials with multifunctionalities just by selecting associated MOF components and integrating them in a specific way.[63-64] For example, employing MOFs with different pore structure as components leads to the formation of hierarchical composite MOFs. The pore structure of hierarchical composite MOFs can be tuned by just changing the composition order of MOF components. The obtained composite MOFs with hierarchical pore structure are widely applied in sorption, separation, storage and molecule recognition.[65] However, the greatest challenge of this strategy

is that different MOFs cannot be integrated as desired due to the different incompatibility of MOF structures and crystallization kinetics. Hence, the selection of MOF components for constructing composite MOFs should be careful. To date, the successfully-synthesized composite MOFs are mainly among analogue MOF structures.

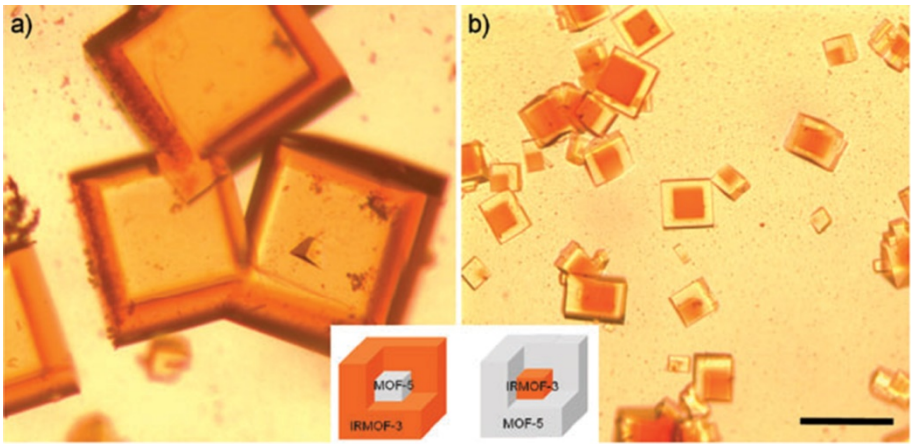

Figure 1.6. Microscope images of representative core–shell MOFs (a. IRMOF-3(shell)@MOF-5(core); b. MOF-5(shell)@IRMOF-3(core)). Scale bar, 200 mm. [Reprinted with permission from ref. 64. Copyright 2009 The Royal Society of Chemistry]

1.2.2.4 MOF thin films

Until now, most of the research attentions are mainly focusing on developing new MOF structures and functionalizing them for desired applications in bulk powder phase. However, some advanced applications, such as sensing, membrane-based separation, optical and electronic devices, and electrodes,[45, 47, 66] require MOFs assembled as thin films on given surfaces. More importantly, thin film process also facilitates the synthesis of composite MOFs, especially for those cannot prepare by normal bulk MOF synthesis methods (Figure 1.7). By this mean, the deposited quantity of each MOF component can be controlled during the fabrication process of heterostructured MOF thin films, which leads to the rational tunability of target

properties compare to bulk composite MOFs. As a promising synthetic strategy for improving the properties and performance of MOF materials, it will be discussed in detail below.

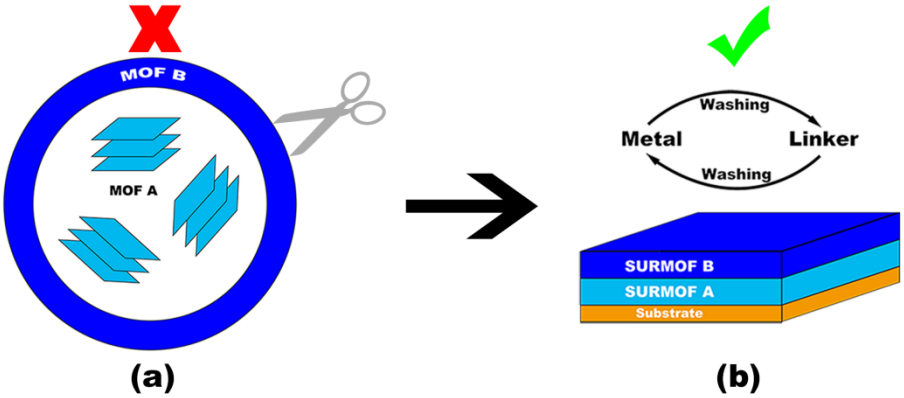

Figure 1.7. Schematic illustration of (a) free-standing composite MOF **B@A** and (b) heterostructured MOF thin film **B@A**.

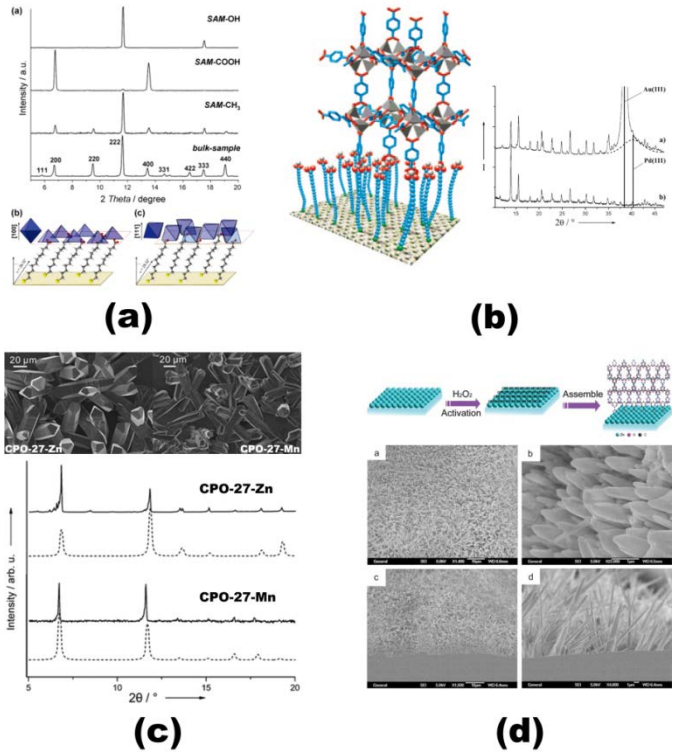

Figure 1.8. (a) Cu_3btc_2 thin films and XRD patterns, (b) MOF-5 thin films and XRD patterns, (c) CPO-27-Zn/Mn thin films SEM images and XRD patterns, (d)

Zn_3btc_2 thin films and XRD patterns. [Reprinted with permission from ref. 72 (a) and 71 (b); Adapted with permission from ref. 76 (a) and 78 (b). Copyright 2007 and 2005 American Chemistry Society; and 2010 and 2009 The Royal Society of Chemistry, respectively]

1.3 MOF thin films

1.3.1 Fabrication techniques

More recently, MOF thin films have attracted rapidly growing research interest due to their advanced applications as stated above.[66] Thus, the development of fabrication techniques for assembling MOFs as thin films into such specific substrates and devices becomes an important issue. So far, a number of different techniques have been proposed for the fabrication of MOF thin films, which can be classified into 5 catalogues generally summing up from the recent reviews.[45, 66-68] They are listed as follow.

1.3.1.1 Direct growth

Direct growth means immersing a substrate in the reaction solutions containing metal salts and organic linkers under solvothermal conditions. The growth of MOF thin films took place on the liquid-solid interface of substrate surface and solution in a more or less intergrown and continuous fashion. Interestingly, it has been found that the growth of MOF thin films by using this method is influenced by the surface nature of substrate, especially its acid/base properties.[69-70] For example, the acid linker-containing Cu_3btc_2 can only grow on an basic surface such as alumina, while the MOF of $Zn_2(bdc)_2(dabco)$ (bdc = terephthalate, dabco = 1,4-diazabicyclo[2.2.2]octane) with both acidic and basic linkers can grow on both acid silica and basic alumina. Because it seems that the linker with carboxylate groups cannot modify the acid substrate, which decreases the ability of heterogeneous

nucleation and growth. In order to overcome the selective growth of MOF thin films on various substrates, chemical modification of substrates is indispensable through which the connection between MOF thin films and substrates is established. Self-assembly monolayers (SAMs), including 16-mercaptohexadecanoic acid (MHDA), (4,(4-pyridyl)phenyl)-methanethiol (PPMT), 11-mercaptoundecanol (MUD), hydroxyl (-OH), 3-aminopropyltriethoxysilane (APTES), *etc*., have been widely used to modify the surface of substrates for directing the growth of MOF thin film.[69, 71-73] The applicability of direct growth methods is extended by employing SAMs as surface modificator.

Up to now, a number of MOF types, such as Cu_3btc_2 (Figure 1.8a),[72] MOF-5 (Figure 1.8b),[71] Zn_2bdc_2dabco,[69] $Mn(HCO_2)_2$,[70] ZIF-22,[74] ZIF-8/SIM-1,[75] CPO-27-M (M = Ni, Co, Mg, Zn and Mn) (Figure 1.8c)),[76] MIL-47,[77] Zn_3btc_2 (Figure 1.8d),[78] and so on, have been fabricated as thin films on various substrates by using direct growth method.

1.3.1.2 Liquid-phase epitaxy (LPE)

How to control the growth of MOF thin films with specific thickness, homogeneity, and preferred crystallographic orientation plays a key role in some advanced applications. Nevertheless, it seems impossible to control the quality of obtained MOF thin films by using the direct growth method. Liquid-phase epitaxy (LPE, also known as Layer-by-Layer (LbL)), which was originally designed for polyelectrolytes held together by ionic interactions,[79] and relies on the stepwise, layer-by-layer dosing of components onto the substrate, has been emerged. Compare to the direct growth, LPE is a promising method for the fabrication of MOF thin film with controllable quality. As shown in Figure 1.9, the general idea of the stepwise LPE growth technique is that metal and linker component solutions are sequentially dosed onto the

surface of SAM-functionalized substrate in a layer-by-layer fashion with rinsing an appropriate solvent between each step to remove the unreacted and/or weakly physisorbed species. The obtained thin films are so-called surface mounted MOFs (SURMOFs). The thin films fabricated by LPE display many advantages: (1) homogeneous and smooth; (2) controllable thickness just by varying the number of deposition cycles; (3) preferred crystallographic orientation; and (4) lower defect density than the bulk powder synthesized by conventional solvothermal methods.[45, 66-67] Moreover, combining with the surface plasmon resonance (SPR) technique[80-81] and quartz crystal microbalance (QCM) sensor,[82] the stepwise LPE growth process can be monitored *in situ* by recording the oscillation frequency change of the QCM sensor, which allows for direct process control and provides insight into the mechanism of SURMOF growth.

Until now, many MOF types (mainly Cu/Zn paddlewheel-based MOF structures) have been fabricated as thin films on various substrates using stepwise LPE technique, among which SURMOF Cu_3btc_2 that is one of the most intensively studied cases. Herein, SURMOF Cu_3btc_2 is used as a typical example to illustrate the details of stepwise LPE growth method. Prior to the growth process, cleaned substrate is immersed in SAM solution for some time to functionalize its surface. In each LPE deposition cycle, the functionalized substrate was first exposed to $Cu(OAc)_2$ solution for 5 min and then H_3btc linker solution for 10 min. Each subsequent step of dosing components was separated by a washing step of 5 min with ethanol. After repeating a certain cycles, the SURMOF Cu_3btc_2 would be obtained. Interestingly, the crystallographic orientation of as-synthesized SURMOF Cu_3btc_2 is determined by the SAMs used for functionalizing the substrates. Specifically, SURMOF Cu_3btc_2 shows the orientation of (100) and (111) on MHDA and MUD/PPMT/-OH SAMs-functionalized surface, respectively.[83] This

phenomenon can be found in other MOF types as well.[84-85] Note that, all of the work in this dissertation are based on this method.

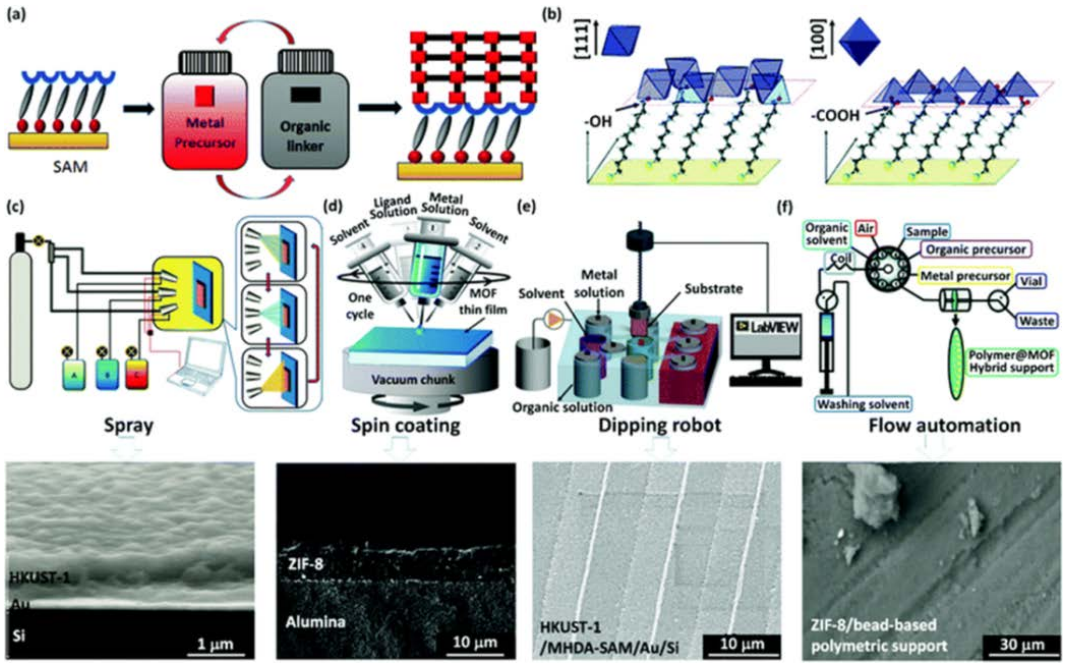

Figure 1.9. Schematic representations of the stepwise LPE method for fabrication of MOF thin-films, highlighting the well-controlled thin-film growth and the control of crystallite orientation by surface functionalization with SAM; and of the corresponding designs of various automatic set-ups for more efficiency in the large-scale processing. [Reprinted with permission from ref. 67. Copyright 2017 The Royal Society of Chemistry]

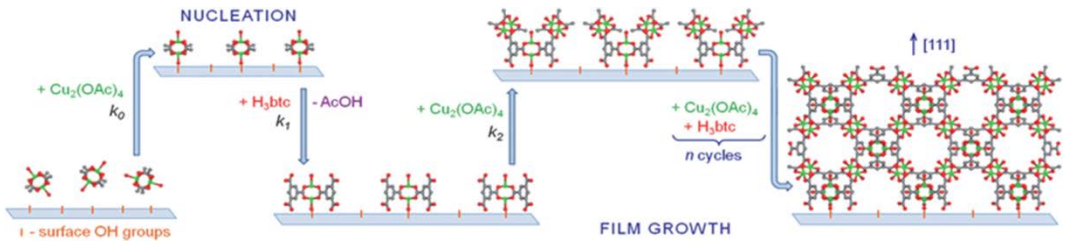

Figure 1.10. Schematic representation of the proposed model for Cu_3btc_2 nucleation and growth on oxide surfaces. [Reprinted with permission from ref. 82. Copyright 2012 The Royal Society of Chemistry]

SURMOFs have attracted a lot of attentions over the past decades due to the controllable thin film quality and potential applications. However, the growth mechanism behind stepwise LPE is still unclear now though several literatures have been published to discuss it.[82, 86-87] But it is widely accepted that the pre-formed SBUs is necessary for the nucleation of SURMOFs (Figure 1.10), otherwise the growth would be hindered.[88]

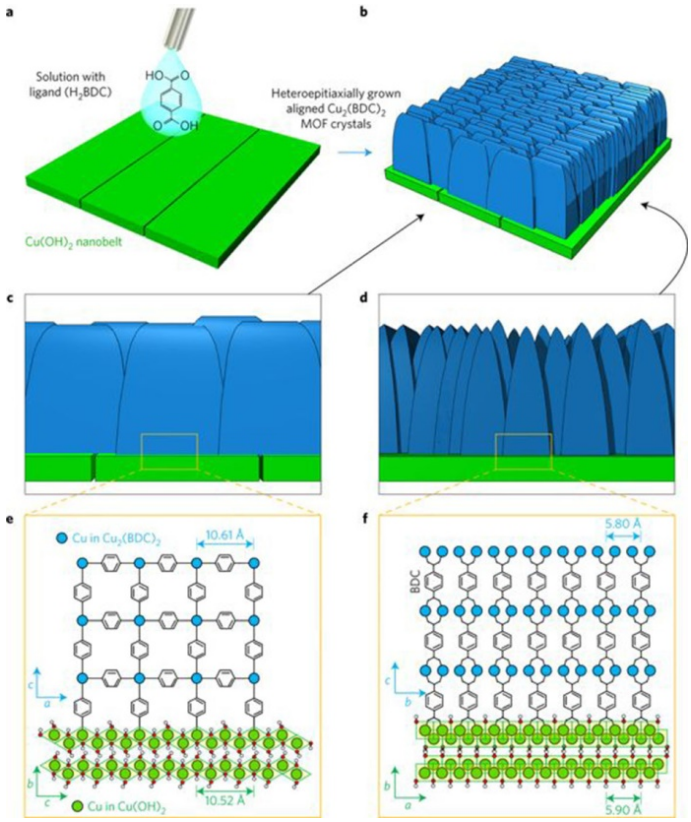

Figure 1.11. Schematically illustration of nanobelts converted Cubdc thin film by using substrate-seeded heteroepitaxy. [Reprinted with permission from ref. 91. Copyright 2017 Macmillan Publishers Limited, part of Springer Nature]

1.3.1.3 Substrate-seeded heteroepitaxy

In this synthetic method, solid substrate itself or with pre-deposited metal oxide/hydroxide nanostructure is used as metal source, which is then soaked in linker solution to form MOF thin films under solvothermal synthesis condition. The substrate-seeded heteroepitaxy differs from the LPE growth method in

which both metallic and organic linker solutions are separately provided. The solution attacks the surface of metal precursor to dissociate metal ions at the solid-liquid interface, and then deprotonated linkers further coordinate with dissociative metal ions to form MOFs anchored on the surface of metal precursor. Normally, MOF@metal precursor composites are obtained by using this method.

For example, MIL-53(Al) membrane on the mechanically strong support of α-Al_2O_3 disc was synthesized via substrate-seeded heteroepitaxy method by which free standing membrane with a size as large as centimeter scale was obtained.[89] The synthesis of ZIF-8, Cu_3btc_2, Cubdc (Figure 1.11) and Cu_2bdc_2dabco films were reported by this method as well, in which $ZnO/Cu(OH)_2$ nanostructures were firstly deposited on the support and then the metal precursor covered substrate reacted in the linker solution to form MOF films.[90-91] The resulted MOF@MO_x composites normally exhibit many unique properties that are from the integration of two species.[92-93]

1.3.1.4 Electrochemical deposition

Recently, a novel synthetic method was developed for MOF thin films fabrication, which is so-called electrochemical deposition. In general, three kinds of approaches have been reported so far for the use of electrochemical reactions to fabricate MOF thin-films, which are anodic, cathodic and electrophoretic deposition. In the anodic deposition process, MOF film forms on a metal connected at the anode within the electrolytic cell and the organic linker is dissolved in the electrolyte. After applying a voltage, anodic metal dissociate to generate the metal ions that further react with the organic linkers to form a target MOF anchoring on its surface. Differing from the anodic deposition, in the cathodic deposition process the electrodes are used as a source of electrons (normally are conductive and stable substrate like FTO, ITO glass) instead of as the MOF precursors and the metallic and linker

precursors are dissolved in the electrolyte. When applying a voltage, a high-concentrated alkali region near the cathode is formed in which organic linkers are deprotonated and further react with metal ions to form MOF particles. After a period of time, the accumulated MOF particles anchor on the cathode to form MOF films. For electrophoretic deposition, surface-charged MOF particles that are dispersed in the electrolyte are drove to accumulate on the opposite-charged electrode and form a MOF film under the electric field between anode and cathode.

Many types of MOF films have been prepared by using electrochemical deposition technique. Among them, UIO-66 is representative example which can be fabricated as film by all three approaches.[94-95]

1.3.1.5 Bottom-up modular assembly

It is difficult to assemble 2-dimensional (2D) MOFs as films on specific substrate due to its structural flexibility and the absence of spacers between adjacent layers. In order to solve this problem, bottom-up modular assembly approach, which combines layer-by-layer growth process and the Langmuir–Blodgett (LB) method, was developed to fabricate ultrathin 2D MOF thin films. Generally speaking, the pre-formed 2D MOF powder are firstly well dispersed in organic solvent by ultrasonication, afterwards suspending the mixture on top of water, at last transferring the suspended 2D MOF nanosheets on substrates by a simple stamping process. This method has been applied in many MOF types, especially the porphyrin-based 2D MOFs.[96-97]

Not only so, many other novel methods such as chemical vapor deposition (CVD),[98] atomic layer deposition (ALD),[99] are also emerged for fabricating MOF thin films. While these techniques normally require high technical threshold and have limited applicability, so they are not discussed in detail in this dissertation.

Although many methods have been developed for the synthesis of MOF thin films, the applicability of each method is limited. Hence, a universal approach for fabricating MOF thin films, especially that with high controllability of MOF thin film quality, is still pursuing by chemists.

1.3.2 Applications of MOF membranes/thin films

MOF membranes/thin films have a wide application scope from fundamental research to industry production process.[66, 100-101]

Separation: The chemical separation process in MOF materials can be divided into two types that are adsorption-storage driven separation and kinetic driven separation. As its name implies, adsorption-storage method utilizes the high adsorption capacity of specific adsorbates to separate from others, which are normally used in bulk MOFs. While for kinetic separation method, it takes advantage of the intrinsic properties of MOFs like the size/shape difference between pore opening of MOFs and adsorbates, and also the different affinities to adsorbates. This method is applied based on MOF films or membranes. MOF-5,[102] Cu_3btc_2,[103] MIL-53,[104] ZIF series,[105-107] *etc*. have been fabricated as membranes/films to study the gas or liquid separation.

Chemical sensing: QCM-based sensing is one of the most straightforward approaches which can detect the mass change accurate to nanograms. Integrating MOFs on QCM sensor is a smart design for chemical sensing application. SURMOFs, grown on QCM sensors by using stepwise LPE technique, are promising in volatile organic compounds (VOCs) sensing. For instance, Tu and Fischer developed a novel heterostructured SURMOF (donated as hetero-SURMOF) Cu_3btc_2(up)@Cu_2ndc_2dabco(down) (ndc = 1,4-naphthalenedicarboxylate) which shows prominent sensing efficiency to VOCs with different kinetic diameter.[108]

In addition, many other chemical sensing mechanisms, such as stress induced chemical detection, colloidal crystal-based sensing and luminescence-based detecting, together with MOF films generated sensors were also emerged over the past decades.[45]

Electronic and optoelectronic devices: Actually, the high porosity and non-conductivity of electrons in MOFs are not in favor of their applications in electronic and optoelectronic devices. However, incorporating metal nodes/linkers with intrinsic electrical, optical, and mechanical properties into the reticula structure of MOFs is an efficient way to tune the conductivity and photoabsorption of MOF materials. Although this field is only in its incipiency, many new fundamental insights relevant to integrating MOFs with such devices have already been gained.

Talin et al. have realized the tunability of electrical conductivity in Cu_3btc_2 by infiltrating the nanopores with redox-active, conjugated guest molecule of 7,7,8,8-tetracyanoquinododimethane (TCNQ).[109] Actually, the TCNQ guest molecules coordinate with the binuclear copper paddlewheels in the framework, which leads to strong electronic coupling between the dimeric Cu SBUs and results in the enhancement of conductivity. Besides, the progress of optoelectronic property in MOFs has been made as well, in which the porphyrin-based MOF thin films exhibiting superior photophysical properties, including large charge-carrier mobility and an unusually large charge-carrier generation efficiency were fabricated.[110] These synthetic efforts pave the way for electronic and optoelectronic applications of MOF materials.

Catalysis: Catalytic active functional species loaded MOF films, such as Pd@MOF-5,[71] and Bi_2O_3@Cu_3btc_2[111] have been developed as catalysts for the reactions of hydrogenation and dye degradation.

1.4 Motivation and outlines

As having been discussed previously, MOF thin films are promising in many application fields (e.g., sensors, membrane based separation, electronics, *etc*). Nevertheless, there are two primary challenges facing in practical applications for MOF thin film-based materials and devices: (1) developing advanced film fabrication and patterning techniques which are effective for integration of MOF materials into related devices with high quality and performance; (2) discovering novel MOF materials with specific functionalities. As for the first concern, various techniques have been emerged for the growth of uniform MOF thin films or patterns. Among these synthetic methods, stepwise LPE technique has been intensively studied and developed for the fabrication of well-controlled MOF thin films. Still, how to control the quality of SURMOFs and what the underlying mechanisms allowing for the fine-tuning of SURMOF fabrication process are not clear. Regarding to the second concern, some synthetic attempts such as fabricating heterostructured SURMOFs and loading functional species in SURMOFs have been devoted. Despite of this, continuous efforts still need before stepping into real-world applications. Starting from these challenges, the studies of this dissertation are aiming at understanding of the SURMOFs growth process, including improving the quality controllability of SURMOFs and the synthesis of lattice-mismatched heterostructured SURMOFs, and further exploiting this knowledge to develop novel SURMOFs and seek their potential applications. The detailed descriptions of each chapter are listed below.

Chapter 2 presents the thin film quality enhancement of Cu-paddlewheel-based SURMOFs (Cu_3btc_2 and Cubdc) by integrating a certain amount of water in the linker solution during the stepwise LPE growth process. By systematically studying the impact of water content on the quality

of obtained SURMOFs, we find that integrating 5% (v/v) water in the linker solution is the best condition for synthesizing SURMOFs with high quality, namely high crystallinity, preferred crystallographic orientation, high porosity, dense and homogenous morphology, and low defect density. Unfortunately, when applying this strategy to another Cu-paddlewheel-based SURMOFs Cu_2bdc_2dabco, the target SURMOFs cannot be obtained. Finally, we analyze the impact of water on the quality controllability of Cu-paddlewheel-based SURMOFs from the linker deprotonation and surface etching of thin films.

Chapter 3 focuses on the fabrication of lattice mismatched hetero-SURMOF $Cu_2ndc_2dabco@Cu_3btc_2$. According to the former research, Cu_3btc_2 can be sequentially deposited on the top of SURMOF Cu_2ndc_2dabco to obtain hetero-SURMOF $Cu_3btc_2@Cu_2ndc_2dabco$. Nevertheless, the heterostructure with reversed order cannot be obtained using the same growth method and conditions. In order to solve this synthetic problem, the surface of pre-formed SURMOF Cu_3btc_2 was functionalized by isophthalate ligands with flexible spacing chain and end -OH group. By interface functionalization, the hetero-SURMOF $Cu_2ndc_2dabco@Cu_3btc_2$ is successfully prepared. Prior to the growth of the hetero-SURMOF, the binding configuration of isophthalate ligands deposited at the external surface of SURMOF Cu_3btc_2 was explored firstly. The success of this strategy suggests that this methodology of interface functionalization probably can be generalized as a universal method for fabricating other hetero-SURMOFs or even hetero-bulk MOFs.

Chapter 4. In this chapter, we developed a novel 2D-3D hybrid hetero-SURMOF Cu_3btc_2@SURMOF-2 (Cubdc/bpdc/TF-bdc, bpdc = biphenyl-4,4'-dicarboxylate, TF-bdc = tetrafluoroterephthalate) by using stepwise LPE technique, which shows prominent VOCs adsorption properties. Instead of continuous film, discrete Cu_3btc_2 particles were deposited on top of

SURMOF-2, and the crystallographic orientation of top-deposited Cu_3btc_2 particles is determined by the linker used in the bottom SURMOF-2. Herein, the upper randomly-distributed Cu_3btc_2 particles enhance the VOCs adsorption capacity of bottom SURMOF-2 which was retrained by its surface barrier. The total storage capacity of hetero-SURMOF Cu_3btc_2@SURMOF-2 is higher than that of both component phases. Moreover, the hetero-SURMOF shows preferred adsorption ability to large VOC molecules, which can be even tuned by using different linkers in bottom SURMOF-2. Considering the unique VOCs adsorption properties, hetero-SURMOF Cu_3btc_2@Cubdc shows great potential in the sensing, recognition and adsorption of VOCs.

Chapter 5 presents the defects creation in SURMOF HKUST-1 by partially substituting the parent H_3btc with three kinds of truncated linkers isophthalic acid (H_2ip), 5-hydroxyisophthalic acid (H_2OH-ip) and 3,5-pyridindicarboxylic acid (H_2pydc) via two methods based on stepwise LPE, mixing method and alternating method. The obtained thin films were characterized by X-Ray diffraction (XRD), infrared reflection-absorption spectroscopy (IRRAS) and Raman spectroscopy to confirm that the incorporation of defects in HKST-1 did not change the overall structure. The defects integrated in SURMOF HKUST-1 were characterized by the measurements of ^1H nuclear magnetic resonance spectroscopy (NMR), time-of-flight secondary ion mass spectroscopy (ToF-SIMS), ultraviolet-visible (UV-Vis) spectroscopy, methanol vapor sorption and scanning electron microscope (SEM). The advantages of defects incorporation in SURMOF HKUST-1 of two strategies are compared at last.

Chapter 6 includes the experimental details and analytical procedures in Chapter 2-5. The details of organic ligands synthesis and fabrication of SURMOFs by stepwise LPE method, various characterizations (such as XRD,

IRRAS, TGA, sorption isotherms, SEM, NMR, UV-Vis, ToF-SIMS and Raman) are described. In addition, the supplementary data of Chapter 2 is also given in this chapter.

Chapter 7: In last chapter, we summarize the studies of this dissertation and the outlooks are also given. This dissertation focuses on the methodologies for the fabrication and improvement the quality of SURMOFs, and further multifunctionalizes SURMOFs to gain enhanced or create new functions by establishing heterostructure and incorporating defects.

1.5 References

[1] B.-L. Su, C. Sanchez, X.-Y. Yang, *Hierarchically Structured Porous Materials: From Nanoscience to Catalysis, Separation, Optics, Energy, and Life Science*, Wiley-VCH, Weinheim **2011**.

[2] J. Rouquerol, D. Avnir, C. Fairbridge, D. Everett, J. Haynes, N. Pernicone, J. Ramsay, K. Sing, K. Unger, *Pure Appl. Chem.* **1994**, *66*, 1739.

[3] J. P. Arenas, M. J. Crocker, *Sound Vib.* **2010**, *44*, 12.

[4] Z. Wang, J. Yu, R. Xu, *Chem. Soc. Rev.* **2012**, *41*, 1729.

[5] J. Yu, R. Xu, *Chem. Soc. Rev.* **2006**, *35*, 593.

[6] S. Kitagawa, R. Kitaura, S. Noro, *Angew. Chem. Int. Ed.* **2004**, *43*, 2334.

[7] O. M. Yagh, H. Li, *J. Am. Chem. Soc.* **1995**, *117*, 10401.

[8] Y. Kinoshita, T. H. I. Matsubara, Y. Saito, *Bull. Chem. Soc. Jpn.* **1959**, *32*, 1221.

[9] B. P. Block, S. H. Rose, C. W. Schaumann, E. S. Roth, J. Simkin, *J. Am. Chem. Soc.* **1962**, *84*, 3200.

[10] K. Susumu, K. Mitsuru, *Bull. Chem. Soc. Jpn.* **1998**, *71*, 1739.

[11] S. Horike, S. Shimomura, S. Kitagawa, *Nat. Chem.* **2009**, *1*, 695.

[12] O. M. Yagi, G. Li, H. Li, *Nature* **1995**, *378*, 703.

[13] M. Kondo, T.Yoshitomi, K. Seki, H.Matsuzaka, S. Kitagawa, *Angew. Chem. Int. Ed.* **1997**, *36*, 1725.

[14] D. Riou, G. Ferey, *J. Mater. Chem.* **1998**, *8*, 2733.

[15] A. Schneemann, V. Bon, I. Schwedler, I. Senkovska, S. Kaskel, R. A. Fischer, *Chem. Soc. Rev.* **2014**, *43*, 6062.

[16] S. R. Batten, N. R. Champness, X.-M. Chen, J. Garcia-Martinez, S. Kitagawa, L. Öhrström, M. O'Keeffe, M. Paik Suh, J. Reedijk, *Pure Appl. Chem.* **2013**, *85*, 1715.

[17] D. J. Tranchemontagne, J. L. Mendoza-Cortes, M. O'Keeffe, O. M. Yaghi, *Chem. Soc. Rev.* **2009**, *38*, 1257.

[18] M. J. Kalmutzki, N. Hanikel, O. M. Yaghi, *Sci. Adv.* **2019**, *4*.

[19] R. Banerjee, A. Phan, Bo Wang, C. Knobler, H. Furukawa, M. O'Keeffe, O. M. Yaghi, *Science* **2008**, *319*, 939.

[20] H. Furukawa, K. E. Cordova, M. O'Keeffe, O. M. Yaghi, *Science* **2013**, *341*, 1230444.

[21] A. O. Yazaydın, A. I. Benin, S. A. Faheem, P. Jakubczak, J. J. Low, R. R. Willis, R. l. Q. Snurr, *Chem. Mater.* **2009**, *21*, 1425.

[22] J. Qian, Q. Li, L. Liang, T. T. Li, Y. Hu, S. Huang, *Dalton Trans.* **2017**, *46*, 14102.

[23] K. Schlichte, T. Kratzke, S. Kaskel, *Micropor. Mesopor. Mater.* **2004**, *73*, 81.

[24] L. H. Wee, C. Wiktor, S. Turner, W. Vanderlinden, N. Janssens, S. R. Bajpe, K. Houthoofd, G. Van Tendeloo, S. De Feyter, C. E. Kirschhock, J. A. Martens, *J. Am. Chem. Soc.* **2012**, *134*, 10911.

[25] S. Horike, M.Dinca, K. Tamaki, J. R. Long, *J. Am. Chem. Soc.* **2008**, *130*, 5854.

[26] Y. K. Hwang, D. Y. Hong, J. S. Chang, S. H. Jhung, Y. K. Seo, J. Kim, A. Vimont, M. Daturi, C. Serre, G. Ferey, *Angew. Chem. Int. Ed.* **2008**, *47*, 4144.

[27] A. Herbst, A. Khutia, C. Janiak, *Inorg. Chem.* **2014**, *53*, 7319.

[28] M. Bosch, M. Zhang, H.-C. Zhou, *Adv. Chem.* **2014**, *2014*, 1.

[29] M. Kandiah, M. H. Nilsen, S. Usseglio, S. Jakobsen, U. Olsbye, M. Tilset, C. Larabi, E. A. Quadrelli, F. Bonino, K. P. Lillerud, *Chem. Mater.* **2010**, *22*, 6632.

[30] S. Bernt, V. Guillerm, C. Serre, N. Stock, *Chem. Commun.* **2011**, *47*, 2838.

[31] H. Deng, S. Grunder, K. E. Cordova, C. Valente, H. Furukawa, M. Hmadeh, F. Gándara, A. C. Whalley, Z. Liu, S. Asahina, H. Kazumori, M. O'Keeffe, O. Terasaki, J. F. Stoddart, O. M. Yaghi, *Science* **2012**, *336*, 1018.

[32] J. R. Li, R. J. Kuppler, H. C. Zhou, *Chem. Soc. Rev.* **2009**, *38*, 1477.

[33] J. Juan-Alcañiz, J. Gascon, F. Kapteijn, *J. Mater. Chem.* **2012**, *22*, 10102.

[34] K. K. Tanabe, S. M. Cohen, *Chem. Soc. Rev.* **2011**, *40*, 498.

[35] H. Deng, C. J. Doonan, H. Furukawa, R. B. Ferreira, J. Towne, C. B. Knobler, B. Wang, O. M. Yaghi, *Science* **2010**, *327*, 846.

[36] A. Helal, Z. H. Yamani, K. E. Cordova, O. M. Yaghi, *Natl. Sci. Rev.* **2017**, *4*, 296.

[37] N. Stock, S. Biswas, *Chem. Rev.* **2012**, *112*, 933.

[38] R. J. Marshall, C. L. Hobday, C. F. Murphie, S. L. Griffin, C. A. Morrison, S. A. Moggach, R. S. Forgan, *J. Mater. Chem. A* **2016**, *4*, 6955.

[39] A. Umemura, S. Diring, S. Furukawa, H. Uehara, T. Tsuruoka, S. Kitagawa, *J. Am. Chem. Soc.* **2011**, *133*, 15506.

[40] F. J. Carmona, C. R. Maldonado, S. Ikemura, C. C. Romao, Z. Huang, H. Xu, X. Zou, S. Kitagawa, S. Furukawa, E. Barea, *ACS Appl. Mater. Inter.* **2018**, *10*, 31158.

[41] M. Tu, C. Wiktor, C. Rosler, R. A. Fischer, *Chem. Commun.* **2014**, *50*, 13258.

[42] L. H. Wee, Y. Li, K. Zhang, P. Davit, S. Bordiga, J. Jiang, I. F. J. Vankelecom, J. A. Martens, *Adv. Funct. Mater.* **2015**, *25*, 516.

[43] P. Deria, J. E. Mondloch, O. Karagiaridi, W. Bury, J. T. Hupp, O. K. Farha, *Chem. Soc. Rev.* **2014**, *43*, 5896.

[44] M. Li, D. Li, M. O'Keeffe, O. M. Yaghi, *Chem. Rev.* **2014**, *114*, 1343.

[45] M. Tu, S. Wannapaiboon, R. A. Fischer, *Inorg. Chem. Front.* **2014**, *1*, 442.

[46] L. J. Murray, M. Dinca, J. R. Long, *Chem. Soc. Rev.* **2009**, *38*, 1294.

[47] L. E. Kreno, K. Leong, O. K. Farha, M. Allendorf, R. P. Van Duyne, J. T. Hupp, *Chem. Rev.* **2012**, *112*, 1105.

[48] A. H. Chughtai, N. Ahmad, H. A. Younus, A. Laypkov, F. Verpoort, *Chem. Soc. Rev.* **2015**, *44*, 6804.

[49] Q. L. Zhu, Q. Xu, *Chem. Soc. Rev.* **2014**, *43*, 5468.

[50] Q. Yang, Q. Xu, H. L. Jiang, *Chem. Soc. Rev.* **2017**, *46*, 4774.

[51] C. Rösler, R. A. Fischer, *CrystEngComm* **2015**, *17*, 199.

[52] M. Meilikhov, K. Yusenko, D. Esken, S. Turner, G. Van Tendeloo, R. A. Fischer, *Eur. J. Inorg. Chem.* **2010**, *2010*, 3701.

[53] H. R. Moon, D. W. Lim, M. P. Suh, *Chem. Soc. Rev.* **2013**, *42*, 1807.

[54] D. Mustafa, E. Breynaert, S. R. Bajpe, J. A. Martens, C. E. Kirschhock, *Chem. Commun.* **2011**, *47*, 8037.

[55] C.-Y. Sun, S.-X. Liu, D.-D. Liang, K.-Z. Shao, Y.-H. Ren, Z.-M. Su, *J. Am. Chem. Soc.* **2009**, *131*, 1883.

[56] Z. Wang, S. M. Cohen, *Chem. Soc. Rev.* **2009**, *38*, 1315.

[57] Z. Wang, S. M. Cohen, *J. Am. Chem. Soc.* **2009**, *131*, 16675.

[58] Z. Fang, B. Bueken, D. E. De Vos, R. A. Fischer, *Angew. Chem. Int. Ed.* **2015**, *54*, 7234.

[59] S. Dissegna, K. Epp, W. R. Heinz, G. Kieslich, R. A. Fischer, *Adv. Mater.* **2018**, *30*, e1704501.

[60] Z. Fang, J. P. Durholt, M. Kauer, W. Zhang, C. Lochenie, B. Jee, B. Albada, N. Metzler-Nolte, A. Poppl, B. Weber, M. Muhler, Y. Wang, R. Schmid, R. A. Fischer, *J. Am. Chem. Soc.* **2014**, *136*, 9627.

[61] J. Canivet, M. Vandichel, D. Farrusseng, *Dalton Trans.* **2016**, *45*, 4090.

[62] W. Zhang, M. Kauer, O. Halbherr, K. Epp, P. Guo, M. I. Gonzalez, D. J. Xiao, C. Wiktor, F. X. Liabrés i Xamena, C. Wöll, Y. Wang, M. Muhler, R. A. Fischer, *Chem. Eur. J.* **2016**, *22*, 14297.

[63] S. Furukawa, K. Hirai, Y. Takashima, K. Nakagawa, M. Kondo, T. Tsuruoka, O. Sakata, S. Kitagawa, *Chem. Commun.* **2009**, *34*, 5097.

[64] K. Koh, A. G. Wong-Foy, A. J. Matzger, *Chem. Commun.* **2009**, *41*, 6162.

[65] Y. Gu, Y. N. Wu, L. Li, W. Chen, F. Li, S. Kitagawa, *Angew. Chem. Int. Ed.* **2017**, *56*, 15658; *Angew. Chem*. **2017**, *129*, 15864.

[66] A. Betard, R. A. Fischer, *Chem. Rev.* **2012**, *112*, 1055.

[67] J. Liu, C. Wöll, *Chem. Soc. Rev.* **2017**, *46*, 5730.

[68] B. Liu, R. A. Fischer, *Sci. China Chem.* **2011**, *54*, 1851.

[69] D. Zacher, A. Baunemann, S. Hermes, R. A. Fischer, *J. Mater. Chem.* **2007**, *17*, 2785.

[70] M. Arnold, P. Kortunov, D. J. Jones, Y. Nedellec, J. Kärger, J. Caro, *Eur. J. Inorg. Chem.* **2007**, *2007*, 60.

[71] S. Hermes, F. Schröder, R. Chelmowski, C. Wöll, R. A. Fischer, *J. Am. Chem. Soc.* **2005**, *127*, 13744.

[72] E. Biemmi, C. Scherb, T. Bein, *J. Am. Chem. Soc.* **2007**, *129*, 8054.

[73] E. Biemmi, A. Darga, N. Stock, T. Bein, *Micropor. Mesopor. Mater.* **2008**, *114*, 380.

[74] A. Huang, H. Bux, F. Steinbach, J. Caro, *Angew. Chem. Int. Ed.* **2010**, *49*, 4958.

[75] S. Aguado, J. Canivet, D. Farrusseng, *Chem. Commun.* **2010**, *46*, 7999.

[76] A. Bétard, D. Zacher, R. A. Fischer, *CrystEngComm* **2010**, *12*, 3768.

[77] A. Centrone, Y. Yang, S. Speakman, L. Bromberg, G. C. Rutledge, T. A. Hatton, *J. Am. Chem. Soc.* **2010**, *132*, 15687.

[78] X. Zou, G. Zhu, I. J. Hewitt, F. Sun, S. Qiu, *Dalton Trans.* **2009**, 3009.

[79] G. Decher, *Science* **1997**, *277*, 1232.

[80] O. Shekhah, H. Wang, S. Kowarik, F. Schreiber, M. Paulus, M. Tolan, C. Sternemann, F. Evers, D. Zacher, F. A. Fischer, C. Wöll, *J. Am. Chem. Soc.* **2007**, *129*, 15118.

[81] O. Shekhah, H. Wang, D. Zacher, R. A. Fischer, C. Wöll, *Angew. Chem. Int. Ed.* **2009**, *48*, 5038; *Angew. Chem.* **2009**, *121*, 5138.

[82] V. Stavila, J. Volponi, A. M. Katzenmeyer, M. C. Dixon, M. D. Allendorf, *Chem. Sci.* **2012**, *3*, 1531.

[83] J. Liu, O. Shekhah, X. Stammer, H. K. Arslan, B. Liu, B. Schüpbach, A. Terfort, C. Wöll, *Materials* **2012**, *5*, 1581.

[84] S. M. Chen, M. Liu, Z. G. Gu, W. Q. Fu, J. Zhang, *ACS Appl. Mater. Inter.* **2016**, *8*, 27332.

[85] B. Liu, M. Tu, R. A. Fischer, *Angew. Chem. Int. Ed.* **2013**, *52*, 3402.

[86] A. Summerfield, I. Cebula, M. Schroder, P. H. Beton, *J. Phys. Chem. C* **2015**, *119*, 23544.

[87] G. Delen, D. Z. Ristanović, L. D. B. Mandemaker, P. D. B. M. Weckhuysen, *Chem. Eur. J.* **2018**, *24*, 187.

[88] S. Wannapaiboon, M. Tu, R. A. Fischer, *Adv. Funct. Mater.* **2014**, *24*, 2696.

[89] Y. Zhang, Q. Gao, Z. Lin, T. Zhang, J. Xu, Y. Tan, W. Tian, L. Jiang, *Sci. Rep.* **2014**, *4*, 4947.

[90] K. Khaletskaya, S. Turner, M. Tu, S. Wannapaiboon, A. Schneemann, R. Meyer, A. Ludwig, G. Van Tendeloo, R. A. Fischer, *Adv. Funct. Mater.* **2014**, *24*, 4804.

[91] P. Falcaro, K. Okada, T. Hara, K. Ikigaki, Y. Tokudome, A. W. Thornton, A. J. Hill, T. Williams, C. Doonan, M. Takahashi, *Nat. Mater.* **2017**, *16*, 342.

[92] W. W. Zhan, Q. Kuang, J. Z. Zhou, X. J. Kong, Z. X. Xie, L. S. Zheng, *J. Am. Chem. Soc.* **2013**, *135*, 1926.

[93] G. Cai, W. Zhang, L. Jiao, S.-H. Yu, H.-L. Jiang, *Chem* **2017**, *2*, 791.

[94] I. Stassen, M. Styles, T. Van Assche, N. Campagnol, J. Fransaer, J. Denayer, J.-C. Tan, P. Falcaro, D. De Vos, R. Ameloot, *Chem. Mater.* **2015**, *27*, 1801.

[95] I. Hod, W. Bury, D. M. Karlin, P. Deria, C. W. Kung, M. J. Katz, M. So, B. Klahr, D. Jin, Y. W. Chung, T. W. Odom, O. K. Farha, J. T. Hupp, *Adv. Mater.* **2014**, *26*, 6295.

[96] R. Makiura, S. Motoyama, Y. Umemura, H. Yamanaka, O. Sakata, H. Kitagawa, *Nat. Mater.* **2010**, *9*, 565.

[97] G. Xu, T. Yamada, K. Otsubo, S. Sakaida, H. Kitagawa, *J. Am. Chem. Soc.* **2012**, *134*, 16524.

[98] I. Stassen, M. Styles, G. Grenci, H. V. Gorp, W. Vanderlinden, S. D. Feyter, P. Falcaro, D. D. Vos, P. Vereecken, R. Ameloot, *Nat. Mater.* **2016**, *15*, 304.

[99] E. Ahvenniemi, M. Karppinen, *Chem. Mater.* **2016**, *28*, 6260.

[100] P. Falcaro, R. Ricco, C. M. Doherty, K. Liang, A. J. Hill, M. J. Styles, *Chem. Soc. Rev.* **2014**, *43*, 5513.

[101] V. Stavila, A. A. Talin, M. D. Allendorf, *Chem. Soc. Rev.* **2014**, *43*, 5994.

[102] Y. Liu, Z. Ng, E. A. Khan, H.-K. Jeong, C.-b. Ching, Z. Lai, *Micropor. Mesopor. Mater.* **2009**, *118*, 296.

[103] H. Guo, G. Zhu, I. J. Hewitt, S. Qiu, *J. Am. Chem. Soc.* **2009**, *131*, 1646.

[104] Y. Hu, X. Dong, J. Nan, W. Jin, X. Ren, N. Xu, Y. M. Lee, *Chem. Commun.* **2011**, *47*, 737.

[105] A. Huang, Y. Chen, N. Wang, Z. Hu, J. Jiang, J. Caro, *Chem. Commun.* **2012**, *48*, 10981.

[106] Q. Song, S. K. Nataraj, M. V. Roussenova, J. C. Tan, D. J. Hughes, W. Li, P. Bourgoin, M. A. Alam, A. K. Cheetham, S. A. Al-Muhtaseb, E. Sivaniah, *Energ. Environ. Sci.* **2012**, *5*, 8359.

[107] Y. Ban, Y. Li, Y. Peng, H. Jin, W. Jiao, X. Liu, W. Yang, *Chem. Eur. J.* **2014**, *20*, 11402.

[108] M. Tu, R. A. Fischer, *J. Mater. Chem. A* **2014**, *2*, 2018.

[109] A. A. Talin, A. Centrone, A. C. Ford, M. E. Foster, V. Stavila, P. Haney, R. A. Kinney, V. Szalai, F. E. Gabaly, H. P. Yoon, F. Léonard, M. D. Allendorf, *Science* **2014**, *343*, 66.

[110] J. Liu, W. Zhou, J. Liu, I. Howard, G. Kilibarda, S. Schlabach, D. Coupry, M. Addicoat, S. Yoneda, Y. Tsutsui, T. Sakurai, S. Seki, Z. Wang, P. Lindemann, E. Redel, T. Heine, C. Wöll, *Angew. Chem. Int. Ed.* **2015**, *54*, 7441.

[111] W. Guo, Z. Chen, C. Yang, T. Neumann, C. Kubel, W. Wenzel, A. Welle, W. Pfleging, O. Shekhah, C. Wöll, E. Redel, *Nanoscale* **2016**, *8*, 6468.

Chapter 2

Control of water content for enhancing the quality of copper paddle-wheel-based MOF thin films grown by Layer-by-Layer liquid-phase epitaxy*

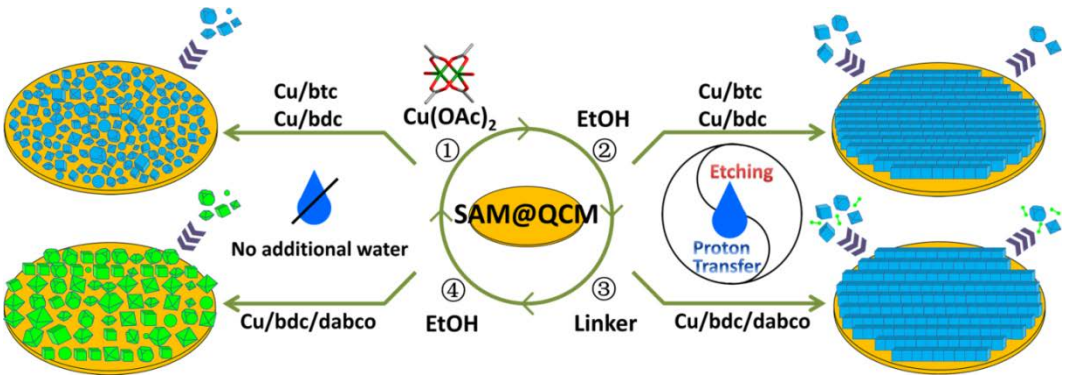

*The results of this chapter are published and reproduced from: "Z. Wang, K. Rodewald, R. Medishetty, B. Rieger, and R. A. Fischer, *Cryst. Growth Des.* **2018**, 18, 7451−7459" with the Copyright 2018 American Chemistry Society.

Abstract

Metal−organic framework (MOF) thin films with high crystallinity, preferred orientation, homogeneous texture, and enhanced porous properties are desired to satisfy many practical applications. Surface mounted MOF crystallite thin films (SURMOFs), prepared via a stepwise liquid-phase epitaxy technique, have attracted great interest. Although many efforts have been devoted to this field, it still remains a significant challenge to prepare SURMOFs with high quality reproducibly in an efficient way. In the synthesis of MOF bulk materials, coordination modulators (normally are acids or bases) have been successfully used to improve the properties of obtained materials. However, non-neutral additives are too reactive for Cu paddle-wheel-based SURMOFs to survive. Introducing water as a mild additive to the growth process provides an efficient strategy for the growth of SURMOFs. Herein, the growth of three kinds of Cu paddle-wheel-based SURMOFs (Cu_3btc_2, Cubdc, Cu_2bdc_2dabco) is systematically investigated by varying the water content in the linker solution during the stepwise liquid phase epitaxial growth process (btc = 1,3,5- benzentricarboxylate; bdc = 1,4-benzendedicarboxylate; dabco = 1,4-diazabicyclo[2.2.2]octane). Grazing incidence X-ray diffraction (GIXRD), scanning electron microscopy (SEM), methanol sorption behavior, and infrared reflection absorption spectroscopy (IRRAS) are employed to characterize the quality of as-deposited SURMOFs. The strategy of integrating water in the linker solution could provide a potentially versatile route for the fabrication of a wide range of MOF thin films with enhanced characteristics. The addition of 5% water turned out to yield dense, highly crystalline, oriented, and porous Cu_3btc_2 SURMOFs, whereas water contents above 30% yielded less dense films with lower surface coverage. Above 70% water content SURMOF growth was no longer possible. Similar enhanced quality is found for Cubdc

SURMOFs; however growth of Cu_2bdc_2dabco is not possible in the presence of water, and rather Cubdc SURMOFs were obtained.

2.1 Introduction

Thin film devices have a broad application in optical, electronic applications,[1-4] plasma-enhancement detection,[5] chemical sensing,[6-7] photovoltaics,[8-9] *etc*., which originate from their unusual physiochemical properties such as unique surface chemistry, high aspect ratio and quantum-size effect. Many of these application prospects heavily rely on the quality of thin films (crystallinity, orientation, morphology, surface roughness and defect density). High quality thin films are always pursued in the practical applications, because it is greatly beneficial to obtain enhanced properties and fabricate devices with high performance and long life time.[10-12] In addition, these are also ideal candidates for fundamental studies and mechanistic understanding. However, fabrication of thin films with high quality still remains a significant challenge for each given class of materials. Summarizing huge number of reports, it turns out that solution-based deposition and film growth techniques are most often employed as being a relatively cheap, versatile, flexible and scalable fabricating technique.[13-16]

Metal-organic frameworks (MOFs) are a family of microporous crystalline hybrid materials, which show great applications in a broad range from fundamental research life sciences to practical applications in industry,[7, 17-23] due to their large internal surface area, controlled porosities, tunable cavities, *etc*. [24-26] MOF thin films are receiving increasing attention in recent years because they are promising candidates in many advanced applications.[3-4, 7, 27-28] Abundant techniques, including *in situ*,[29-30] secondary growth,[31-32] *ex situ*[33] and stepwise liquid-phase epitaxy (stepwise LPE; also called

layer-by-layer (LbL) deposition),[34-36] have been developed for integrating MOFs onto specific substrates and devices as thin films. Among them, the stepwise LPE method has emerged as an important synthetic strategy to allow the MOF to grow with a well-controlled film thickness even down to the lower nano scale regime with exceptionally smooth surface morphology in case of optimizing the growth parameters during the fabrication process. In this technique, self-assembled organic monolayer (SAM) modified substrates are sequentially exposed to metal and linker solutions with rinsing solvent between successive deposition steps to remove not reacted or weakly physisorbed components.[37] The resulted thin films are called surface mounted MOFs (SURMOFs). Moreover, combining with surface plasmon resonance (SPR) technique[34, 38] and quartz crystal microbalance (QCM) sensor[39], the stepwise LPE growth process can be monitored *in-situ* by recording the oscillation frequency change of QCM sensor during the fabrication process. This allows for direct process control and provides insight into the mechanism of SURMOF fabrication. Although the utility of this technique has been illustrated *via* the successful deposition of several MOF systems (mainly are Cu/Zn paddlewheel-based MOF structures)[34, 40-43], well-controlled and highly reproducible film growth has remained quite elusive to date. Moreover, limited attention has been devoted to systematically explore the underlying mechanism and the full set of possible growth parameters which control the quality of the resulting films. Learning from the synthesis strategies known to manipulate and optimize the growth of bulk MOF crystals presents a potentially powerful route to improve the quality of MOF thin films.

Among the synthetic methods available for controlling the growth of bulk MOF crystals, the addition of Brønsted acids or bases in the synthesis process is widely used to control the resulting crystal size and morphology.[44-48] In fact, one of our previous works demonstrated the beneficial effect of coordination

modulators to the synthesis of MOF thin films. MOF-5 isotype SURMOFs based on carboxylpyrazolate linkers were grown with enhanced crystallinity, orientation and sorption capacity by mixing appropriate amount of acetic acid (*i.e.* acetate as the competing ligand) into the solution used for the step of metal ion (Zn^{2+}) dosing.[44] The applicability of stronger Brønsted acids or bases in the precursor solutions is limited especially for Cu paddlewheel-based SURMOFs (such as Cu_3btc_2 (btc = benzene-1,3,5-tricarboxylate),[34] pillar-layered M_2L_2P[40] and SURMOF-2 family[43]) due to their poor resistant ability to acid and base. Considering the lability of Cu paddlewheel-based MOFs, we decided to investigate water as a mild coordination modulator or additive.[49]

Previously, the growth of Cu_3btc_2 SURMOFs was found to be highly susceptible to the environmental humidity (EH) and/or undefined water content in the solvents, based on our experience. The intentional addition of defined amounts of water in the synthesis process can weaken the influence of EH and we anticipated a more reproducible growth behavior and enhanced quality thin films. Furthermore, the water content of the solution is likely to influence the "proton transfer" between acetate groups of the copper ion source $Cu(OAc)_2$ and carboxyl groups of linker during the acetate *vs.* linker substitution reaction, which is the crucial process in the stepwise layer-by-layer growth of Cu_3btc_2 SURMOFs.[50] As these processes involve adsorption/desorption equilibria at the liquid-solid interface of the growing SURMOF, water also contribute to the etching of the growing SURMOFs, for example by removing miss-oriented nuclei and crystallizes and this effect may contribute to the evolution of crystal size, shape, orientation and crystal density at the surface (*e.g.* surface coverage).

In the present work, we systematically explore the influence of water on the stepwise layer-by-layer LPE growth of Cu paddle wheel based MOFs through mixing various amount of water in linker solutions, with emphasis on the Cu_3btc_2 system. Under the synergistic effect of promoted crystal growth and etching of water, highly crystalline, orientated and homogenous SURMOFs can be obtained (Figure 2.1), however there is an optimum set of parameters for achieving a smooth surface coverage. The obtained SURMOFs were characterized by grazing incidence X-ray diffraction (GIXRD), scanning electron microscope (SEM), methanol sorption behavior and infrared reflection absorption spectroscopy (IRRAS). The strategy was also applied to two related systems, namely Cubdc (bdc = terephthalate) and Cu_2bdc_2dabco (dabco = 1,4-Diazabicyclo[2.2.2]octane). The characterization results indicated that SURMOFs of Cubdc with high crystallinity, preferred orientation and dense texture were synthesized by mixing proper amount of water in linker solution. Interestingly in the case of Cu_2bdc_2dabco, water turned out to be an inappropriate modulator as the presence of additional water led to the formation of Cubdc instead of the targeted Cu_2bdc_2dabco.

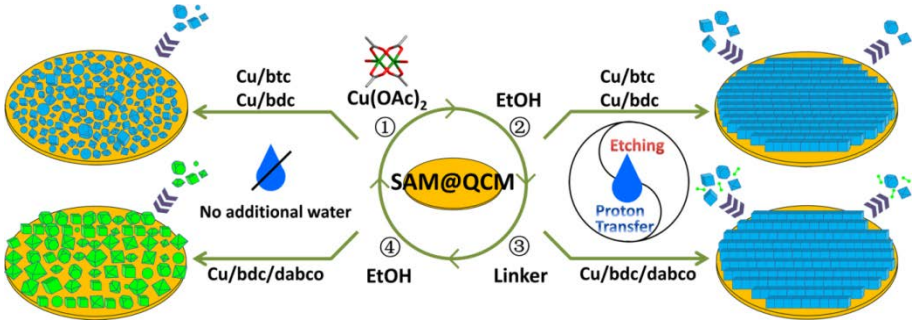

Figure 2.1. Schematic illustration presenting the influence of water on the growth of Cu paddlewheel-based SURMOFs. Note that, blue polyhedrons represent Cu_3btc_2 or Cubdc particles and related coordination species; and green polyhedrons (dumbbells) mean Cu_2bdc_2dabco (dabco molecules).

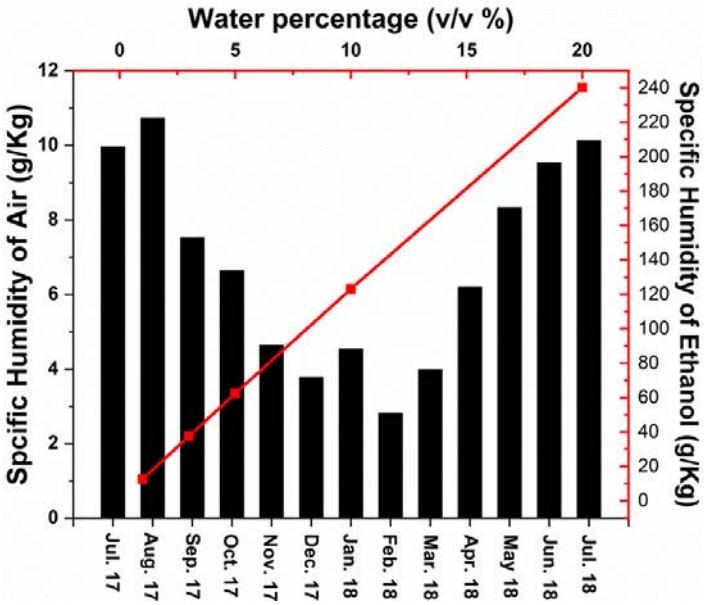

Figure 2.2. The specific humidity of air in Garching and the specific humidity of linker solution (integrated with different amount of water, here only 1-20% is shown). In the case of Cu_3btc_2 SURMOFs, the fabrication processes were repeated time to time in the span of whole year and the quality shows no great disparities. For the parts of Cubdc and Cu_2bdc_2dabco SURMOFs, the fabrication was done in summer time (from May to July of 2018) of Garching, Germany. The specific humidity of air was calculated from the monthly average relative humidity (RH), temperature and pressure by using the Clausius-Clapeyron equation. Herein, the monthly climate data is from the Meteorological Institute Munich, Ludwig-Maximilians-Universität München (LMU). Moreover, the specific humidity of linker solution was also calculated. Here only shows the range of 1-20% for clarity.

2.2 Results and Discussion

2.2.1 Cu_3btc_2 SURMOFs

Growth of Cu_3btc_2 SURMOFs. According to our research experience, the growth of Cu_3btc_2 SURMOF is susceptible to EH, which means that the

quality of Cu_3btc_2 SURMOFs fabricated in different periods is diverse. In order to explore the best condition of humidity level for fabricating high quality Cu_3btc_2 SURMOFs, different amount of water varying from EH (no additional water) to 100% (volume ratio) was mixed in H_3btc linker solution. Herein, the specific humidity of ambient air and the linker solution (with different amounts of intentionally added water) is given in Figure 2.2. Note that the addition or rising water contents to the solution of $Cu(OAc)_2$ in absolute ethanol is impractical because of chemical instability.[51] The Cu_3btc_2 SURMOFs were fabricated by using stepwise, layer-by-layer LPE technique. In a typical preparation, the MHDA SAM functionalized QCM substrate was alternatively dosed with $Cu(OAc)_2$ and H_3btc linker solutions (containing defined amounts of water) in a continuous flow mode, with an ethanol washing step between precursor dosing stages. The quantity of Cu_3btc_2 deposited on the substrate was simply controlled by the cycling number.

The growth processes of Cu_3btc_2 SURMOFs were monitored *in-situ* by the Q-sense instrument with recording the QCM frequency as shown in Figure 2.3a. Viewing from QCM frequency change curves, it is noticeable that the mass of Cu_3btc_2 deposited on the substrate increases over the same period with the raise of water content in H_3btc solution from the range of EH to 70%. Closer inspection of the frequency change over the period of the rinsing step after H_3btc dosing (Figure 2.3b) indicates that some pre-formed parts were removed from the surface of film. However, very limited amount of MOF deposited on the substrate is observed when the water content is more than 70%. One plausible reason for the loss of deposition could be the massive competition of water with the growth components (linkers) *via* hydrogen bonding interactions between water and H_3btc, preventing the efficient chemisorption of the carboxylate groups of btc to Cu paddlewheels mounted on the gold surface of substrate[52]. In summary, the integrating water in H_3btc

solution boosted the SURMOF deposition efficiency in a specific range (up to 70%).

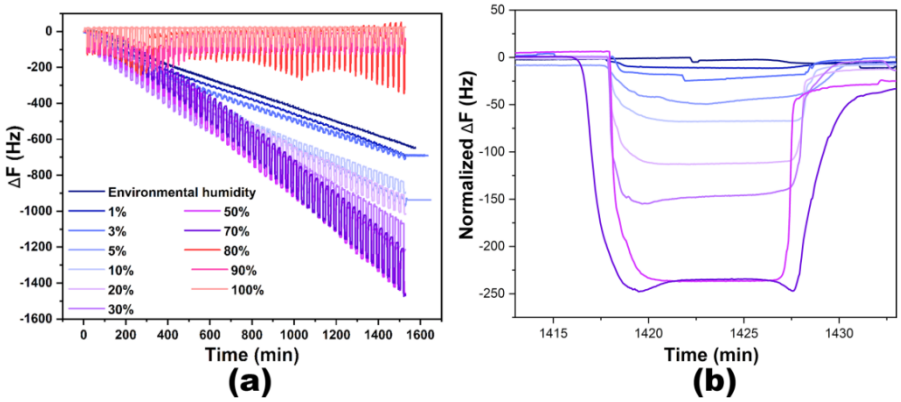

Figure 2.3. QCM frequency as a function of time recorded in situ during the stepwise LPE growth of (a) Cu_3btc_2 SURMOFs and the comparison of the depth of gaps appeared during the rinsing stage after (b) H_3btc.

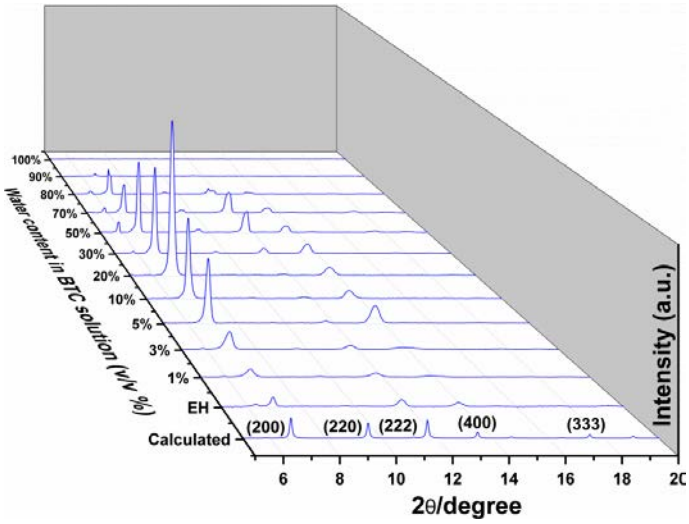

Figure 2.4. The comparison of out-of-plane 3D XRD patterns of Cu_3btc_2 SURMOFs fabricated with different amount of water in linker solution (EH = environmental humidity).

Quality characterization of Cu_3btc_2 SURMOFs. The crystallinity and orientation of obtained SURMOFs was probed by GIXRD presented in Figure 2.4. The patterns show qualitatively that the crystallinity (relative peak intensity)

of obtained Cu_3btc_2 SURMOFs is enhanced by integrating water in H_3btc solution (up to 70%) compared to that grown under EH. In detail, the crystallinity enhances gradually with the increase of water content in H_3btc solution, and culminates at the percentage of 20% afterwards begins to reduce. While the water content exceeds 70%, some unknown phase was deposited on the substrate. The Cu_3btc_2 SURMOFs fabricated within the water range of 5–20% in H_3btc solution, which only show (200) and (400) peaks, are more uniform with respect to the preferred crystallite orientation than others.

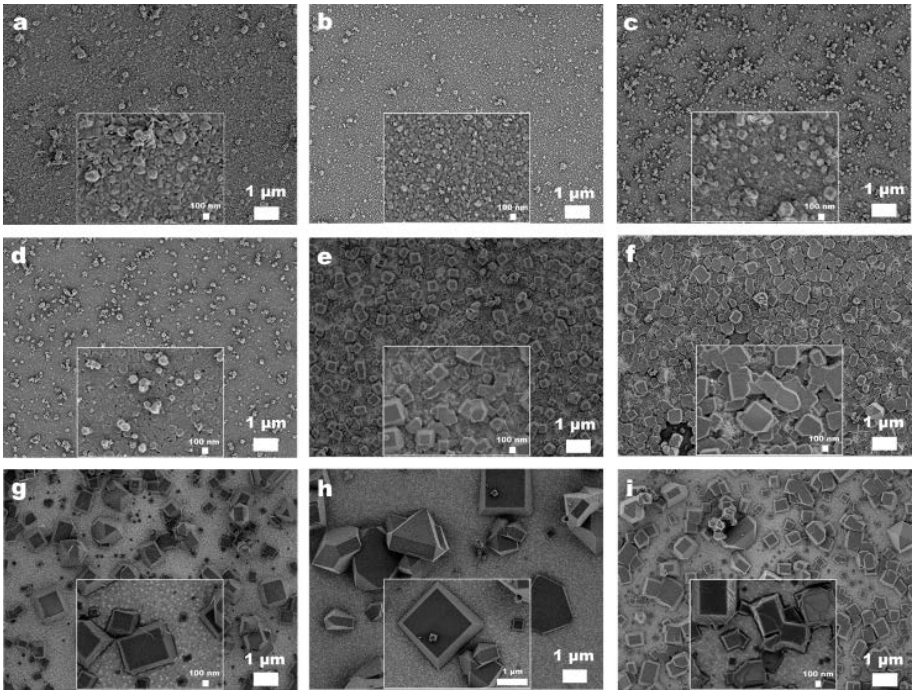

Figure 2.5. SEM images of Cu_3btc_2 SURMOFs fabricated with different water content in H_3btc solution: (a) EH, (b) 1%, (c) 3%, (d) 5%, (e) 10%, (f) 20%, (g) 30%, (h) 50%, (i) 70%.

Combining the data of QCM frequency change and XRD patterns, we can speculate that the integration of water in H_3btc solution accelerated the nucleation of Cu_3btc_2 SURMOFs and promoted further crystal growth. Meanwhile, water etched out some pre-formed MOFs as well, and the washed-out amount augments with the raise of water content.[53-54] The quality

of deposited thin films can be rationally controlled under the synergistic effect of promoted crystal growth and surface etching, which is realized by adjusting the water content integrated in H_3btc solution. Concluding from XRD patterns, integrating additional 5–20% water in H_3btc solution (in this range the influence of EH is much less competitive than the integrated water) would be an acceptable range for fabrication highly-crystalline and orientated Cu_3btc_2 SURMOFs as judged by the GIXRD.

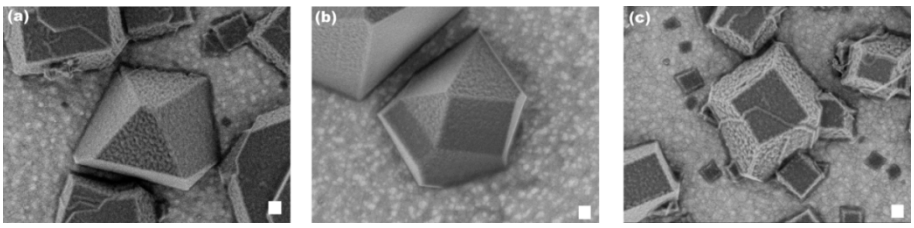

Figure 2.6. SEM images of Cu_3btc_2 SURMOFs fabricated with (a) 30%, (b) 50% and (c) 70% water content in linker solution. Scale bar: 100 nm.

In order to assess the influence of additional water on the morphology of Cu_3btc_2 SURMOFs, SEM images (Figure 2.5) were recorded under the GB mode by which real surface features of thin film can be observed.[55] The SURMOF thin films are composed of more or less dense and interconnected MOF particles depending on the water content. In particular, the size of these MOF particles increases from the nano to micro meter range with rising water content in H_3btc solution. This is primarily assigned to both, a promoted nucleation and as well crystal growth efficiency of Cu_3btc_2. The visual proof of the etching effect by the water is also available in Figure 2.6, in which the surface morphology of micrometer Cu_3btc_2 particles is shown. The rough surface of micrometer Cu_3btc_2 particles is similar to that reported and discussed in literatures.[53] The sample prepared with 5% water shows more flat and homogeneous surface morphology and texture than others (Figure 2.5d). Note that there are some nanoparticles/islands located on the top of film,

which cannot be avoided. Because it is determined by the island growth mechanism involving a relatively small number of initial MOF nuclei on the surface, followed by subsequent growth and extension to a layer of film.[56]

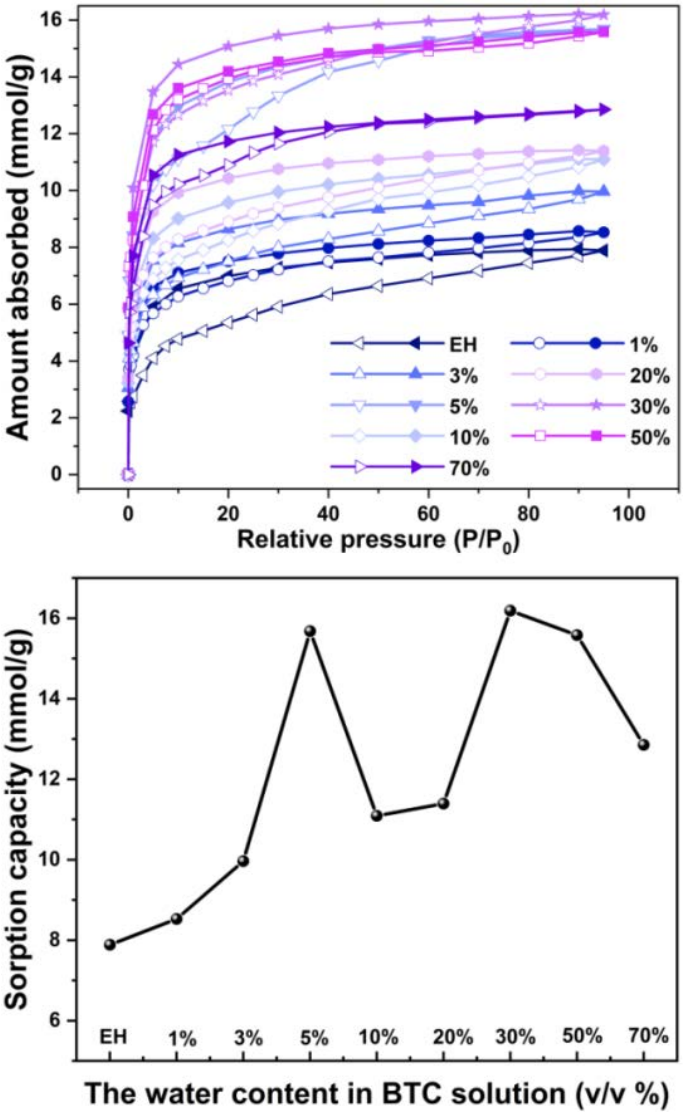

Figure 2.7. Methanol sorption isotherms (up) and the comparison of the sorption capacity (down) of Cu_3btc_2 SURMOFs prepared with water content range from EH to 70% in H_3btc solution. The saturated vapor pressure P_0 of methanol at 25 °C is 0.169 bar.

Methanol sorption experiments were also employed to probe and compare the porosity of Cu_3btc_2 SURMOFs with reference material. Herein, a

He gas flow containing a controlled partial pressure of methanol vapor was introduced into the BEL-QCM cell maintained at a constant temperature of 25 °C. The mass of methanol adsorbed and desorbed was recorded following stabilization of the substrate frequency. The methanol isotherm data for Cu_3btc_2 SURMOFs are presented in Figure 2.7.

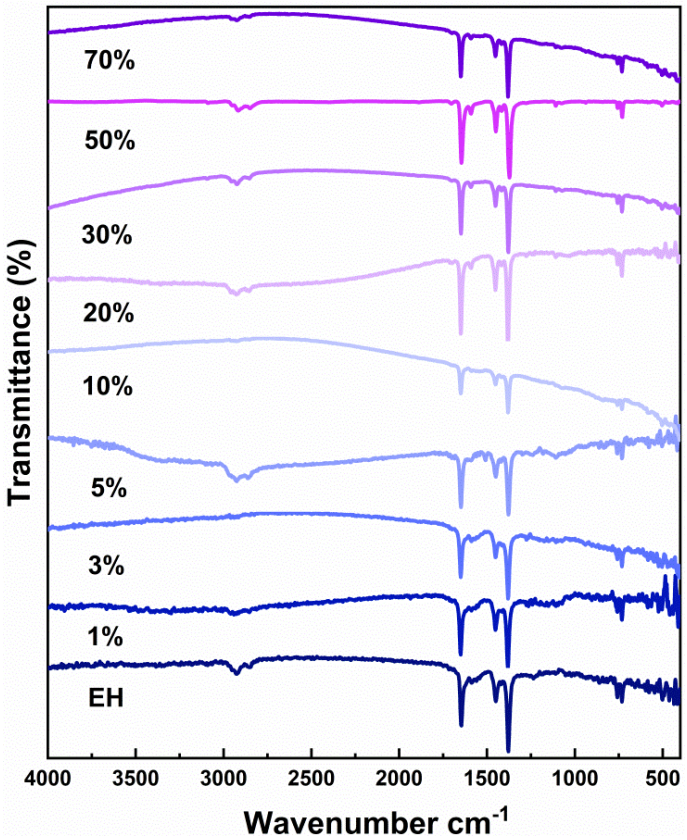

Figure 2.8. IRRAS spectra of Cu_3btc_2 SURMOFs fabricated with water content in H_3btc solution from EH to 70%. The labelling colors of spectra are corresponding to former.

Integrating water in H_3btc solution during the fabrication process enhanced the methanol adsorption capacity from 7.89 mmol g^{-1} (EH) to 15.68 mmol g^{-1} (5% water) at P/P_0 = 0.95. This is ascribed to the enhanced crystallinity and compactness of Cu_3btc_2 SURMOFs, and a decrease in the amount of amorphous, non-porous phases of Cu_3btc_2. However, further

increasing water content resulted in a small decrease of adsorption capacity, which is probably due to the reduction of compactness of Cu_3btc_2 SURMOFs. When raising the water content to 30%, the fabricated Cu_3btc_2 films show a similar sorption behavior as bulk one. By comprehensively analyzing the GIXRD, surface morphology (SEM) and methanol sorption isotherms (QCM), it is concluded that integrating a level of 5% water into H_3btc ethanol solution is the best parameter for fabricating Cu_3btc_2 SURMOFs with high crystallinity, orientation, homogeneous morphology and texture and enhanced methanol sorption capacity at the given experimental set-up for layer-by-layer LPE at 40°C using the Q-Sense instrument as described in the experimental part.

The recorded IRRAS spectra of Cu_3btc_2 SURMOFs show no differences (see Figure 2.8), and all of the peaks are typically from Cu_3btc_2. Specifically, the weak bands at 732 and 759 cm^{-1} are characteristic for phenyl groups as well as bands located at 1030 and 1108 cm^{-1}. The strong bands at 1379 and 1450 cm^{-1}, and 1589 and 1647 cm^{-1} are assigned to COO symmetric and asymmetric stretching respectively.[38, 57]

2.2.2 Growth and characterization of Cubdc SURMOFs

Cubdc SURMOF (also called SURMOF-2) is a 2D MOF thin film.[43] It is composed of Cu paddlewheel and terephthalate, which has a similar node structure as Cu_3btc_2. Hence, the strategy of integrating water in liker solution was applied to Cubdc SURMOF system. Similarly, Cubdc SURMOFs were fabricated by using stepwise LPE technique with different amount of water integrated in H_2bdc solution. The QCM frequency curves are presented in Figure 2.9. Unlike Cu_3btc_2 SURMOF, the integration of additional water decreased the quantity of Cubdc deposited on substrate.

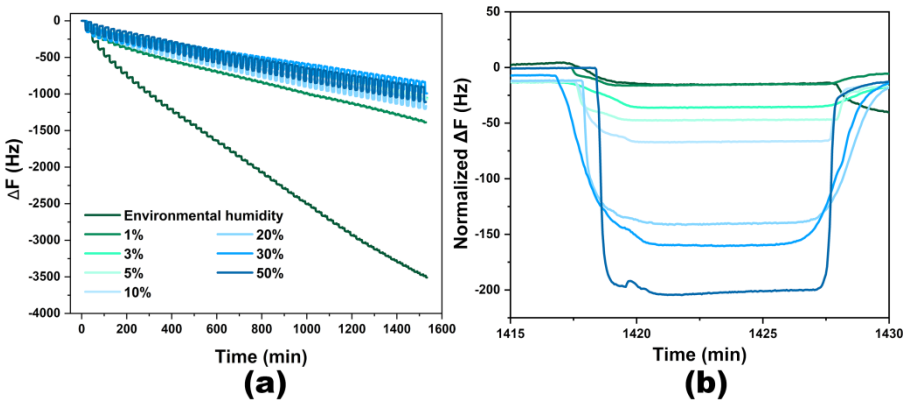

Figure 2.9. QCM frequency as a function of time recorded in situ during the stepwise LPE growth of (a) Cubdc SURMOFs and the comparison of the depth of gaps appeared during the rinsing stage after (b) H_2bdc.

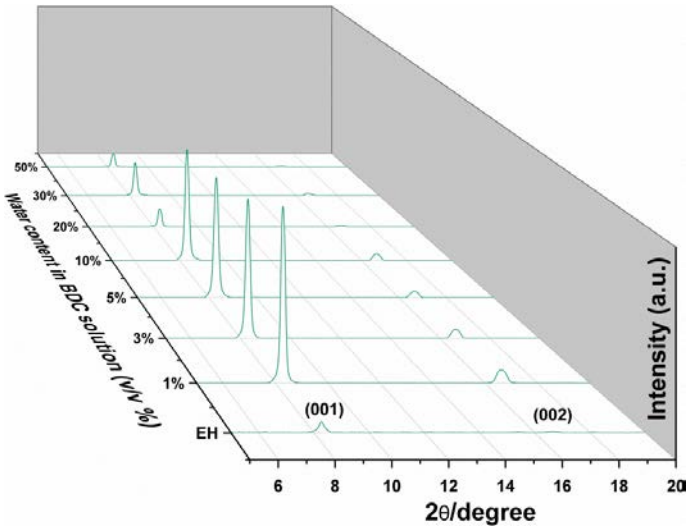

Figure 2.10. The comparison of out-of-plane 3D XRD patterns of Cubdc SURMOFs fabricated with different amount of water in linker solution (EH = environmental humidity).

GIXRD patterns were measured on the SURMOFs to probe the influence of water on the growth of Cubdc SURMOFs. As shown in Figure 2.10, the addition of water in H_2bdc solution enhances the crystallinity of Cubdc SURMOFs greatly even at an EH-comparable amount of 1%. The crystallinity begins to decrease to a low level with continuously increasing the water

content to 20%. In conclusion, 1–10% would be a reasonable range of water content to prepare highly crystallized Cubdc SURMOFs. Due to the 2D structure, the obtained oriented Cubdc SURMOFs only show the (001)/(002) direction in all cases.

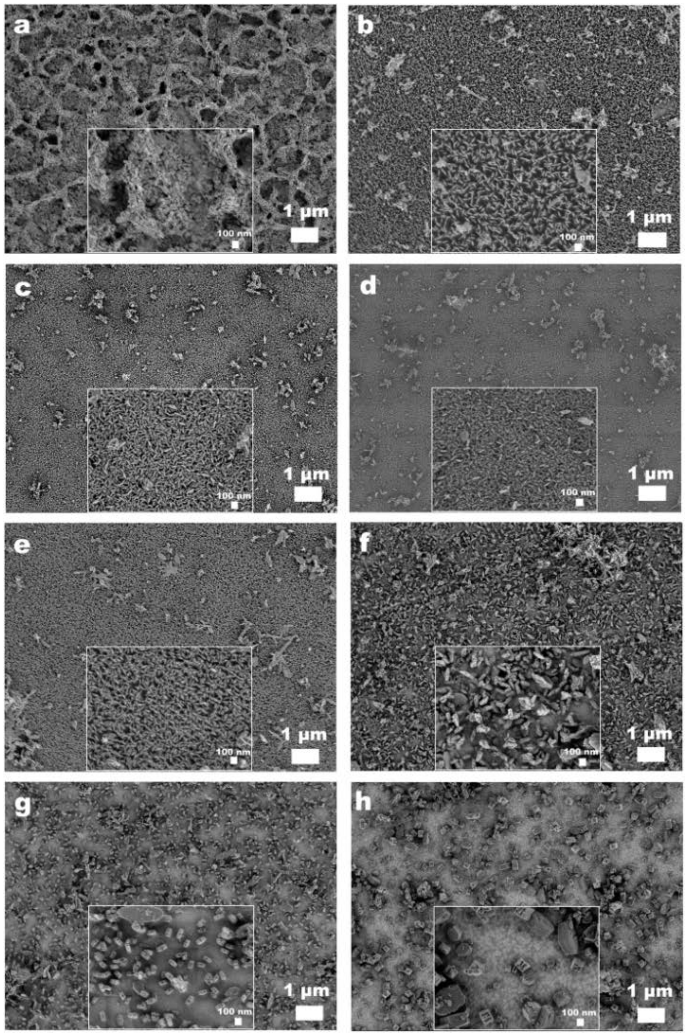

Figure 2.11. SEM images of Cubdc SURMOFs prepared by adding different amount of water in H_2bdc solution: (a) EH, (b) 1%, (c) 3%, (d) 5%, (e) 10%, (f) 20%, (g) 30%, (h) 50%.

The morphology of Cubdc SURMOFs was characterized by SEM measurements, which are shown in Figure 2.11. Viewing from Figure 2.11a, the SURMOF fabricated under EH is composed by lots of irregular particles

and shows a disordered and inhomogeneous morphology. With the addition of water (up to 10%) in H_2bdc solution, the particles are becoming more regular-shaped and larger (Figure 2.11b-e). These needle-like particles further stack to form flat, dense and homogenous film, among which the sample fabricated with 5% water shows the best quality. The quality of SURMOFs begins to go down when the water content exceed 10%. Considering the size growth of particles and their rugged surface, the synergistic effect of promoted crystal growth and surface etching from water can be seen as well in the growth process of Cubdc SURMOFs.

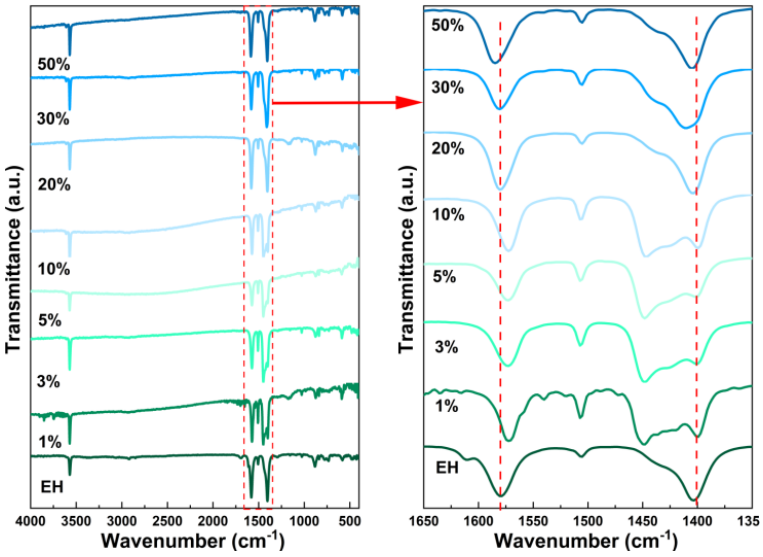

Figure 2.12. IRRAS spectra of Cubdc SURMOFs fabricated with different water content in H_2bdc solution.

The IRRAS spectra are presented in Figure 2.12, which are corresponding to the reported one in general.[58] Inspecting the fingerprint region of the carboxylate group (1350–1650 cm^{-1}, Figure 6 right), the two peaks located around 1580 and 1400 cm^{-1} are assigned to its asymmetric and symmetric stretching, respectively. An extra peak appeared at 1450 cm^{-1} in the spectra of the SURMOF samples fabricated with 1, 3, 5 and 10% water in H_2bdc solution, which is assigned to the symmetric stretching of COO as well.

Considering the reduced intensity of the symmetric stretching band, it is believed that the additional peak of 1450 cm^{-1} is spilt from the 1400 cm^{-1} peak with a blue shift of 50 cm^{-1}. Moreover, the asymmetric stretching peak of COO in the above-mentioned samples shows a red shift about 6 cm^{-1} to 1574 cm^{-1}. According to the literature, the carboxylate group in bidentate coordination mode shows a decrease in the asymmetrical vibration frequency and an increase in the symmetrical vibration frequency (smaller separation) as compared to those of carboxylate in unidentate coordination state.[59-60] From this assignments it is deduced that numerous unidentate-coordinated Cu-bdc species are present in Cubdc SURMOFs fabricated without additional water. However, integrating a proper amount of water (1–10%) in the H_2bdc solution can remove these unidentate-coordinated Cu-bdc species and promote the "paddlewheel" type coordination (bridging-bidentate coordination mode). Interestingly, the peak of the COO symmetric stretching goes back again when the water content is more than 10%. A water content above a critical threshold seems to destroy the Cu-paddlewheel and promotes the formation of unidentate-coordinated Cu-bdc species.[61] By comparing the relative intensity of two peaks of 1400 and 1450 cm^{-1}, the SURMOF prepared with 5% water contains the lowest defect density of unidentate carboxylates. In summary, integrating 5% water in H_2bdc solution is the best condition for fabricating Cubdc SURMOFs with high crystallinity, homogenous morphology and low defect density.

2.2.3 The growth of Cu_2bdc_2dabco SURMOFs

The strategy of integrating water in linker solution was also applied to Cu_2bdc_2dabco system, which is another closely related Cu paddlewheel-based SURMOF. Unfortunately, Cu_2bdc_2dabco SURMOFs with enhanced properties were not obtained; instead, addition of water caused the formation of the 2D Cubdc SURMOF, rather than the pillared 3D system Cu_2bdc_2dabco. The

characterizations of XRD, SEM and methanol sorption (Figure 2.13–15) on prepared SURMOFs confirm the presence of Cubdc rather than Cu_2bdc_2dabco. This observation is assigned to the initial reaction stage during the layer-by-layer growth. The apical sites of paddlewheel dinuclear Cu clusters obviously prefer water molecules Cu-OH_2, probably also involving hydrogen bonds to the solvent (ethanol) instead of the Cu-N bond with dabco, when additional water was integrated in linker solution.[61] Also, dabco is a relatively strong Brønsted base (pKa = 8.8). It is likely that water favors the protonation of dabco. Hence, a generalized strategy of integrating water in linker solution is not straight forward for the synthesis of pillar-layered type of MOF thin films. It may be possible to modify the growth protocol by separation of the bdc/dabco linker solution and moving from a two-step to a three-step protocol.

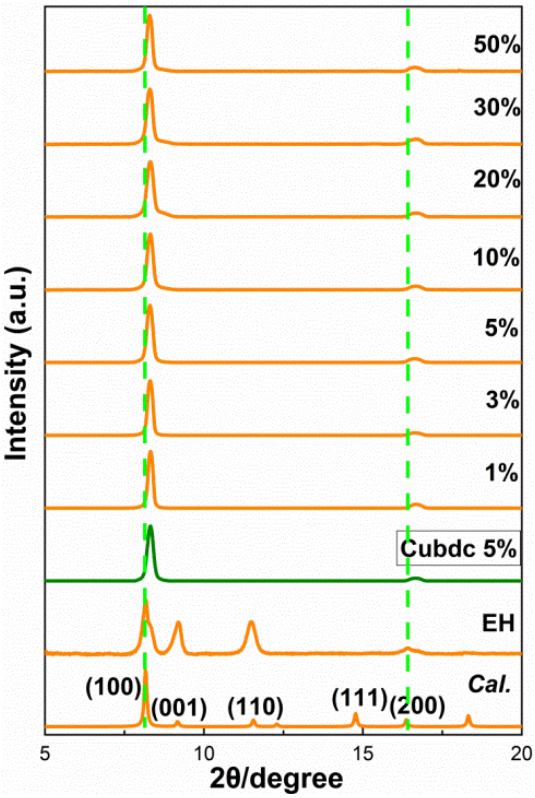

Figure 2.13. The comparison of out-of-plane 3D XRD patterns of Cu/bdc/dabco SURMOFs fabricated with different amount of water in linker solution. The orange are the XRD patterns of Cu/bdc/dabco SURMOFs, the

green is the XRD pattern of Cubdc SURMOF synthesized with 5% water in H_2bdc solution (the best quality). The sample prepared under EH is Cu_2bdc_2dabco, which can be confirmed from the characteristic XRD peaks corresponding to the (100), (001) and (110) peaks of calculated. However, the XRD peaks of those samples prepared with additional water in linker solution show a shift to high angle and corresponding to that of Cubdc.

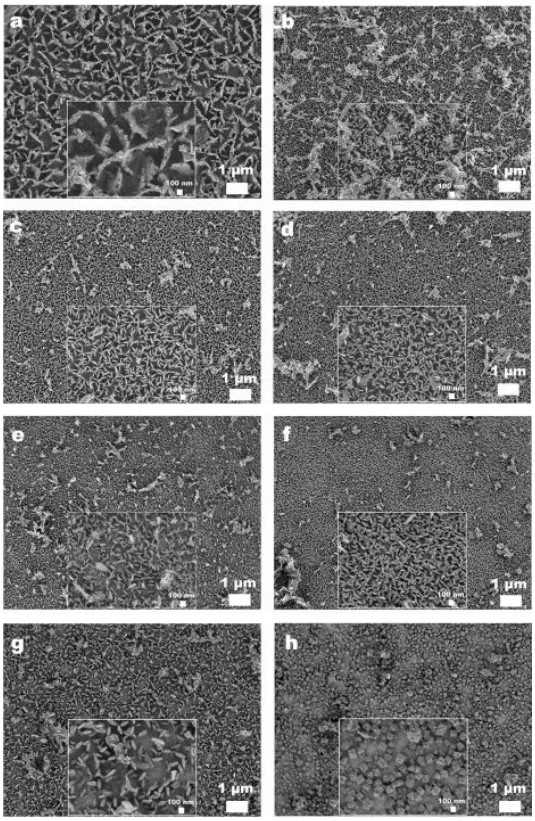

Figure 2.14. SEM images of Cu/bdc/dabco SURMOFs fabricated with different water content in linker solution: (a) EH, (b) 1%, (c) 3%, (d) 5%, (e) 10%, (f) 20%, (g) 30%, (h) 50%. As we can see from the images, the sample fabricated under EH shows different morphology from others. The morphologies of rest samples are more close to Cubdc in which needle-like MOF particles stack to form thin film and particle size were growing with increasing the water content in linker solution. SEM images provide another

evidence of the failure growth of Cu_2bdc_2dabco with water integrated in linker solution.

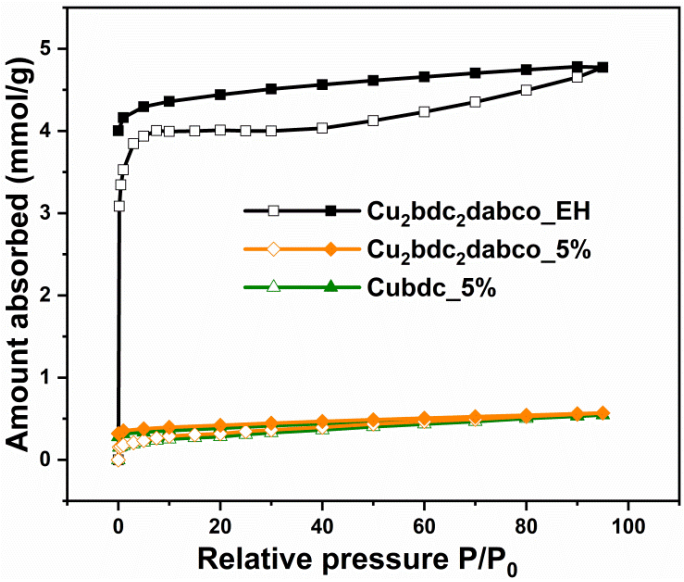

Figure 2.15. The methanol sorption isotherms of the Cu_2bdc_2dabco SURMOFs fabricated without additional water, Cu/bdc/dabco and Cubdc both with 5% water in linker solution. The methanol sorption capacity of Cu_2bdc_2dabco SURMOF is 4.77 mmol g-1, while the value of Cu/bdc/dabco and Cubdc SURMOFs are 0.57 and 0.55 mmol g-1 respectively. The huge difference of methanol sorption capacity from Cu_2bdc_2dabco SURMOF, together with close value to Cubdc SURMOF, demonstrates that the sample of Cu/bdc/dabco SURMOF fabricated with water in linker solution has the same structure as Cubdc rather than Cu_2bdc_2dabco.

2.2.4 Interpretation of the quality enhancement of Cu paddlewheel-based SURMOFs with water content

As analyzed above, the water molecule promotes the nucleation and crystal growth of SURMOFs. It is noteworthy that H_2bdc (pK_a1: 3.52, pK_a2: 4.46) and H_3btc (pK_a1: 3.12, pK_a2: 3.89, pKa3: 4.70) show a lower pK_a than acetic acid (4.76),[62] hence benzene carboxylic acid linkers tend to dissociate preferentially in the environment with rising amounts of water. The underlying

mechanism of promotion effect is that the presence of water significantly enhances the “proton transfer” from carboxyl groups of linker to acetate groups of $Cu(OAc)_2$ to form deprotonated linkers and AcOH.[50] Furthermore, the deprotonated linkers replace the acetates to coordinate with Cu paddlewheel to generate MOFs. While the product AcOH and other unreacted species are washed out with the continuous flow. On the contrary, with insufficient water accessible in the growth process an inefficient proton transfer reaction limits the nucleation and further growth of MOFs.

Along with the promotion effect on the coordination bond formation, the effect of etching also plays a significant role in control the crystallite size, orientation and surface coverage of SURMOFs. As described in the literature,[61] water molecules interact with COO groups to dissociate linkers from the framework, which leads to the etching of mis-oriented MOF particles from film. Moreover, water molecules affect the structure of Cu paddlewheels as well. As shown in Figure 2.16, the addition of massive water in the growth process could induce the Cu dimer paddlewheels converting to Cu monomers.[63] Obviously, the more water in linker solution, stronger the etching effect is. Actually, the promotion effect and etching effect are working at the same time in the SURMOF growth process from two opposite directions. Rational control of water content in linker solution is crucial to obtain SURMOFs with high quality.

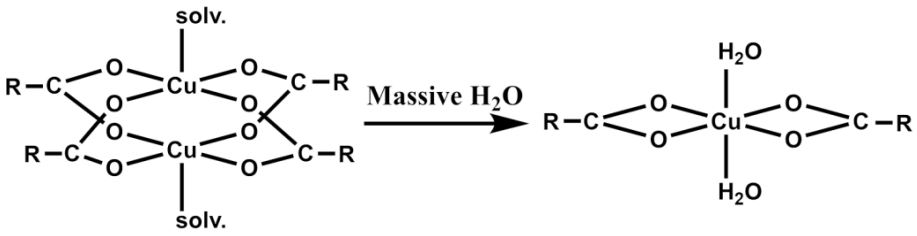

Figure 2.16. The conversion from Cu dimer paddlewheel to Cu monomer with massive water in the SURMOF fabrication process.

2.3 Conclusions

In conclusion, the integration of water in linker solution can provide a significant enhancement in the quality of SURMOFs fabricated by stepwise LPE technique. From our studies, it is concluded that integrating 5% (of volume) water in linker solution is best condition to fabricate SURMOFs with high crystallinity, preferred orientation, homogenous texture and enhanced sorption capacity in both cases, Cu_3btc_2 and Cubdc SURMOFs. Moreover, additional water also showed the ability of controlling the defects in Cubdc SURMOF. However, the integration of additional water in growth process is not easily transferable to any kind of Cu paddle wheel based SURMOF. For example, the deposition of Cu_2bdc_2dabco SURMOFs is disfavored by water addition. Nevertheless, the parameter space of the stepwise layer-by-layer LPE is large and further modification of growth protocols may allow optimized SURMOF growth also for more complex multi component MOFs. In addition to the optimization of the water content, we propose that the pH regime of the SURMOF growth (buffer solutions) may also influence the deposition process as the coordination bond equilibria are pH dependent.

2.4 References

[1] T. Ikeda, O. Tsutsumi, *Science* **1995**, *268*, 1873.

[2] X. Jia, C. Fuentes-Hernandez, C.-Y. Wang, Y. Park, B. Kippelen, *Sci. Adv.* **2018**, *4*, 1705.

[3] M. D. Allendorf, A. Schwartzberg, V. Stavila, A. A. Talin, *Chem. Eur. J.* **2011**, *17*, 11372.

[4] Z.-G. Gu, A. Pfriem, S. Hamsch, H. Breitwieser, J. Wohlgemuth, L. Heinke, H. Gliemann, C. Wöll, *Micropor. Mesopor. Mater.* **2015**, *211*, 82.

[5] L. E. Kreno, J. T. Hupp, R. P. Van Duyne, *Anal. Chem.* **2010**, *82*, 8042.

[6] G. Dai, *Sensor Actuat. B-Chem.* **1998**, *53*, 8.

[7] L. E. Kreno, K. Leong, O. K. Farha, M. Allendorf, R. P. Van Duyne, J. T. Hupp, *Chem. Rev.* **2012**, *112*, 1105.

[8] H. Zhou, Q. Chen, G. Li, S. Luo, T.-b. Song, H.-S. Duan, Z. Hong, J. You, Y. Liu, Y. Yang, *Science* **2014**, *345*, 542.

[9] J. Liu, W. Zhou, J. Liu, I. Howard, G. Kilibarda, S. Schlabach, D. Coupry, M. Addicoat, S. Yoneda, Y. Tsutsui, T. Sakurai, S. Seki, Z. Wang, P. Lindemann, E. Redel, T. Heine, C. Wöll, *Angew. Chem. Int. Ed.* **2015**, *54*, 7441.

[10] E. Ugur, A. D. Sheikh, R. Munir, J. I. Khan, D. Barrit, A. Amassian, F. Laquai, *ACS Energy Lett.* **2017**, *2*, 1960.

[11] W. Zhang, S. Pathak, N. Sakai, T. Stergiopoulos, P. K. Nayak, N. K. Noel, A. A. Haghighirad, V. M. Burlakov, D. W. deQuilettes, A. Sadhanala, W. Li, L. Wang, D. S. Ginger, R. H. Friend, H. J. Snaith, *Nat. Commun.* **2015**, *6*, 10030.

[12] S. Muthukumar, C. R. Gorla, N. W. Emanetoglu, S. Liang, L. Y., *J. Cryst. Growth* **2001**, *225*, 197.

[13] Y. Chen, Z. Fan, Z. Zhang, W. Niu, C. Li, N. Yang, B. Chen, H. Zhang, *Chem. Rev.* **2018**, *118*, 6409.

[14] J. Liu, C. Wöll, *Chem. Soc. Rev.* **2017**, *46*, 5730.

[15] N. Stock, S. Biswas, *Chem. Rev.* **2012**, *112*, 933.

[16] A. Betard, R. A. Fischer, *Chem. Rev.* **2012**, *112*, 1055.

[17] P. Horcajada, R. Gref, T. Baati, P. K. Allan, G. Maurin, P. Couvreur, G. Ferey, R. E. Morris, C. Serre, *Chem. Rev.* **2012**, *112*, 1232.

[18] M. Yoon, R. Srirambalaji, K. Kim, *Chem. Rev.* **2012**, *112*, 1196.

[19] K. Sumida, D. L. Rogow, J. A. Mason, T. M. McDonald, E. D. Bloch, Z. R. Herm, T. H. Bae, J. R. Long, *Chem. Rev.* **2012**, *112*, 724.

[20] H. Wu, Q. Gong, D. H. Olson, J. Li, *Chem. Rev.* **2012**, *112*, 836.

[21] M. P. Suh, H. J. Park, T. K. Prasad, D. W. Lim, *Chem. Rev.* **2012**, *112*, 782.

[22] C. Wang, T. Zhang, W. Lin, *Chem. Rev.* **2012**, *112*, 1084.

[23] J. R. Li, J. Sculley, H. C. Zhou, *Chem. Rev.* **2012**, *112*, 869.

[24] H. Furukawa, K. E. Cordova, M. O'Keeffe, O. M. Yaghi, *Science* **2013**, *341*, 1230444.

[25] H. L. Li, M. Eddaoudi, M. O'Keeffe, O. M. Yaghi, *Science* **1999**, *402*, 276.

[26] H. C. Zhou, S. Kitagawa, *Chem. Soc. Rev.* **2014**, *43*, 5415.

[27] G. Givaja, P. Amo-Ochoa, C. J. Gomez-Garcia, F. Zamora, *Chem. Soc. Rev.* **2012**, *41*, 115.

[28] P. Falcaro, R. Ricco, C. M. Doherty, K. Liang, A. J. Hill, M. J. Styles, *Chem. Soc. Rev.* **2014**, *43*, 5513.

[29] G. Lu, J. T. Hupp, *J. Am. Chem. Soc.* **2010**, *132*, 7832.

[30] M. Kubo, W. Chaikittisilp, T. Okubo, *Chem. Mater.* **2008**, *20*, 2887.

[31] Y. S. Li, F. Y. Liang, H. Bux, A. Feldhoff, W. S. Yang, J. Caro, *Angew. Chem. Int. Ed.* **2010**, *49*, 548.

[32] L. Dumée, L. He, M. Hill, B. Zhu, M. Duke, J. Schütz, F. She, H. Wang, S. Gray, P. Hodgson, L. Kong, *J. Mater. Chem. A* **2013**, *1*, 9208.

[33] C. M. Doherty, G. Grenci, R. Ricco, J. I. Mardel, J. Reboul, S. Furukawa, S. Kitagawa, A. J. Hill, P. Falcaro, *Adv. Mater.* **2013**, *25*, 4701.

[34] O. Shekhah, H. Wang, S. Kowarik, F. Schreiber, M. Paulus, M. Tolan, C. Sternemann, F. Evers, D. Zacher, F. A. Fischer, C. Wöll, *J. Am. Chem. Soc.* **2007**, *129*, 15118.

[35] H. K. Arslan, O. Shekhah, J. Wohlgemuth, M. Franzreb, R. A. Fischer, C. Wöll, *Adv. Funct. Mater.* **2011**, *21*, 4228.

[36] D. Witters, S. Vermeir, R. Puers, B. F. Sels, D. E. De Vos, J. Lammertyn, R. Ameloot, *Chem. Mater.* **2013**, *25*, 1021.

[37] M. Tu, S. Wannapaiboon, R. A. Fischer, *Inorg. Chem. Front.* **2014**, *1*, 442.

[38] O. Shekhah, H. Wang, D. Zacher, R. A. Fischer, C. Wöll, *Angew. Chem. Int. Ed.* **2009**, *48*, 5038; *Angew. Chem.* **2009**, *121*, 5138.

[39] V. Stavila, J. Volponi, A. M. Katzenmeyer, M. C. Dixon, M. D. Allendorf, *Chem. Sci.* **2012**, *3*, 1531.

[40] B. Liu, M. Tu, R. A. Fischer, *Angew. Chem. Int. Ed.* **2013**, *52*, 3402.

[41] X. J. Yu, J. L. Zhuang, J. Scherr, T. Abu-Husein, A. Terfort, *Angew. Chem. Int. Ed.* **2016**, *55*, 8348.

[42] S. Wannapaiboon, M. Tu, R. A. Fischer, *Adv. Funct. Mater.* **2014**, *24*, 2696.

[43] J. Liu, B. Lukose, O. Shekhah, H. K. Arslan, P. Weidler, H. Gliemann, S. Brase, S. Grosjean, A. Godt, X. Feng, K. Mullen, I. B. Magdau, T. Heine, C. Wöll, *Sci. Rep.* **2012**, *2*, 921.

[44] S. Wannapaiboon, K. Sumida, K. Dilchert, M. Tu, S. Kitagawa, S. Furukawa, R. A. Fischer, *J. Mater. Chem. A* **2017**, *5*, 13665.

[45] D. Feng, Z. Y. Gu, J. R. Li, H. L. Jiang, Z. Wei, H. C. Zhou, *Angew. Chem. Int. Ed.* **2012**, *51*, 10307.

[46] N. A. Khan, J. W. Jun, S. H. Jhung, *Eur. J. Inorg. Chem.* **2010**, *2010*, 1043.

[47] D. J. Tranchemontagne, J. R. Hunt, O. M. Yaghi, *Tetrahedron* **2008**, *64*, 8553.

[48] H. Guo, Y. Zhu, S. Qiu, J. A. Lercher, H. Zhang, *Adv. Mater.* **2010**, *22*, 4190.

[49] N. C. Burtch, H. Jasuja, K. S. Walton, *Chem. Rev.* **2014**, *114*, 10575.

[50] R. S. Blake, P. S. Monks, A. M. Ellis, *Chem. Rev.* **2009**, *109*, 861.

[51] H. Grasdalen, I. Svare, *Acta Chem. Scand.* **1971**, *25*, 1089.

[52] B. Zhang, J. Zhang, C. Liu, X. Sang, L. Peng, X. Ma, T. Wu, B. Han, G. Yang, *RSC Adv.* **2015**, *5*, 37691.

[53] M. Todaro, G. Buscarino, L. Sciortino, A. Alessi, F. Messina, M. Taddei, M. Ranocchiari, M. Cannas, F. M. Gelardi, *J. Phys. Chem. C* **2016**, *120*, 12879.

[54] J. R. Álvarez, E. Sánchez-González, E. Pérez, E. Schneider-Revueltas, A. Martínez, A. Tejeda-Cruz, A. Islas-Jácome, E. González-Zamora, I. A. Ibarra, *Dalton Trans.* **2017**, *46*, 9192.

[55] M. Suga, S. Asahina, Y. Sakuda, H. Kazumori, H. Nishiyama, T. Nokuo, V. Alfredsson, T. Kjellman, S. M. Stevens, H. S. Cho, M. Cho, L. Han, S. Che, M. W. Anderson, F. Schüth, H. Deng, O. M. Yaghi, Z. Liu, H. Y. Jeong, A. Stein, K. Sakamoto, R. Ryoo, O. Terasaki, *Prog. Solid State Chem.* **2014**, *42*, 1.

[56] A. Summerfield, I. Cebula, M. Schroder, P. H. Beton, *J. Phys. Chem. C* **2015**, *119*, 23544.

[57] O. Zybaylo, O. Shekhah, H. Wang, M. Tafipolsky, R. Schmid, D. Johannsmann, C. Wöll, *Phys. Chem. Chem. Phys.* **2010**, *12*, 8092.

[58] E. Redel, Z. Wang, S. Walheim, J. Liu, H. Gliemann, C. Wöll, *Appl. Phys. Lett.* **2013**, *103*, 091903.

[59] G. B. Deacon, R. J. Phillips, *Coord. Chem. Rev.* **1980**, *33*, 227.

[60] Y. Lu, J. D. Miller, *J. Colloid. Interf. Sci.* **2002**, *256*, 41.

[61] K. Tan, N. Nijem, P. Canepa, Q. Gong, J. Li, T. Thonhauser, Y. J. Chabal, *Chem. Mater.* **2012**, *24*, 3153.

[62] E. A. Braude, F. C. Nachod, *Determination of organic structures by physical methods*, Academic Press, New York **1955**.

[63] P. Sharrock, M. Melník, *Can. J. Chem.* **1985**, *63*, 52.

Chapter 3

Directing the hetero-growth of lattice-mismatched SURMOFs by functionalizing the interface*

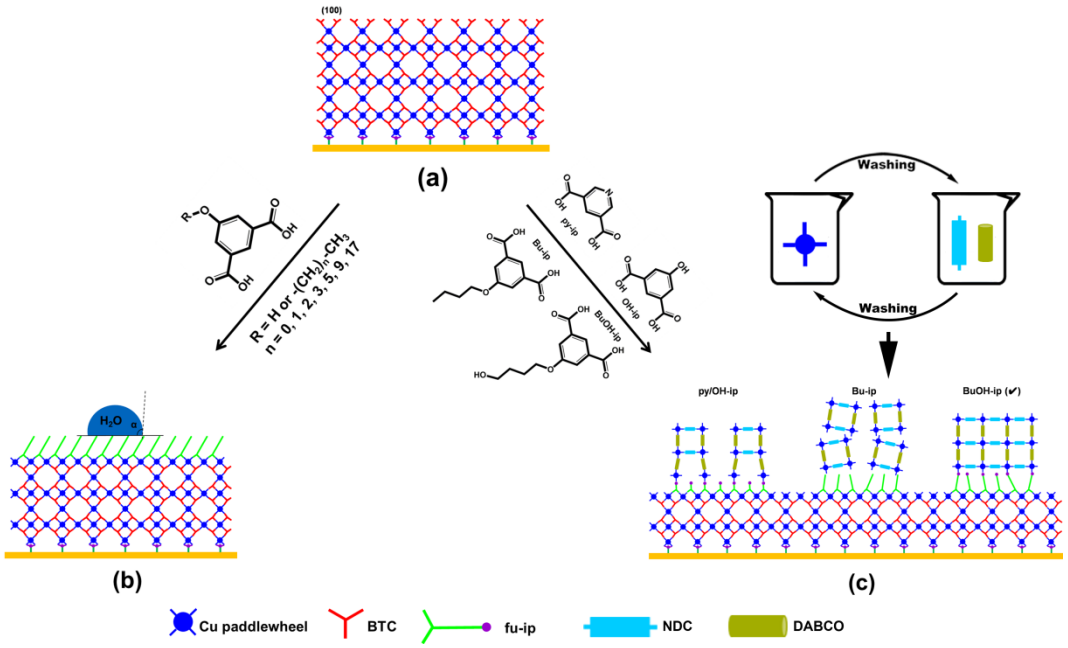

* The results of this chapter are published and reproduced from: "Z. Wang, S. Wannapaiboon, K. Rodewald, M. Tu, B. Rieger and R. A. Fischer, *J. Mater. Chem. A* **2018**, 6, 21295–21303" with the Copyright 2018 The Royal Society of Chemistry.

Abstract

Heterostructured metal-organic framework materials (MOF-on-MOF or core-shell MOFs) feature synergistic properties of the hetero-architecture. Selective modification of the interface between the different MOF crystallites by mimicking a self-assembled organic monolayer (SAM) of suitably functionalized isophatale (fu-ip) ligands allows for the oriented growth of the lattice-mismatched $Cu_2ndc_2dabco@Cu_3btc_2$ (**A**@**B**) using a stepwise liquid-phase epitaxial (LPE) deposition approach. Prior to growth of the hetero-structured surface mounted MOF (hetero-SURMOF), the binding configuration of a range of fu-ip ligands deposited at the external surface of SURMOF **B** was explored. Among many possibilities, only the configuration of fu-ip ligands in the “head-on” fashion binding on the external surface of SURMOF **B** proper exposition of the nucleation directing terminal functional groups is valid to act as template for the oriented hetero-growth of SURMOF **A** on top of SURMOF **B**. The quartz crystal microbalance (QCM) frequency change profiles, the infrared reflection absorption spectra (IRRAS) and the water contact angle (WCA) measurements confirm the presence of the valid configuration of fu-ip on the external surface of SURMOF **B**. The fu-ip ligands containing the functional sidechain at the fifth position with long flexible aliphatic spacers and coordination active functional terminal groups reveals the most efficient for growing of porous, high-crystalline, lattice-mismatched hetero-SURMOFs. The concept is expected to be a good reference for the fabrication of other types of hetero-SURMOFs.

3.1 Introduction

The surfaces of material with abundant dangling chemical bonds and defects play dominant roles in many physical and chemical processes, especially at the nanoscale regime.[1-4] Surface modification, which creates such a desired functionality at the external surfaces of materials by binding of surface ligands, is an essential technique for enhancing the characteristic features of materials as well as improving the synthetic and processing procedures for various applications. Understanding the interaction of the ligands with the surface of materials can benefit for fine tuning and rational design of material properties.[1, 4] Many studies have discussed various strategies to tame and make use of surface ligands,[5-10] including thiols binding to noble metal and quantum dot nanoparticles for controlling sizes and shapes,[5, 11-12] silane coupling agents for modifying the surface of silica,[13] amines functionalizing the surface of metal-organic framework (MOF) catalysts for improving the capacity of CO_2 capture,[14-15] *etc*.

MOFs are a novel family of porous crystalline materials constructed by coordination bonds between metallic nodes and organic linkers. The high porosity of MOFs, in combination with other unique properties such as flexibility and high variability of structural compositions,[16-18] makes MOFs to be promising candidates for many applications such as storage,[19] separation[20] and catalysis[21]. In addition, theoretical simulation of MOFs recently plays an important role in the interpretation of the structure–property relationship and prediction of novel structures and properties.[22-24] In particular, MOF downscaling and thin film deposition has developed for membrane-based separation and filtration,[25-26] chemical sensing,[27] optical and electronic devices.[28-29] Surface mounted MOFs (so-called SURMOFs), fabricated by using a stepwise liquid phase epitaxial (LPE) approach,[30-33] feature high

crystallinity, well-defined crystallite orientation and size, homogeneity and well-controlled film thickness and roughness. One advanced concept of functionalizing bulk MOF powders and SURMOFs is homoepitaxial and/or heteroepitaxial growth of one type of MOF on the external surface of a particular type of MOF (MOF-on-MOF or core-shell MOFs).[34-38] Heterostructured MOFs have attracted rapid-growing research interests because of the integrated properties from each MOF component as well as the emerged properties from the synergistic heterostructured unit.[39-44] However, the synthesis of heterostructured SURMOFs still remains a challenge, especially for the lattice-mismatched heterostructures consisting of three dimensional (3D) MOFs with different unit cell parameters and even different different structural types.[45-46] Herein, the hetero-SURMOFs can be also regarded as “core-shell” because the bottom SURMOF is enveloped by top SURMOF from all directions. Only one example of 3D hetero-SURMOF of an outer@inner type of Cu_3btc_2@Cu_2ndc_2dabco has been reported so far (**B**@**A**; **A** and **B** are the inner and outer MOF component, respectively; btc: benzene-1,3,5-tricarboxylate, ndc: 1,4-naphtalene dicarboxylate, dabco: 1,4-diazabicyclo(2.2.2)octane).[46] Surprisingly, the growth of hetero-SURMOF **A**@**B** with inverse ordering of **A** and **B** cannot be achieved in this previous study. This observation is attributed to the inefficient template effect of the tilted carboxylate terminated groups of the btc linkers at the external surface of **B**, which inhibits the further heteroepitaxial growth of **A**. However, the inefficient template effect of tilted-oriented carboxylate groups at the external surface of SURMOF **B** can be settled through modification with surface ligands consisting of flexible functional groups at the other end of the ligands.

Hereby, we illustrate the success of this strategic procedure to solve the failure growth of hetero-SURMOF **A**@**B** by functionalizing the interface using various functionalized isophthalate ligands owing controllable functional

groups at the fifth position of the ligands (fu-ip). Specifically, the incorporated fu-ip ligands perform as a template in a similar fashion as self-assembly monolayer (SAM).[47] The binding of fu-ip on the external surface of SURMOF **B** by their carboxylate head groups may leave the additional functional terminal groups to be anchoring sites for the nucleation and further growth of SURMOF **A**. It is noteworthy that several configurations may appear when binding the fu-ip ligands onto surface of SURMOF **B**. Nevertheless, only the configuration which binds the fu-ip ligands on the external surface of SURMOF **B** with the "head-on" fashion is valid for fabricating such a hetero-SURMOF **A**@**B**. Hence, it is necessary to study the effects of fu-ip implementation on the external surface of SURMOF **B** in details prior to employing for the fabrication of hetero-SURMOFs.

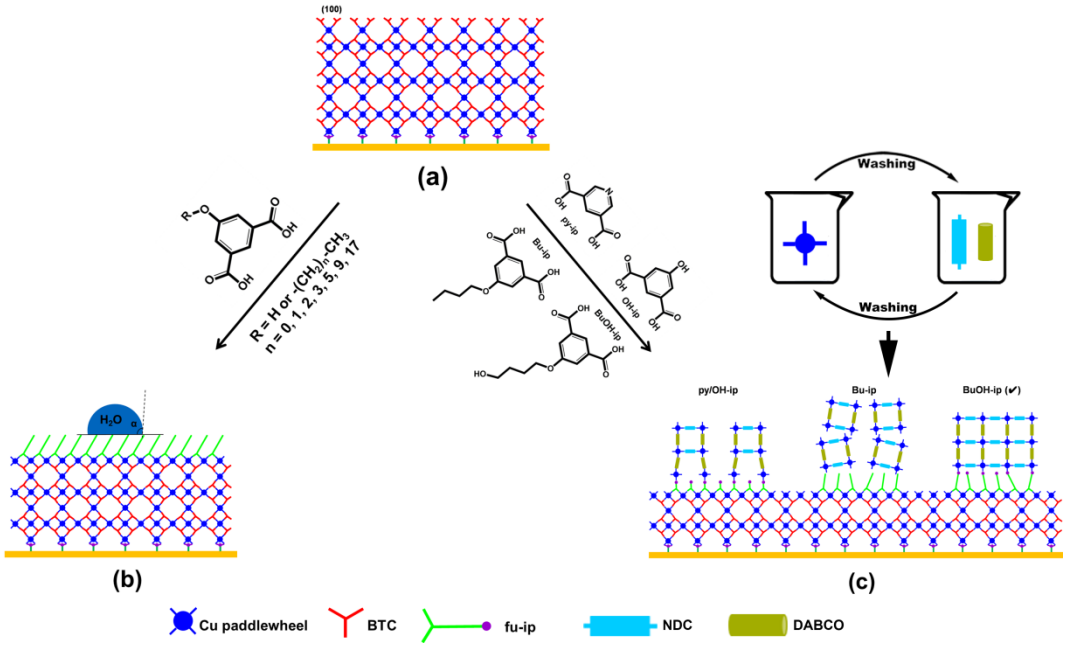

Figure 3.1 Schematic illustration of (a) SURMOF Cu_3btc_2 (**B**) along (100) direction mounted on the carboxylate-functionalized Au-coated surface of a quartz crystal microbalance (QCM) substrate; (b) an implementation of fu-ip ligands (consisting of hydrophobic functional groups at the fifth position) on the external surface of SURMOF **B**; (c) hetero-growth of SURMOF **A**

(Cu_2ndc_2dabco) on the top of SURMOF **B** after functionalizing the interface with different kinds of fu-ip ligands. (Blue: Cu paddlewheel, red: btc linker, green and violet: fu-ip ligand)

In this present work, a first series of fu-ip (fu = hydroxy (OH), methoxy (Me), ethoxy (Et), propoxy (Pr), butoxy (Bu), hexyloxy (He), decyloxy (De) and octadecyloxy (Od)) ligands are employed to study their binding on the external surface of SURMOF **B** (Figure 3.1b). Afterwards, we explore the template effects of a second series of fu-ip ligands with different functional groups at the fifth position (fu = pyridine (py), OH, Bu and 4-hydroxybutoxy (BuOH)) on the fabrication of inverted-ordering hetero-SURMOF **A@B** by inserting them at the interface between the two SURMOF phases (Figure 3.1c)**.** The success of our strategy suggests this methodology of interface functionalization probably can be generalized as a universal method for fabricating lattice-mismatched hetero-SURMOFs or even hetero-bulk MOFs.

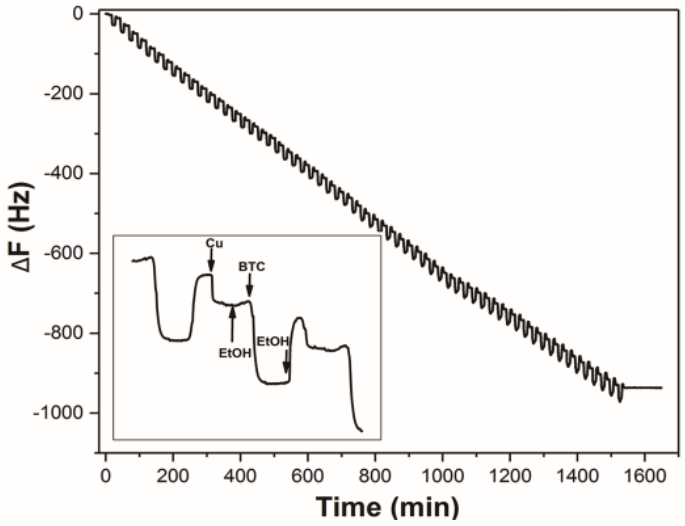

Figure 3.2. QCM frequency as a function of time recorded in situ during the stepwise liquid phase epitaxial growth of SURMOF **B** (60 cycles) on the carboxylate-terminated Au covered QCM substrate. Inset: QCM profile of deposition step.

3.2 Results and Discussion

3.2.1 Implementation of fu-ip ligands on the external surface of SURMOF Cu_3btc_2 (B)

Film fabrication and characterization. Firstly, SURMOF **B** was fabricated on the carboxylate-SAM functionalized QCM substrates by using the stepwise LPE approach for a total 60 cycles. The phase purity, crystallite orientation, and adsorption capacity of the pre-formed SURMOF **B** samples were characterized in order to verify and standardize the quality of the samples. Since the SURMOF **B** samples were taken out of the fabrication cell for characterization, the LPE fabrication of SURMOF **B** for another 5 cycles were performed prior to the surface functionalization in order to remove the surface defects created during the characterization.[48] After that, fu-ip ligands (fu = OH, Me, Et, Pr, Bu, He, De and Od) were subsequently implemented on the external surface of SURMOF **B** by alternate dosing of $Cu(OAc)_2$ and fu-ipH_2 for a total 5 cycles (similar to the LPE process of SURMOF **B**).

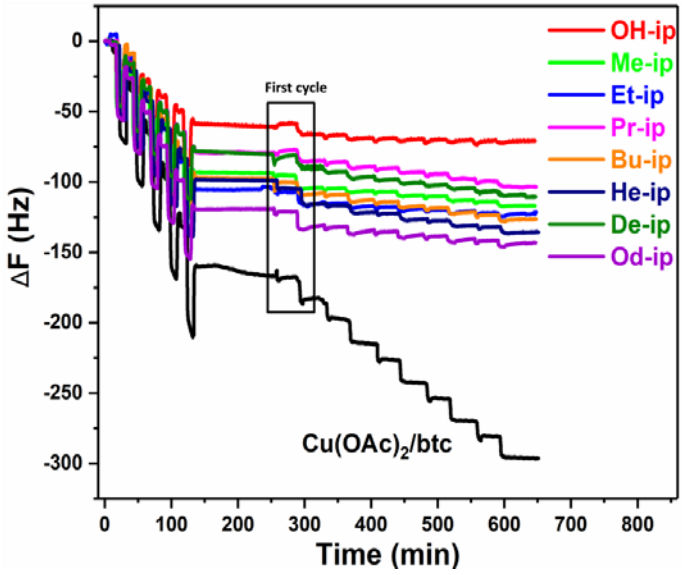

Figure 3.3. The QCM frequency profiles during the implementation process of fu-ip ligands on the external surface of SURMOF **B** (color curves) in

comparison with the second dosing of $Cu(OAc)_2$/btc for a further growth of SURMOF **B** (black curve). The first dosing cycle of $Cu(OAc)_2$/fu-ip is shown in the box.

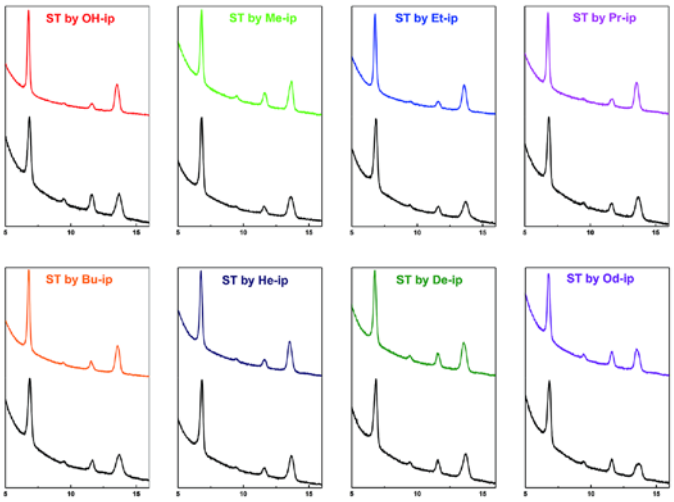

Figure 3.4. The comparison of out-of-plane XRD patterns of SURMOF **B** before (black curve) and after (color curve) the implementation of fu-ip ligands on its external surface. The term ST abbreviates surface termination.

During the whole LPE fabrication process, the change of QCM frequency was *in situ* monitored (as shown in Figure 3.2 and 3.3). Comparing the QCM frequency profiles during the implementation process (Fig. 3.3), the total frequency change of dosing 5-cycles $Cu(OAc)_2$/fu-ipH_2 (color curves) is much less than that of dosing 5-cycles $Cu(OAc)_2$/H_3btc (black curve). This observation indicates the efficient termination of the SURMOF **B** external surface by the fu-ip ligands showing a small QCM frequency change at the first dosing step of $Cu(OAc)_2$/fu-ipH_2. Interestingly, the further dosing steps of $Cu(OAc)_2$/fu-ipH_2 steps do not show a significant change of QCM frequency, indicating that the $Cu(OAc)_2$/fu-ipH_2 dosing selectively leads to the surface termination of SURMOF **B** without further growth of another hetero-SURMOF containing fu-ip ligands at the outer part. In comparison, the further growth of

SURMOF **B** on the pre-formed sample is possible by continuely dosing $Cu(OAc)_2/H_3btc$ (black curve).

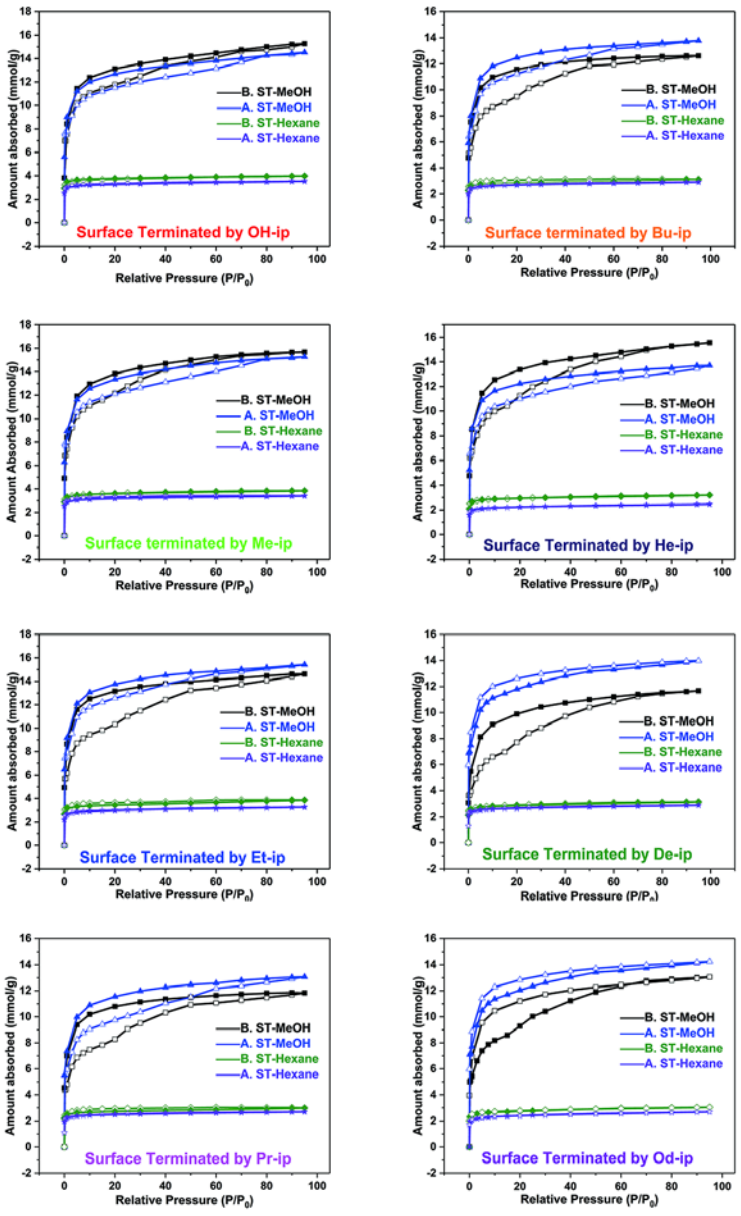

Figure 3.5. The comparison of methanol and *n*-hexane sorption isotherms of SURMOF **B** before and after the implementation of fu-ip ligands on its external surface. Adsorption and desorption are labelled with the hollow symbols and solid symbols, respectively. Herein, B. ST represents “before surface termination” and A. ST means “after surface termination”.

The distinct GIXRD pattern of SURMOF B suggests good crystallinity and the expected preferred orientation along the (100) crystallographic direction. Moreover, the crystallinity of SURMOF **B** remains after the implementation of fu-ip ligands on its external surface (Figure 3.4). To probe the adsorption capacity of the fu-ip surface modified SURMOF **B**, methanol and *n*-hexane sorptions were measured on the environmental-controlled BEL-QCM instrument at a constant temperature of 25 °C. As shown in Figure 3.5, the sorption isotherms show that the surface termination with a single layer consisting of the fu-ip ligands does not significantly change the porous capacity as well as the pore opening of the SURMOF **B**. Moreover, top-view SEM images (Figure 3.6) of the pristine SURMOF **B** and the films terminated by fu-ip ligands (herein, Me-ip, He-ip and Od-ip were selected as the examples) show flat, oriented and dense films with a similar morphology.

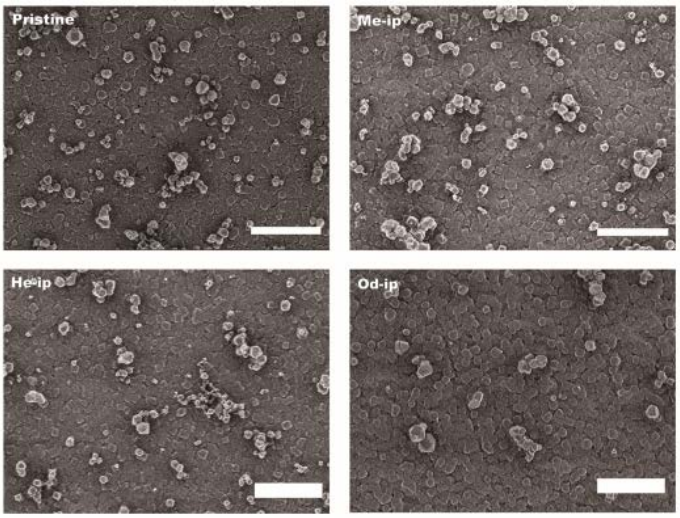

Figure 3.6. Scanning electron microscopic (SEM) images of the pristine SURMOF **B** and the SURMOF **B** samples after the implementation of fu-ip ligands on their external surface. Here, the samples with the Me-ip, He-ip and Od-ip surface termination were selected for comparison with the pristine SURMOF **B**. Note that the scale bar in the SEM images represents a size of 1 μm.

Configuration of the fu-ip ligands at the external surface of SURMOF Cu_3btc_2 (B). In order to further prove the presence of fu-ip ligands at the external surface of SURMOF **B**, IRRAS spectra (Figure 3.7) were measured. According to the IR spectra (Figure 3.7 left), the bands at 732 and 759 cm^{-1}, 1379 and 1450 cm^{-1}, and 1650 cm^{-1} are assigned to symmetric and asymmetric stretching of the phenyl group and the COO group respectively, which are all typical for SURMOF **B**.[49-50] By closer inspection of the spectra in the range of 1470-1560 cm^{-1} (Figure 3.7 right), some weak bands are detected only in the films terminated by fu-ip ligands at the external surface. Comparing with the spectra of pristine SURMOF **B**, the fu-ip terminated films show an increased intensity of the bands at 1540 and 1558 cm^{-1} assigned to the C=C bending of the aromatic ring of btc and fu-ip.[51-52] Moreover, the additional bands appeared at 1472, 1490, 1497, 1507 and 1520 cm^{-1} are assigned to the C-H deformation (bending and scissoring) vibrations of the aliphatic sidechain groups at the fifth position of the fu-ip ligands'.[53-56] Apparently, these bands prove the presence of fu-ip ligands on the surface of SURMOF **B**.

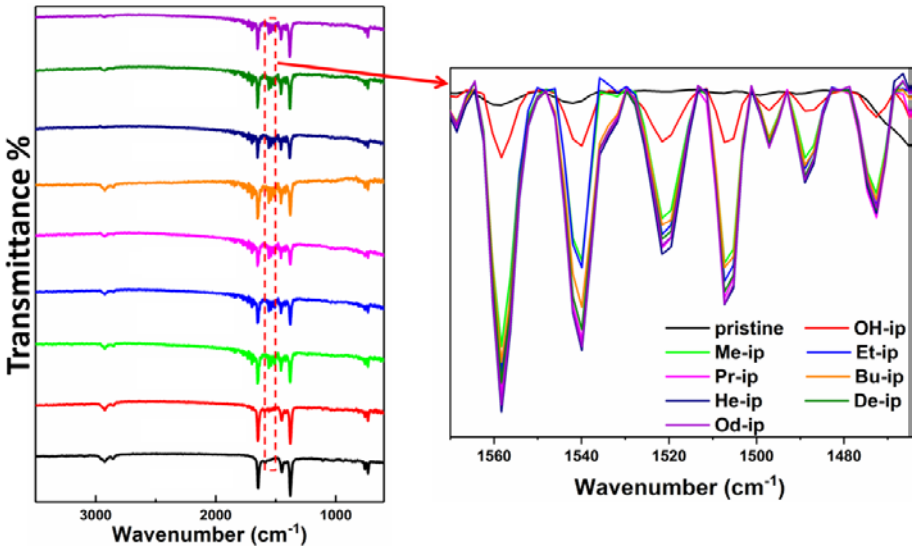

Figure 3.7. The IR spectra of SURMOF **B** before and after the implementation of fu-ip ligands on its external surface (left), and closer inspection of the IR

spectra within the red box area (right). Note that, the spectra are labelled by different colors with respect to the variation of fu-ip ligands in the similar fashion as the ones in Figure 3.3. The OH-ip terminated sample also shows small C-H deformation vibrations bands, which are probably contributed from the acetate units of Cu(OAc)2 binding at the hydroxy pending group.

Moreover, the water contact angle (WCA) of SURMOFs was measured, serving as a complimentary proof to confirm the presence of fu-ip ligands on the external surface of SURMOF **B**. As illustrated in Figure 3.8, OH-ip terminated SURMOF **B** shows a hydrophilic surface with a smaller water contact angle (63°) comparing to the pristine one (71°). However, the other samples terminated with fu-ip ligands containing the hydrophobic groups at the fifth position show a higher water contact angle with respect to the pristine sample.

The WCA is progressively increased with lengthening the carbon chain of the alkoxy side group, indicating the enhanced surface hydrophobicity as a direct consequence from the fu-ip ligands binding at the external surface of SURMOF **B**. Combining the data from the analysis of terminated growth of $Cu(OAc)_2$/fu-ip, and its IRRAS spectra and WCA, we expect that the fu-ip ligands are bound on the external surface of SURMOF **B** by coordination bonds between the coordinated-available Cu-paddlewheel nodes at the external surface and the carboxylate groups of the fu-ip ligands and consequently align the functional group at the fifth position of the fu-ip ligands in the “head-on” fashion as shown in Figure 3.1.

In summary of this part of the study, the above discussed characterization data support the hypothesis that the surface ligands selectively altered the surface properties of SURMOFs such as hydrophilicity/hydrophobicity, while they do not change the intrinsic properties, including crystallinity, crystal

morphology, pore structure and sorption capacity. Thus, the surface termination with appropriately selected fu-ip probably can be used as an efficient approach for functionalizing the external surface of MOF thin films or even bulk MOF materials to facilitate the subsequent growth of another MOF on top of the previously grown MOF. The interface between the two MOF crystallite domains would then act as a nucleation active self-assembled organic monolayer and would not affect the over-all sorption properties of the heterostructure **A**@**B**.

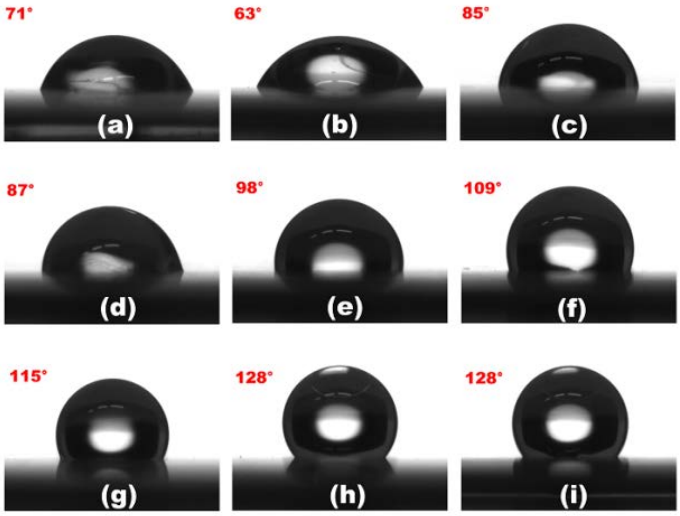

Figure 3.8. Images of the water contact angle measured on (a) pristine SURMOF **B** and fu-ip surface-terminated SURMOF **B** samples by (b) OH-ip, (c) Me-ip, (d) Et-ip, (e) Pr-ip, (f) Bu-ip, (g) He-ip, (h) De-ip, and (i) Od-ip ligands.

3.2.2 Hetero-SURMOF Cu_2ndc_2dabco@Cu_3btc_2 (A@B)

LPE hetero-growth and characterization. Based on the successful implementation of alkoxy-functionalized fu-ip ligands on the external surface of SURMOF **B** discussed in the previous section, we herein apply the procedure for functionalization the external surface of SURMOF **B** for the further growth of lattice-mismatched SURMOF e.g. Cu_2ndc_2dabco (**A**) on top of it. Herein, four kinds of fu-ip ligands (pydc, OH-ip, Bu-ip and BuOH-ip) were selected, of

which the terminated functional groups of the side chain at the fifth position can act as the functional seeding points for the nucleation and the further growth of SURMOF **A**. In details, SURMOF **B** was first fabricated by LPE for 40 cycles and then functionalize its external surface by employing the stepwise LPE of $Cu(OAc)_2$ and the template fu-ipH_2 ligands followed by rinsing with ethanol after each precursor step for 1 cycles. After creating the interface by surface functionalization with the fu-ip ligands, SURMOF **A** was successively grown by the stepwise LPE process for 40 cycles. The corresponding QCM frequency change data are shown in Figure 3.9 from which $Cu(OAc)_2$/fu-ipH_2 ligands and the components of SURMOF **A** are deposited sequentially on top of SURMOF **B**. Interestingly, the continuous stepwise change of QCM frequency is observed during the dosing of the SURMOF **A** precursor solutions, implying the hetero-growth of SURMOF **A** on top of the pre-formed SURMOF **B**.

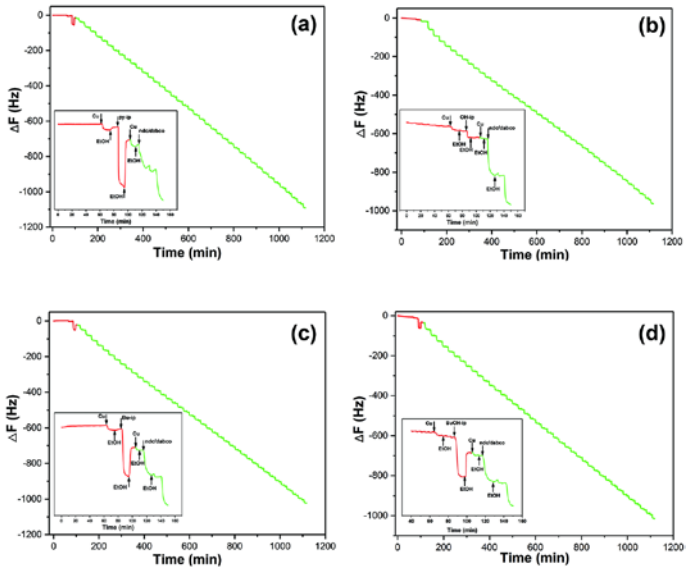

Figure 3.9. QCM frequency as a function of time recorded in situ during the stepwise LPE growth of SURMOF **A** (40 cycles) on the top of the preformed, surface-functionalized SURMOF **B**. In this case, the interface between the two SURMOFs was functionalized by (a) pydc, (b) OH-ip, (c) Bu-ip, (d) BuOH-ip.

Inset: QCM profile during the deposition steps of Cu(OAc)2/fu-ip (red) and SURMOF **A** (green).

The crystallinity of the single SURMOF **B** and the obtained hetero-SURMOF **A@B** was probed by GIXRD (shown in Figure 3.10). According to the XRD patterns, the pre-formed SURMOF **B** (Figure 3.10c) shows a well-matched with the bulk **B** with high crystallinity and a preferred orientation along the (100) crystallographic direction. In addition to the XRD pattern of the pre-formed SURMOF **B**, a new diffraction peak at 2θ around 9.2° (indexed as the (001) of MOF **A**) appears in the XRD pattern of the heterostructure films, which is significantly observed when functionalizing the interface by BuOH-ip (Figure 3.10g). However, there is very weak reflection peak indexed to be SURMOF **A** in the cases of functionalizing the interface with pydc (Figure 3.10d), OH-ip (Figure 3.10e) and Bu-ip (Figure 3.10f), implying that most of the deposited compounds on top of the pre-formed SURMOF **B** during the hetero-growth in these cases is some unknown amorphous coordination polymer rather than the desired SURMOF **A**. Herein, using BuOH-ip ligand for functionalizing the external surface of SURMOF **B** is a good template for a further growth of the oriented SURMOF **A**. The stepwise LPE approach offers the ability to precisely control the composition of the external surface in contrast to one-pot solvothermal synthesis.[31-33] The interface functionalized with py/OH/Bu-ip yields the tilted (py/OH-ip) or no valid (Bu-ip) seeding points at the external surface, which are not sufficient to bind the $Cu(OAc)_2$ units and the nucleation centers of Cu_2ndc_2dabco directly on the SURMOF **B** surface. Hence, the heteroepitaxial growth of the SURMOF **A** on the pre-formed, oriented SURMOF **B** is failed to produce the well-crystallized phase but the amorphous coordination polymer is formed instead,[57-58] though the stepwise and continuous deposition of precursor components for SURMOF **A** is observed in the QCM frequency profiles (Figure 3.9a-c). Moreover, the

influence of the thickness of SURMOF B on the growth of SURMOF **A** was studied as well (shown in Fig. 3.11). A thin SURMOF **B** is not beneficial for depositing SURMOF **A** on its surface, while its influence becomes very weak when the pre-deposition of SURMOF **B** is done for more than 20 cycles.

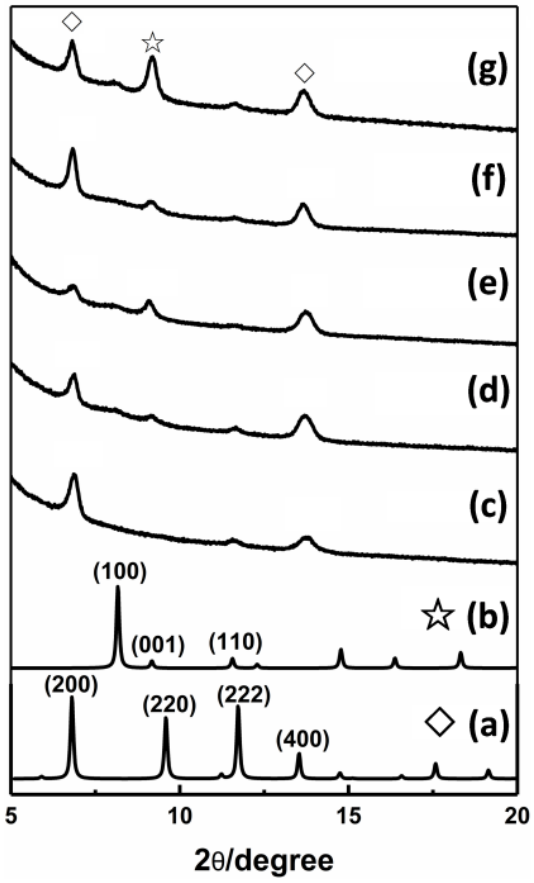

Figure 3.10. Out-of-plane XRD patterns of SURMOFs in comparison with the simulated patterns of the bulk MOFs; (a) simulated pattern of bulk MOF **B**; (b) simulated pattern of bulk MOF **A**; (c) 40-cycles pre-formed SURMOF **B**; and hetero-SURMOFs **A@B** (both are fabricated for 40 cycles) with (d) pydc, (e) OH-ip, (f) Bu-ip, and (g) BuOH-ip functionalization at the interface.

In addition, the surface morphologies and the cross-section of hetero-SURMOF **A@B** were investigated by SEM (Figure 3.12). Unambiguously, the two layer-blocks SURMOF **A** and SURMOF **B** can be

directly distinguished from the cross-sectional SEM image, showing a striking contrast of the dual layer-blocks of SURMOF **A** and SURMOF **B** (Figure 3.12b), which is because of the uneven fracture (blue step in Figure 3.12b) created during the sample preparation. Moreover, the IRRAS spectra shown in Figure 3.13 also prove the presence of both components of SURMOF **A** and SURMOF **B**. In all, SURMOF **A** can be hetero-epitaxially grown with the preferred-orientation along its (001) crystallographic direction on the top of pre-formed SURMOF **B** with the preferred-orientation along its (100) crystallographic direction by modifying the interface between the two lattice-mismatched MOFs with surface-functionalized ligands.

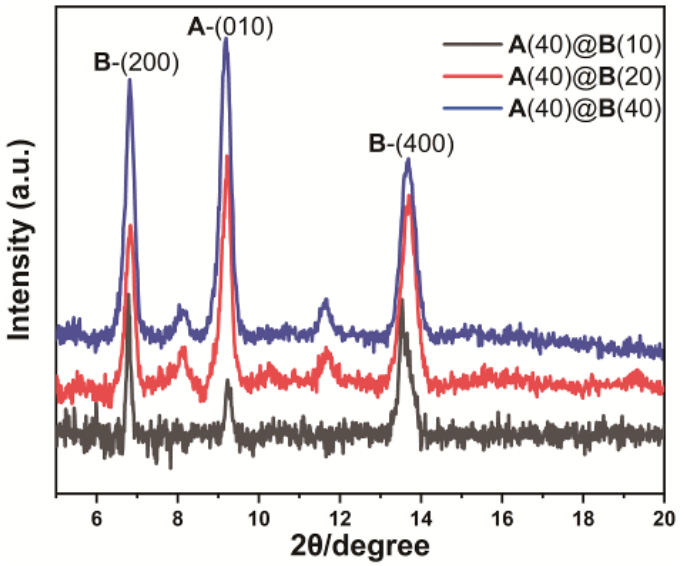

Figure 3.11. The comparison of out-of-plane XRD patterns of hetero-SURMOF **A**@**B** in which 40 cycles SURMOF **A** on SURMOF **B** with different thickness (black: 10 cycles, red: 20 cycles and blue: 40 cycles). The interface between SURMOF **A** and **B** was functionalized with BuOH-ip. For clarity, 40 cycles SURMOF **A** deposited on 10-cycles SURMOF **B** abbreviates to **A**(40)@**B**(10) and the others are similar. Herein, **B**-(200) stands for (200) XRD peak of SURMOF **B** and the rest are the same.

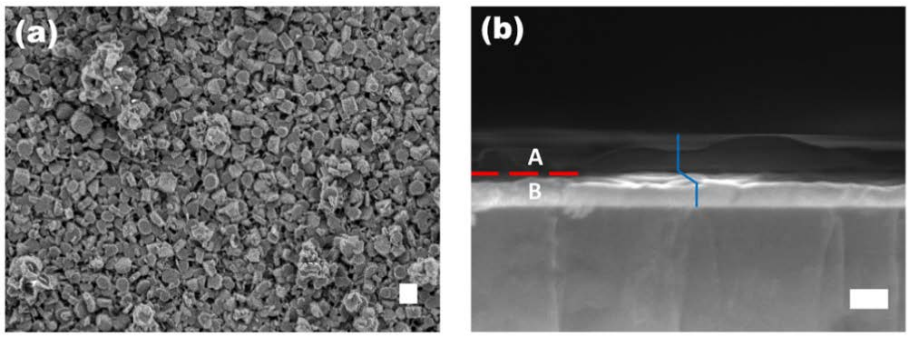

Figure 3.12. SEM images of hetero-SURMOF **A**@**B**: (a) top view; (b) cross-section. Scale bar: 200 nm. SURMOF **B** with ~120 nm thickness is formed at the first layer. After functionalization the interface with BuOH-ip ligands, an additional SURMOF **A** with ~150 nm thickness can be deposited on the top of SURMOF **B**. Note that, the uneven fracture is show by the blue line.

Interestingly, the template effect is improved substantially through using BuOH-ip as the interfacial layer between SURMOF **B** and SURMOF **A**. This emphasizes the influence of the sidechain groups of the fu-ip ligands used for surface termination on the hetero-growth of SURMOF **A**. Specifically, hetero-SURMOF **A**@**B** can be prepared with a high degree of crystallinity of both components when functionalizing the external surface of SURMOF **B** with fu-ip ligands bearing terminating groups which can further act as the seeding points for the hetero-growth of the SURMOF **A** on top of SURMOF **B**. Importantly, the surface-functionalized fu-ip ligands should have a long alkyl spacer between the ip unit and the terminated functional groups, so that they can be flexible to rearrange the positions of the terminated groups in order to be suitable for the further nucleation of the second MOF (herein SURMOF **A**). In other words, these fu-ip ligands imitate the role of SAM substrate surface functionalization in the typical procedure for homostructured growth of SURMOF by LPE process. In details, the surface-terminated BuOH-ip ligands

have the hydroxy end groups acting alike that of 11-mercaptoundecanol (MUD) SAM which is normally used as a functionalized template for fabricating SURMOFs on the gold surface.[59-60] These functional groups serve as coordination sites for the formation of uniform and *c*-axial oriented $Cu(OAc)_2$ units, which result in continuous growth of (001)-oriented SURMOF **A** on the pre-formed SURMOF **B** by sequential stepwise exposure to the $Cu(OAc)_2$ and H_2ndc/dabco solutions. Lacking a long-chain spacer as well as lacking nucleation reactive functional groups at the terminated position of the selected interfacial ligands leads to the inefficient growth of the desired highly crystalline hetero-SURMOFs, as shown by the examples pydc, OH-ip and Bu-ip ligands for the interface functionalization.

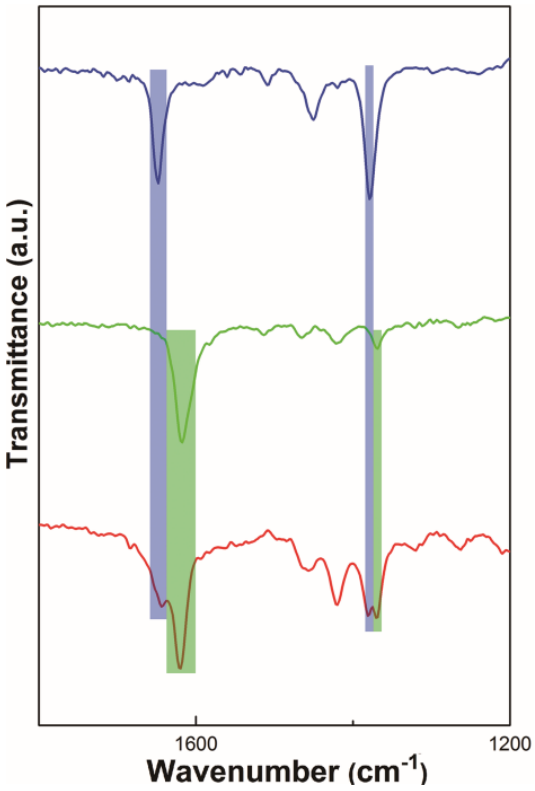

Figure 3.13. IRRAS spectra of SURMOF **B** (blue), SURMOF **A** (green) and hetero-SURMOF **A@B** (red). As demonstration, the hetero-SURMOF **A@B** generally reveals a combination of the IR bands between the single

components of SURMOF **A** and **B**, highlighting the existence of both components within the hetero-SURMOF.

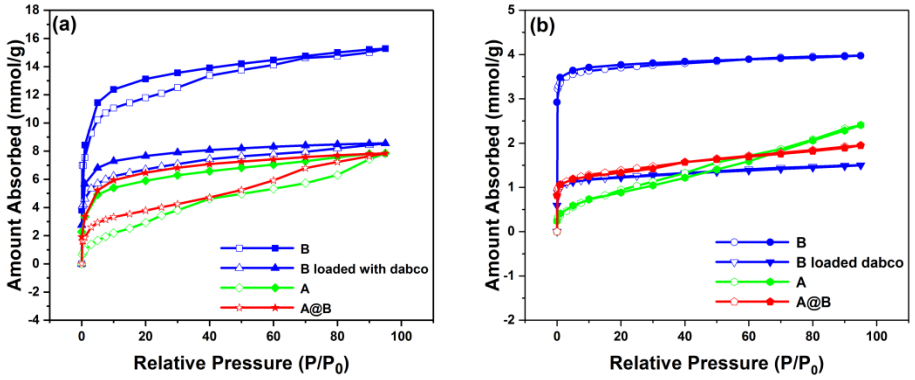

Figure 3.14 The organic solvents sorption isotherms of the homo- and hetero-SURMOFs using (a) methanol and (b) n-hexane as probe molecules.

Sorption properties of hetero-SURMOF $Cu_2ndc_2dabco@Cu_3btc_2$ (A@B). Combining MOFs with different structures into one composite may generate unique properties. The synergetic effects arise from the combination of diverse porous properties of each component. Such kinds of heterostructured MOF materials have potential for application in separation, storage and molecular recognition.[44, 46] It is noteworthy that MOF **B** has a larger pore size (13.2 Å in diameter and an aperture of 9 Å) than MOF **A** (range from 5.7 × 5.7 to 7.5 × 7.5 $Å^2$). With a large pore size and volume, MOF **B** shows outstanding storage capacity for gases and volatile organic compounds (VOCs)[61-62] while for MOF **A**, the tailoring of the pore opening and modulation of hydrophilic or hydrophobic properties provide more opportunities for tailoring the permeation selectivity for the sorption of gases and VOCs.[57] Thus, it is suggested that hetero-SURMOF **A@B** may have potential for selective storage or recognition of VOCs. The methanol and *n*-hexane sorption isotherms, shown in Figure 3.14, were measured on a BEL-QCM instrument at a constant temperature of 25 °C. Presumably, the sorption capacity of hetero-SURMOF **A@B** should be similar to that of the reported **B@A**,[46] which

should be located in between the sorption capacity of the two single components SURMOF **A** (7.8 mmol g^{-1} for methanol and 2.4 mmol g^{-1} for *n*-hexane) and SURMOF **B** (~15 mmol g^{-1} for methanol and 4 mmol g^{-1} for *n*-hexane). However, the sorption data presented in Figure 3.14 show that the methanol and *n*-hexane sorption capacity of the hetero-SURMOF **A**@**B** are unexpectedly much lower, which are only 7.8 and 2.0 mmol g^{-1}, respectively. Note that, any etching or degradation of SURMOF **B** upon exposure to the H_2ndc/dabco solution can be ruled out according to the good-crystalline XRD data of the hetero-SURMOF **A**@**B** and the previous proof reported in the literature.[46] The pores of SURMOF **B** are occupied by the dabco molecules *via* binding to the apical positions of the coordinative accessible apical sites the Cu-paddlewheel units is considered as one possible reason for the reduction of total adsorption capacity of the hetero-SURMOF **A**@**B**. In order to verify the speculation, the pre-formed SURMOF **B** was exposed to 0.2 mM dabco solution for 10 min following by the rinsing step with absolute ethanol for 5 min for a total of 40 cycles. Afterwards, the post-treated SURMOF **B** sample was characterized by GIXRD and organic solvents sorption isotherms. The comparison of the XRD data recorded before and after exposing SURMOF **B** to the dabco solution (shown in Figure 3.15) reveals a change of the intensity ratio between (200)/(400) diffraction peaks, which confirms the loading of dabco molecules into the pores of SURMOF **B**.[55, 63] Note that, the change of the (200)/(400) intensity ratio is observed in the XRD patterns of the hetero-SURMOF **A**@**B** as well (Figure 3.10). Moreover, the methanol and *n*-hexane sorption isotherms of the post-treated SURMOF **B** show a closer amount of the total sorption capacity (8.5 mmol g^{-1} for methanol and 1.5 mmol g^{-1} for *n*-hexane) to the hetero-SURMOF **A**@**B** than to the pristine SURMOF **B**. This observation is persuasive to ascribe the unexpected lower sorption capacity of hetero-SURMOF **A**@**B** to the binding of dabco molecules within

the pores of SURMOF **B** during the heteroepitaxial growth of the SURMOF **A** on top of it.

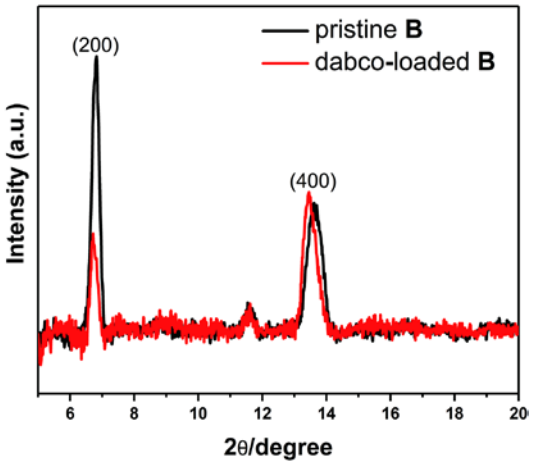

Figure 3.15. The comparison of out-of-plane XRD patterns of pristine SURMOF **B** (black curve) and after the loading of dabco molecules (red curve). After loading, the intensity ratio of (200)/(400) are decreased.

3.3 Conclusions

The implementation of fu-ip ligands containing a side chain with terminal groups at the fifth position on the external surface of SURMOF **B** has been achieved by using the stepwise LPE approach. The fu-ip ligands bind on the external surface of SURMOF **B** by their carboxylate groups and consequently expose their terminal functional groups to the interface, leading to the alteration of the surface properties such as surface hydrophobicity. The implementation of fu-ip ligands does not change the intrinsic properties of SURMOF **B**, including crystallinity, crystallite orientation, surface morphology and sorption isotherms. This modification of the surface can be applied for the growth of lattice-mismatched hetero-SURMOF. The highly crystalline hetero-SURMOF **A@B,** which cannot be deposited by the usual LPE procedure, can be fabricated by engineering an interface between **A** and **B**

with appropriately selected fu-ip ligands. The use of BuOH-ip ligand for the interface modification is found to be an effective choice to modify the topmost tilted carboxylate groups of the pre-formed SURMOF **B** to be suitable for the further nucleation of the SURMOF **A**. This interface functionalization mimics the role of substrate surface modification via SAMs for nucleation of the targeted thin film material deposited using liquid phase techniques. This strategy is expected to be generally efficient for hetero-SURMOF growth, especially lattice-mismatched ones, which could benefit the further development of the MOF-based synergistic unit for targeted applications such as selective sorption, sensing and catalysis.

3.4 References

[1] M. A. Boles, D. Ling, T. Hyeon, D. V. Talapin, *Nat. Mater.* **2016**, *15*, 364.

[2] E. Ozbay, *Science* **2006**, *311*.

[3] C. B. Murray, C. R. Kagan, *Annu. Rev. Mater. Sci.* **2000**, *30*, 545.

[4] A. T. Bell, *Science* **2003**, *299*, 1688.

[5] X. Peng, L. Manna, W. Yang, J. Wickham, E. Scher, A. Kadavanich, A. P. Alivisatos, *Nature* **2000**, *404*, 59.

[6] L. Protesescu, M. Nachtegaal, O. Voznyy, O. Borovinskaya, A. J. Rossini, L. Emsley, C. Coperet, D. Gunther, E. H. Sargent, M. V. Kovalenko, *J. Am. Chem. Soc.* **2015**, *137*, 1862.

[7] R. Cao-Milan, L. D. He, S. Shorkey, G. Y. Tonga, L. S. Wang, X. Zhang, I. Uddin, R. Das, M. Sulak, V. M. Rotello, *Mol. Syst. Des. Eng.* **2017**, *2*, 624.

[8] K. Y. Ko, J. G. Song, Y. Kim, T. Choi, S. Shin, C. W. Lee, K. Lee, J. Koo, H. Lee, J. Kim, T. Lee, J. Park, H. Kim, *ACS Nano* **2016**, *10*, 9287.

[9] P. K. Alaboina, M. J. Uddin, S. J. Cho, *Nanoscale* **2017**, *9*, 15736.

[10] A. Zimpel, T. Preiß, R. Röder, H. Engelke, M. Ingrisch, M. Peller, J. O. Rädler, E. Wagner, T. Bein, U. Lächelt, S. Wuttke, *Chem. Mater.* **2016**, *28*, 3318.

[11] M. K. Corbierre, R. B. Lennox, *Chem. Mater.* **2005**, *17*, 5691.

[12] M. Cargnello, N. L. Wieder, P. Canton, T. Montini, G. Giambastiani, A. Benedetti, R. J. Gorte, P. Fornasiero, *Chem. Mater.* **2011**, *23*, 3961.

[13] K. Möller, T. Bein, *Chem. Mater.* **2016**, *29*, 371.

[14] A. Demessence, D. M. D'Alessandro, M. L. Foo, J. R. Long, *J. Am. Chem. Soc.* **2009**, *131*, 8784.

[15] C. M. Miralda, E. E. Macias, M. Zhu, P. Ratnasamy, M. A. Carreon, *ACS Catal.* **2011**, *2*, 180.

[16] H. Furukawa, K. E. Cordova, M. O'Keeffe, O. M. Yaghi, *Science* **2013**, *341*, 1230444.

[17] H. Li, M. Eddaoudi, M. O'Keeffe, O. M. Yaghi, *Nature* **1999**, *402*, 276.

[18] H. C. Zhou, S. Kitagawa, *Chem. Soc. Rev.* **2014**, *43*, 5415.

[19] L. J. Murray, M. Dinca, J. R. Long, *Chem. Soc. Rev.* **2009**, *38*, 1294.

[20] J. R. Li, J. Sculley, H. C. Zhou, *Chem. Rev.* **2012**, *112*, 869.

[21] A. H. Chughtai, N. Ahmad, H. A. Younus, A. Laypkov, F. Verpoort, *Chem. Soc. Rev.* **2015**, *44*, 6804.

[22] L.-M. Yang, G. Y. Fang, J. Ma, R. Pushpa, E. Ganz, *Phys. Chem. Chem. Phys.* **2016**, *18*, 32319.

[23] L.-M. Yang, G.-Y. Fang, J. Ma, E. Ganz, S. S. Han, *Cryst. Growth Des.* **2014**, *14*, 2532.

[24] L.-M. Yang, P. Vajeeston, P. Ravindran, H. Fjellvag, M. Tilset, *Inorg. Chem.* **2010**, *49*, 10283.

[25] M. Shah, M. C. McCarthy, S. Sachdeva, A. K. Lee, H.-K. Jeong, *Ind. Eng. Chem. Res.* **2012**, *51*, 2179.

[26] Z. G. Gu, H. Fu, T. Neumann, Z. X. Xu, W. Q. Fu, W. Wenzel, L. Zhang, J. Zhang, C. Wöll, *ACS Nano* **2016**, *10*, 977.

[27] L. E. Kreno, K. Leong, O. K. Farha, M. Allendorf, R. P. Van Duyne, J. T. Hupp, *Chem. Rev.* **2012**, *112*, 1105.

[28] M. D. Allendorf, A. Schwartzberg, V. Stavila, A. A. Talin, *Chem. Eur. J.* **2011**, *17*, 11372.

[29] Z.-G. Gu, A. Pfriem, S. Hamsch, H. Breitwieser, J. Wohlgemuth, L. Heinke, H. Gliemann, C. Wöll, *Micropor. Mesopor. Mater.* **2015**, *211*, 82.

[30] O. Shekhah, H. Wang, S. Kowarik, F. Schreiber, M. Paulus, M. Tolan, C. Sternemann, F. Evers, D. Zacher, R. A. Fischer, C. Wöll, *J. Am. Chem. Soc.* **2007**, *129*, 15118.

[31] A. Betard, R. A. Fischer, *Chem. Rev.* **2012**, *112*, 1055.

[32] J. Liu, C. Wöll, *Chem. Soc. Rev.* **2017**, *46*, 5730.

[33] O. Shekhah, J. Liu, R. A. Fischer, C. Wöll, *Chem. Soc. Rev.* **2011**, *40*, 1081.

[34] S. Choi, T. Kim, H. Ji, H. J. Lee, M. Oh, *J. Am. Chem. Soc.* **2016**, *138*, 14434.

[35] S. Furukawa, K. Hirai, K. Nakagawa, Y. Takashima, R. Matsuda, T. Tsuruoka, M. Kondo, R. Haruki, D. Tanaka, H. Sakamoto, S. Shimomura, O. Sakata, S. Kitagawa, *Angew. Chem. Int. Ed.* **2009**, *48*, 1766.

[36] K. Koh, A. G. Wong-Foy, A. J. Matzger, *Chem. Commun.* **2009**, *41*, 6162.

[37] K. Hirai, K. Chen, T. Fukushima, S. Horike, M. Kondo, N. Louvain, C. Kim, Y. Sakata, M. Meilikhov, O. Sakata, S. Kitagawa, S. Furukawa, *Dalton Trans.* **2013**, *42*, 15868.

[38] S. Furukawa, K. Hirai, Y. Takashima, K. Nakagawa, M. Kondo, T. Tsuruoka, O. Sakata, S. Kitagawa, *Chem. Commun.* **2009**, *34*, 5097.

[39] S. Wannapaiboon, M. Tu, R. A. Fischer, *Adv. Funct. Mater.* **2014**, *24*, 2696.

[40] K. Hirai, S. Furukawa, M. Kondo, H. Uehara, O. Sakata, S. Kitagawa, *Angew. Chem. Int. Ed.* **2011**, *50*, 8057.

[41] K. Hirai, S. Furukawa, M. Kondo, M. Meilikhov, Z. Sakata, O. Sakata, S. Kitagawa, *Chem. Commun.* **2012**, *48*, 6472.

[42] M. Tu, S. Wannapaiboon, R. A. Fischer, *Dalton Trans.* **2013**, *42*, 16029.

[43] M. Meilikhov, S. Furukawa, K. Hirai, R. A. Fischer, S. Kitagawa, *Angew. Chem. Int. Ed.* **2013**, *52*, 341; *Angew. Chem.* **2013**, *125*, 359.

[44] S. Wannapaiboon, M. Tu, K. Sumida, K. Khaletskaya, S. Furukawa, S. Kitagawa, R. A. Fischer, *J. Mater. Chem. A* **2015**, *3*, 23385.

[45] Z. Wang, J. Liu, B. Lukose, Z. Gu, P. G. Weidler, H. Gliemann, T. Heine, C. Wöll, *Nano Lett.* **2014**, *14*, 1526.

[46] M. Tu, R. A. Fischer, *J. Mater. Chem. A* **2014**, *2*, 2018.

[47] J. C. Love, L. A. Estroff, J. K. Kriebel, R. G. Nuzzo, G. M. Whitesides, *Chem. Rev.* **2005**, *105*, 1103.

[48] L. Heinke, Z. Gu, C. Wöll, *Nat. Commun.* **2014**, *5*, 4562.

[49] O. Shekhah, H. Wang, D. Zacher, R. A. Fischer, C. Wöll, *Angew. Chem. Int. Ed.* **2009**, *48*, 5038; *Angew. Chem.* **2009**, *121*, 5138.

[50] O. Zybaylo, O. Shekhah, H. Wang, M. Tafipolsky, R. Schmid, D. Johannsmann, C. Wöll, *Phys. Chem. Chem. Phys.* **2010**, *12*, 8092.

[51] R. Morent, N. De Geyter, C. Leys, L. Gengembre, E. Payen, *Surf. Interface Anal.* **2008**, *40*, 597.

[52] M. P. Bernstein, A. L. Mattioda, S. A. Sandford, D. M. Hudgins, *Astrophys. J.* **2005**, *626*, 909.

[53] J. R. Durig, C. Pan, G. A. Guirgis, *Spectrochim. Acta. A. Mol. Biomol. Spectrosc.* **2003**, *59*, 979.

[54] A. Thamri, H. Baccar, C. Struzzi, C. Bittencourt, A. Abdelghani, E. Llobet, *Sci. Rep.* **2016**, *6*, 35130.

[55] W. Guo, M. Zha, Z. Wang, E. Redel, Z. Xu, C. Wöll, *ACS Appl. Mater. Inter.* **2016**, *8*, 24699.

[56] B. Faust, in *Modern Chemical Techniques: An Essential Reference for Students and Teachers* Royal Society of Chemistry (RSC) Publishing, London **1997**, Ch. 3, p. 62.

[57] B. Liu, M. Tu, R. A. Fischer, *Angew. Chem. Int. Ed.* **2013**, *52*, 3402.

[58] D. Zacher, K. Yusenko, A. Betard, S. Henke, M. Molon, T. Ladnorg, O. Shekhah, B. Schupbach, T. de los Arcos, M. Krasnopolski, M. Meilikhov, J. Winter, A. Terfort, C. Wöll, R. A. Fischer, *Chem. Eur. J.* **2011**, *17*, 1448.

[59] E. Biemmi, C. Scherb, T. Bein, *J. Am. Chem. Soc.* **2007**, *129*, 8054.

[60] E. Biemmi, A. Darga, N. Stock, T. Bein, *Micropor. Mesopor. Mater.* **2008**, *114*, 380.

[61] E. Borfecchia, S. Maurelli, D. Gianolio, E. Groppo, M. Chiesa, F. Bonino, C. Lamberti, *J. Phys. Chem. C* **2012**, *116*, 19839.

[62] K. Vellingiri, J. E. Szulejko, P. Kumar, E. E. Kwon, K. H. Kim, A. Deep, D. W. Boukhvalov, R. J. Brown, *Sci. Rep.* **2016**, *6*, 27813.

[63] W. Guo, Z. Chen, C. Yang, T. Neumann, C. Kubel, W. Wenzel, A. Welle, W. Pfleging, O. Shekhah, C. Wöll, E. Redel, *Nanoscale* **2016**, *8*, 6468.

Chapter 4

Molecular funneling: synergistic effect of heterostructured dissimilar metal-organic framework thin films

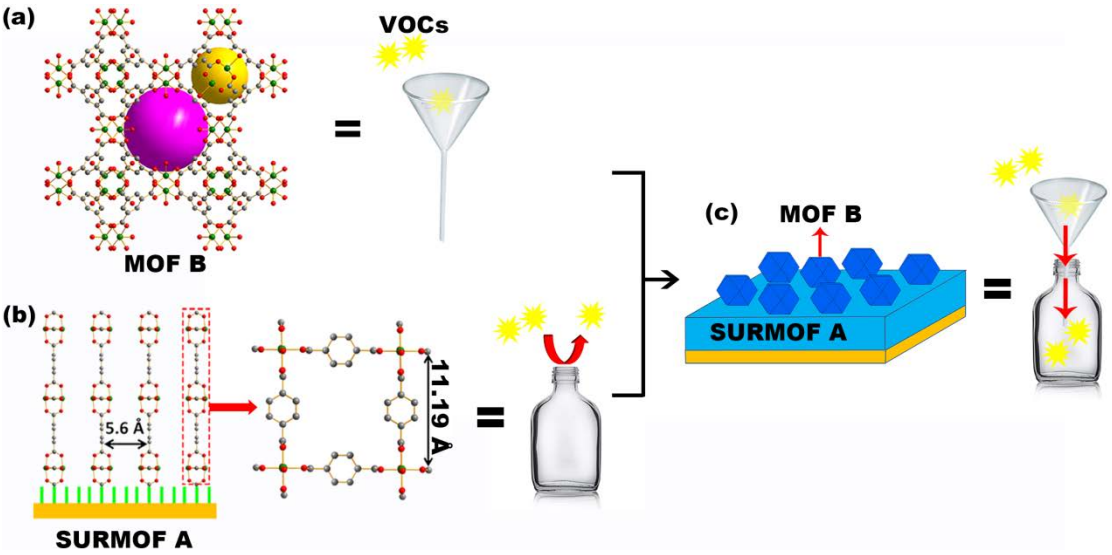

Abstract

A novel heterostructured surface-mounted metal-organic framework (hetero-SURMOF) thin film of the 3-dimensional (3D) Cu_3btc_2 (**B**) on top of the bottom 2D Cubdc (also Cubpdc or CuTF-bdc) (**A**) was developed for volatile organic compounds (VOCs) sensing, recognition and capture. The hetero-SURMOF samples are generally denoted as **B@A** (btc = benzene-1,3,5-tricarboxylate, bdc = terephthalate, bpdc = biphenyl-4,4'-dicarboxylate, TF-bdc = tetrafluoroterephthalate). The obtained **B@A** show *higher* VOCs storage capacity even than that of both homo-SURMOFs **A** and **B**. Moreover, **B@A** shows a *counter-intuitive uptrend* of the adsorption ability with increasing the molecular size of VOCs up to a certain threshold. This phenomenon is different from any known homo-SURMOF and bulk MOF as well, and the novel selective adsorption property can be tuned by functionalized (TF-bdc) or elongated (bpdc) linkers in bottom homo-SURMOF **A**. The unique adsorption property of **B@A** is attributed to the interfacial contact of **A** and **B** and the synergetic property of the whole heterostructure, which results in "molecular funneling".

4.1 Introduction

Over the past few decades, integrating different materials into one structure to generate enhanced or new properties to meet the rising demand for novel and high performance has attracted rapidly growing research interests.[1-2] The concept of heterostructured and hybrid materials has also been applied to metal-organic frameworks (MOFs),[3-6] which are an emerging class of porous materials with lots of excellent properties,[7-8] showing great potential applications in many fields.[9-12] In particular composite MOFs (MOF-on-MOF or core-shell MOFs) usually display such advanced functionalities because of the integrated properties from each MOF component as well as emergent properties from the synergistic heterostructured unit.[5, 13-14] Sensing and elimination of volatile organic compounds (VOCs) is a subject of widespread societal concern associated with environmental and human health issues.[15] In pursuit of materials for VOCs sensing and adsorption, MOFs have been noticed because of the fantastic properties as stated above. To date, plenty of MOFs have been studied on sensing and adsorption of VOCs.[16-22] More recently, composite MOF thin films were developed for sensing VOCs as well.[23-28] Regarding to the wide open parameter space of tuning sorption property of composite MOFs, it is significant to further develop composite MOF materials for VOCs sensing, separation or capture.

The over-all pore structure of composite MOFs can be controlled via scrupulously selecting the individual MOF components, which offer unique sorption properties. For example, encapsulating one MOF with small pores by other MOF with large pores produces composite MOFs possessed of downscaling (from outside to inside) hierarchical pore structure which is promising for separation,[5, 14] and the composite MOFs with a reversed pore structure show great potential applications in storage, sensing and molecular

recognition.[26] We performed a statistical analysis of previously-reported composite MOFs and we found that their total gas/vapor storage capacity C_{AB} is always between or below that of the individual MOF components C_A, and C_B ($C_A \leq C_{AB} \leq C_B$ or $C_{AB} \leq C_A \leq C_B$; C is the specific storage capacity and indices A, B and AB refer to MOF components and the composite MOF, respectively). These observations are quite understandable and in line with accepted concepts of adsorption and molecular transport in porous materials.[13-14, 29-33] Nevertheless, the situation could be changed when strong interaction occurs between the individual MOFs used as components for the composite MOF. For instance, imagine a composite MOF, consisting of a MOF component in which the intrinsic adsorption is restrained by MOF crystallite surface inhibition effects but can be emancipated by the other MOF component due to interfacial interactions being present only in the MOF heterostructure. Such a composite may achieve a higher total storage capacity than that of both components ($C_A \leq C_B < C_{AB}$.).[34-35]

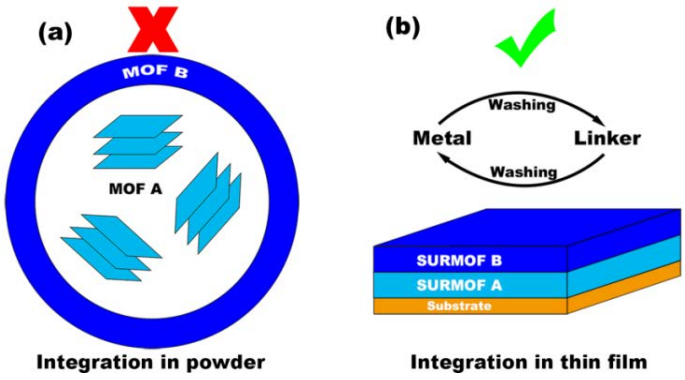

Figure 4.1. Schematic illustration of (a) free-standing composite MOF **B@A** which cannot be synthesized and (b) hetero-SURMOF **B@A** prepared by LPE technique.

We selected Cubdc (bdc = terephthalate, denoted as **A1**) as inner MOF and Cu_3btc_2 (btc = benzene-1,3,5-tricarboxylate, denoted as **B**) as outer MOF to synthesize Cu_3btc_2-on-Cubdc composite heterostructured MOF **B@A1** and

explore its VOCs sorption property. The sorption property of two-dimensional (2D) MOF **A1** is susceptible to VOCs with different size, because the spacing distance of adjacent layers is variant by employing different molecules as spacer.[36-37] Hence, it would be very interesting to study the sorption property of MOF **A1**, especially for those particles confined in a finite space which is formed by other MOFs (Figure 4.1a). Selecting outer MOF for the construction of such composite MOF should be careful, which means that the growth of outer MOF should not affect the pre-formed MOF **A1** and it should have good VOCs sorption property as well. Taking all of these factors into account, MOF **B** which has a rigid 3D structure and preeminent VOCs sorption property is an excellent choice. Nevertheless, growing such a free-standing composite MOF is an enormous challenge from the experimental point of view, because MOF **A1** and **B** have incompatible crystal parameters and totally different crystal habit. Inspired by the fabrication mechanism of stepwise liquid-phase epitaxy (LPE, also known as Layer-by-Layer) in which the metal and linker solutions are alternately dosed,[38] this synthetic problem could be well-settled by transforming the otherwise incompatible free-standing bulk MOFs to thin films, namely, MOF **A1** is fabricated as thin film on a specific substrate followed by sequentially depositing MOF **B** on the top (Figure 4.1b). The MOF thin films synthesized by LPE technique are so-called surface mounted MOFs (SURMOFs), and herein the obtained heterostructured SURMOF is denoted as hetero-SURMOF **B@A1**. To the best of our knowledge, this is the first case of 2D-3D composite MOF materials. Converting MOF bulk powders to thin films provides an efficient solution to solve the synthetic problem of composite MOFs, which has been successfully applied in many cases.[25-26, 39-43] Furthermore, the stepwise LPE thin film fabrication process can efficiently control over the quantity of each component deposited within

hetero-SURMOFs, which results in a rational tunability of target properties compare with bulk composite MOFs.

Compare to the free-standing MOF **A1**, SURMOF **A1** has a different P4 symmetry from that in bulk (P2 or C2) and a larger activation energy barrier for penetration of the external crystallite surface.[44-45] The high energy barrier leads to an unexpected low VOCs storage capacity for homo-SURMOF **A1**. It means that the surface of SURMOF **A1** is blocked and VOCs cannot penetrate.[46] Fortunately, the top-deposited SURMOF **B** has strong interaction with bottom SURMOF **A1** that can overcome this surface barrier and then enhance the total VOCs adsorption. Subsequently, a series of VOCs with a variation of molecular size (kinetic diameter) were selected: methanol (3.6 Å), benzene (5.3–5.9 Å), cyclohexane (6.0–6.2 Å), mesitylene (8.7 Å) and 1,3,5-triisopropylbenzene (9.3 Å), and the sorption property of hetero-SURMOF **B**@**A1** was studied.[25, 47] Moreover, another two analogous SURMOFs, Cubpdc and CuTF-bdc (bpdc = biphenyl-4,4'-dicarboxylate, TF-bdc = tetrafluoroterephthalate, denoted as **A2** and **A3** respectively and named as **A** in general), were also employed to study the VOCs sorption property of hetero-SURMOFs as function of different linkers. Expectedly, the hetero-SURMOF **B**@**A** showed the enhanced uptake capacity $C_A \leq C_B < C_{AB}$. However, in addition and counter intuitively and uptrend adsorption ability with increasing the molecular size of VOCs was obseverd, which is different to the situation of homo-SURMOFs. The obtained hetero-SURMOFs **B**@**A** were firstly characterized by X-ray diffraction (XRD), scanning electron microscope (SEM) and infrared reflection absorption spectrum (IRRAS) to confirm the phases. Then the impact of various parameters on the VOCs sorption behaviors of hetero-SURMOFs **B**@**A** were systematically investigated such as the thickness of upper SURMOF **B** (10, 20 and 40 deposition cycles) and bottom SURMOF **A1** (10, 20, 40 and 60 deposition cycles), the crystallinity of

SURMOF **B** (which is controlled by integrating different amount of water in the H_3btc linker solution during the fabrication process[46]), and finally the linkers adopted in bottom SURMOF **A**.

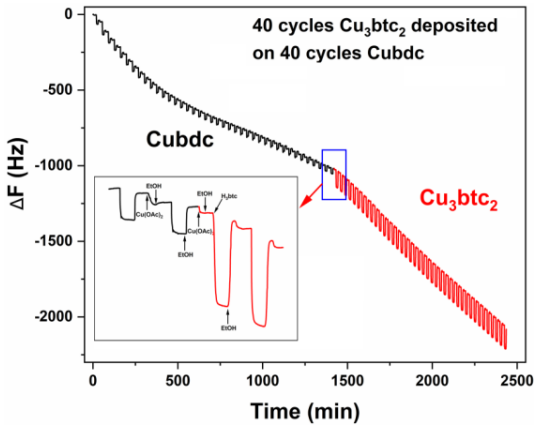

Figure 4.2. The changes in the QCM oscillator frequency (ΔF) as a function of time during the stepwise LPE growth process of hetero-SURMOF **B**@**A1**.

4.2 Results and Discussion

4.2.1 SURMOFs fabrication and characterization

4.2.1.1 SURMOFs fabrication

SURMOFs were synthesized using stepwise LPE method by which thin films featured high crystallinity, well-defined crystallite orientation, homogeneity, and well-controlled thickness and roughness were obtained.[48-49] Combining with surface plasmon resonance (SPR) technique, the growth processes were monitored *in-situ* by recording the oscillation frequency change of QCM sensor.[50-51] Hetero-SURMOFs Cu_3btc_2@Cubdc (**B**@**A1)** were prepared by sequentially depositing SURMOF **B** on top of SURMOF **A** with the same parameters except linker. Note that, specific amount of water (5% H_2O for H_2bdc and 20% H_2O for H_3btc) was integrated into the linker solution in SURMOF fabrication process to control the quality of thin films based on our

previous research.[46] The frequency change of QCM sensor against time curve is shown in Figure 4.2 (only hetero-SURMOF **B**@**A1** presented for clarity), from which it is clear to distinguish the growth region of SURMOF **A1** (40 cycles) and **B** (40 cycles). The hetero-SURMOF with reversed order **A1**@**B** was also fabricated by the same method, the frequency change-time curve, XRD and methanol sorption isotherm are presented in Figure 4.3. We would not put more attention on hetero-SURMOF **A1**@**B** because of its mediocre sorption property.

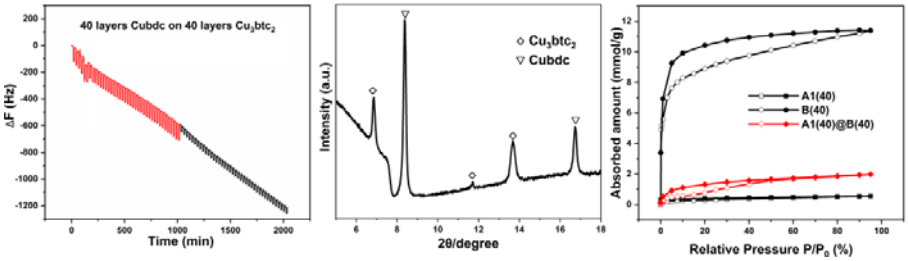

Figure 4.3. (a) The QCM frequency changes against time curve of stepwise LPE growth process of hetero-SURMOF **A1**@**B**; (b) XRD patterns of hetero-SURMOF **A1**@**B**; (c) the comparation of methanol adsorption isotherms of hetero-SURMOF **A1**@**B** and the homo-SURMOF **A1** and **B**. Note that, the hollow shapes are adsorption and solid ones are desorption, the same as below.

4.2.1.2 Characterization of SURMOFs

XRD. The crystallinity and crystallographic orientation of obtained homo- and hetero-SURMOFs were checked by GIXRD and 2D-GIXRD. The XRD patterns of homo-SURMOF **A** (general term of **A1**, Cubpdc (**A2**, bpdc = biphenyl-4,4'-dicarboxylate) and CuTF-bdc (**A3**, TF-bdc = tetrafluoroterephthalate)) and **B** are shown in Figure 4.4, and they correspond to the calculated or reported ones. As also can be seen in Figure 4.4, both signals of SURMOF **A** and **B** are emerged in the XRD patterns of hetero-SURMOFs, which attests the presence of both phases in

heterostructure. The successful growth of SURMOF **B** on the top of SURMOF **A** could ascribe to the structural flexibility of 2D SURMOF **A**, which provides the tolerance for bridging the mis-matched lattices of two frameworks. Interestingly, by analyzing XRD patterns we found that the crystallographic orientation of upper SURMOF **B** is determined by the linkers used in bottom SURMOF **A** despite it solely orients along the (001) direction. Specifically, SURMOF **B** mainly shows the orientation of (100) and (111) on SURMOF **A1** and **A2** respectively, while it has no preferred orientation on SURMOF **A3**. Note that the pre-formed SURMOFs **A** (fabricated with 5% water in linker solution) are quite stable and will not be affected by the component solutions of MOF **B** (with 20% water in linker solution) according to literatures.[52]

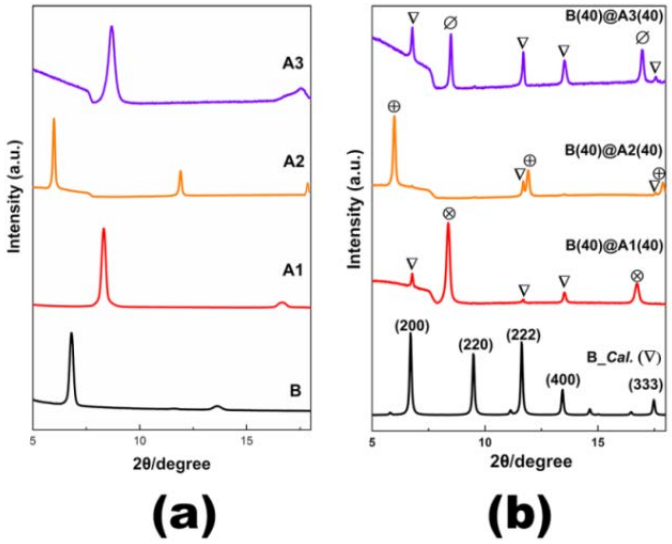

Figure 4.4. The XRD patterns of (a) homo-SURMOF **B**, **A1**, **A2** and **A3**, and (b) hetero-SURMOF **B**@**A1**/**A2**/**A3**. Triangles are the signals of SURMOF **B** and the circles are from SURMOF **A**.

Furthermore, 2D-GIXRD measurements were also performed to confirm the presence of MOF **A** and MOF **B**. The original 2D patterns of hetero-SURMOF **B**@**A**, shown in Figure 4.5, are sliced into a few slices along with different angle. The in-plane XRD patterns (along with 0 or 180°) are

shown in Figure 4.6, from which both peaks from MOF **A** and **B** are observed. Specifically, all of the SURMOF **A** peaks are corresponding to the reported one.[44]

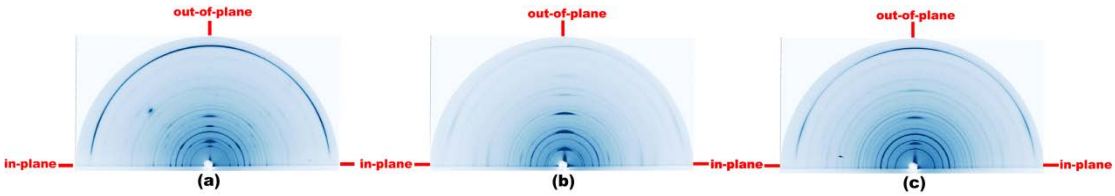

Figure 4.5. The original 2D XRD patterns of hetero-SURMOF (a) **B@A1**, (b) **B@A2**, (c)**B@A3**. As marked in the figure, the horizontal and vertical direction are in-plane and out-of-plane XRD, respectively.

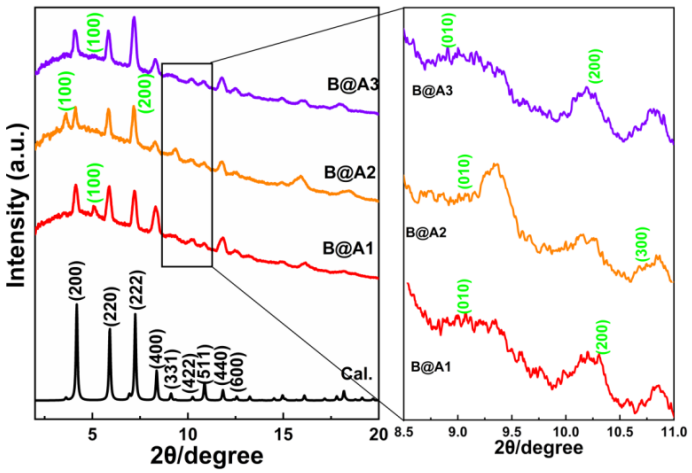

Figure 4.6. The in-plane XRD patterns of hetero-SURMOF **B@A1** (red), **B@A2** (orange) and **B@A3** (violet). The green and black labels of crystallographic plane are from MOF **A** and **B**, respectively. Note that, the 2D-GIXRD measurements were performed under the X-ray with wavelength 0.9607 Å, and the simulate MOF **B** XRD pattern is obtained from Mercury by setting the wavelength as 0.9607 Å.

SEM. The interesting phenomenon of linker determined orientation can be observed directly from the SEM images as well. As shown in Figure 4.7e-g, SURMOF **B** was deposited on the surface of SURMOF **A** as discrete particles

with size ranging from dozens to several hundred nanometers rather than continuous film. A majority of MOF **B** particles appear with square (100) crystallographic plane up on SURMOF **A1** (Figure 4.7e), while most of them show with triangular (111) crystal face up on SURMOF **A2** (Figure 4.7f). Nevertheless, MOF **B** particles disperse randomly on SURMOF **A3** (Figure 4.7g) without preferred orientation. The underlying reason for this phenomenon is not clear up to now. However, when we turn the attention to the "bare" area (no MOF **B** particles covered area), the different morphology of bottom SURMOF **A1**, **A2** and **A3** could decipher the different orientation of upper SURMOF **B**. Viewing from Figure 4.7b-d, SURMOF **A1** thin film is formed by plenty of weaving shuttle-liked nanoparticles (around 20 × 40 nm), for SURMOF **A2** a large number of pine-needle-liked nanostructures (around 10 × 70 nm) intertwine to form dense thin film, and SURMOF **A3** thin film is composed by nanospheres (20~40 nm). It seems that the orientation of upper SURMOF **B** is susceptible to the shape of nanostructures and the mean they interaction with each other within bottom SURMOF **A**.

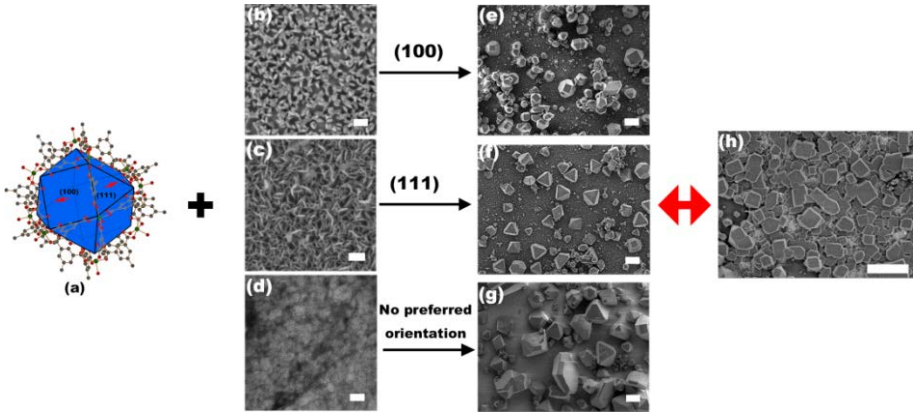

Figure 4.7. (a) Polyhedral structure of MOF **B**; (b-d) SEM images of SURMOF **A1**, **A2** and **A3**; (e-g) SEM images of hetero-SURMOF **B**@**A1**/**A2**/**A3**; (h) SEM images of homo-SURMOF **B** fabricated with 20% water in linker solution. Note that, the scale bar of (b-d) is 100 nm and that of (e-h) is 1 μm.

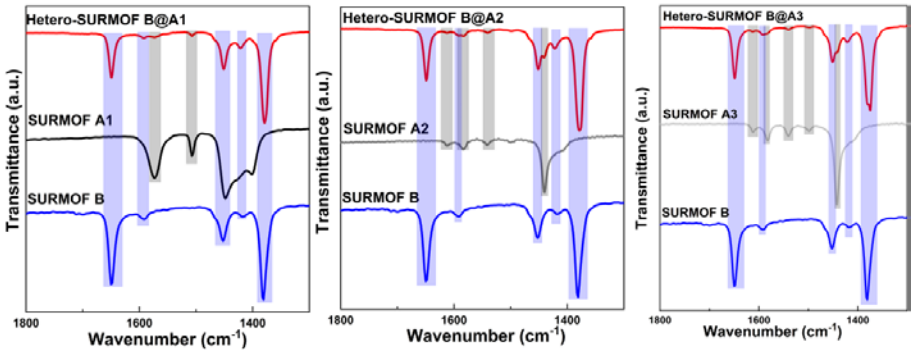

Figure 4.8. The IRRAS spectra of hetero-SURMOF (a) **B@A1**; (b) **B@A2**; (c) **B@A3**. **A2** and **A3** are Cubpdc and CuTF-bdc (bpdc = biphenyl-4,4'-dicarboxylate, TF-bdc = tetrafluoroterephthalate), respectively.

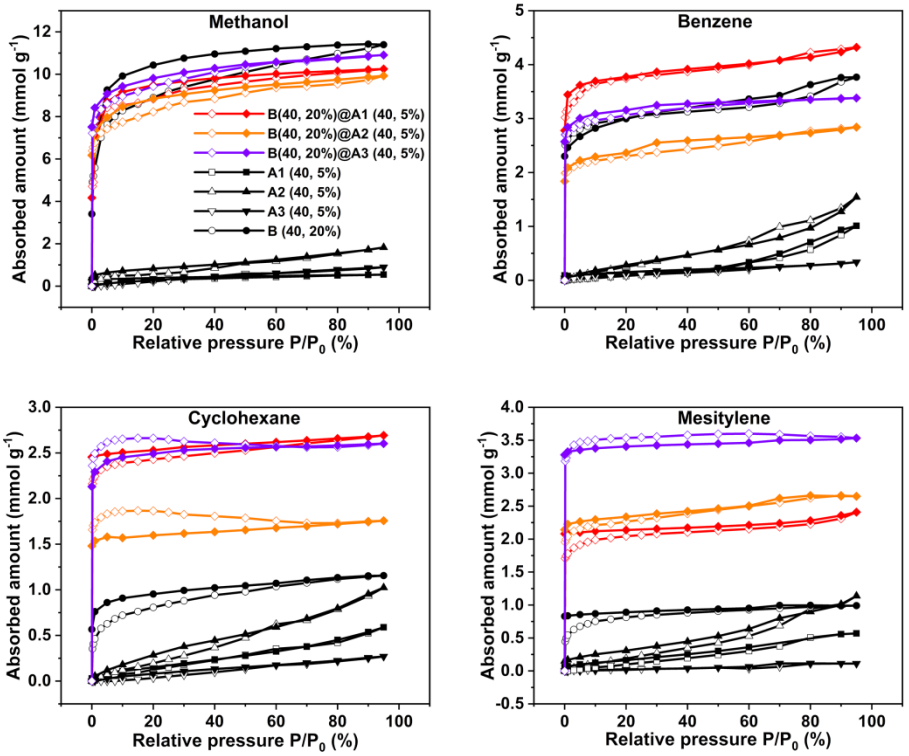

Figure 4.9. The VOCs (methanol, benzene, cyclohexane and mesitylene) sorption isotherms of **B@A1** (red), **B@A2** (orange), and **B@A3** (violate). The **B** (40, 20%) means 40 cycles SURMOF **B** was fabricated with integrating 20% in linker solution, and the rest are similar. The hollow shapes are adsorption process and solid ones are desorption process, the same as below. The

isotherms were measured at 25 °C and the saturated vapor pressure P_0 of methanol, benzene, cyclohexane and mesitylene at 25 °C are 0.169, 0.127, 0.130 and 0.003 bar, respectively.

IRRAS. The IRRAS spectra were recorded to verify the presence of SURMOF **A** and **B** in heterostructures, which are presented in Figure 4.8. By analyzing these spectra, there is no doubt that both signals of SURMOF **A** and **B** are found in heterostructures from which proves the successful synthesis of hetero-SURMOF **B**@**A**.

4.2.2 VOCs adsorption property of hetero-SURMOF B@A.

VOCs sensing and adsorption is a vital application for hetero-SURMOFs with hierarchical pore structure. Heretofore, many examples of heterostructured SURMOFs have been reported for VOCs sensing.[25-26, 39-41, 43, 53] The VOCs sensing ability of these hetero-SURMOFs substantially depend upon the different accessibility of each SURMOF component to VOC molecules. Unfortuitously, there is no exception that the VOCs storage capacity of reported hetero-MOFs locates between or below that of MOF components. In this work, homo-SURMOF **B** exhibits a good VOCs adsorption property, but homo-SURMOF **A** has a quite low storage capacity. However, the integrated hetero-SURMOFs **B**@**A** show higher VOCs (especially for large VOCs) storage capacity beyond this range. The VOCs sorption isotherms of homo- and hetero-SURMOF **B**@**A** (both are 40 cycles) are shown in Figure 4.9. As we can see, the adsorption capacities of **B**@**A**, especially for cyclohexane and mesitylene, are drastically enhanced to several times as high as homo-SURMOF **B**. Note that, the isotherms of **B** and **B**@**A** are not typical Type I isotherm, which is probably because of the interaction between VOC molecules and MOFs. The interaction between adsorbent and adsorbate leads to the bifurcation of adsorption and desorption branches.

Table 4.1. The VOCs storage capacity[a)] (adsorption **ability**[b)]) of homo-SURMOF **B** and hetero-SURMOF **B@A1/A2/A3**.

Adsorbate	**B**	**B@A1**	**B@A2**	**B@A3**
methanol	11.39 (**1**)	10.25 (**0.90**)	9.93 (**0.87**)	10.92 (**0.96**)
benzene	3.77 (**1**)	4.32 (**1.15**)	2.84 (**0.75**)	3.38 (**0.90**)
cyclohexane	1.17 (**1**)	2.69 (**2.30**)	1.76 (**1.50**)	2.60 (**2.22**)
mesitylene	0.99 (**1**)	2.41 (**2.43**)	2.65 (**2.68**)	3.53 (**3.57**)

a): mmol g^{-1}; b): The adsorption ability of homo-SURMOF **B** are set as 1, and those of hetero-SURMOF **B@A1/A2/A3** are defined as the adsorption capacity normalized by that of homo-SURMOF **B**.

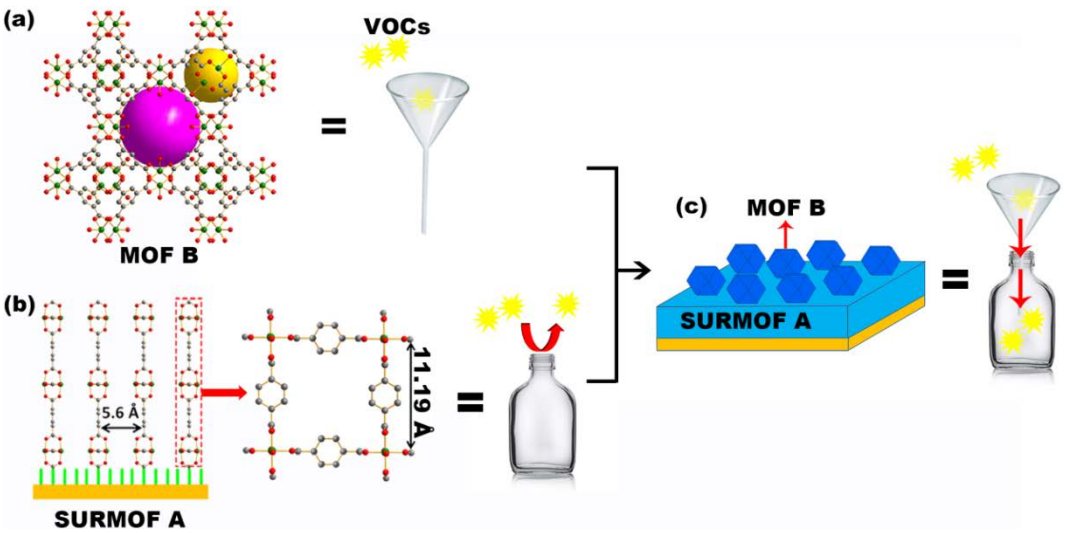

Figure 4.10. The structure of (a) SURMOF **A1** ("container"), (b) MOF **B** ("funnel"), and (c) hetero-SURMOF **B@A1** (assembly of "funnel" and "container"). (Atom identification: blue: Cu, red: btc, gray: carbon, and green: self-assembly monolayers (SAMs)). Note that, hydrogen atoms do not present here for clarity.

The VOCs adsorption ability of **B@A**, defined as the storage capacity normalized by that of homo-SURMOF **B**, is listed in Table 4.1 and it shows the VOC selective enhancement. The methanol adsorption ability **B@A** is close to

that of **B**, while for hydrocarbons the hetero-SURMOFs unprecedentedly show an uptrend storage capacity with increasing the size of VOCs. Such a property is different to that of homo-SURMOF **B**. With increasing the size of VOCs, the storage capacity/adsorption ability of **B** decreases due to the limitations of pore structure. However, the antithetic situation of **B**@**A** mainly attributes to the emancipated intrinsic storage capacity of bottom SURMOF **A**. We attribute this phenomenon to a strong interaction between top-deposited MOF **B** particles and pre-formed MOF **A** thin film. This strong interaction appears to overcome the (known) surface barrier of **A** at the interface between the two MOF components.

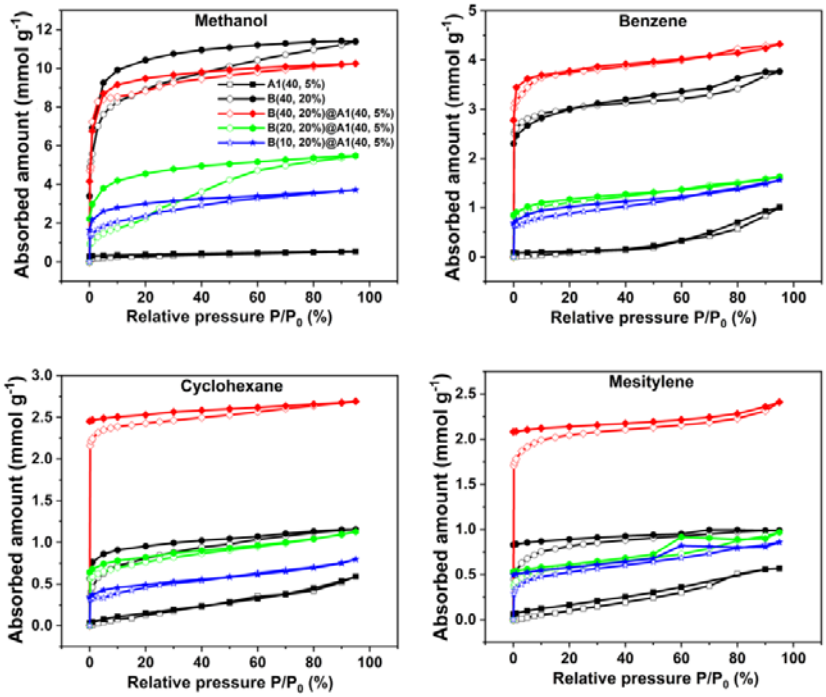

Figure 4.11. The VOCs sorption isotherms of **B**(10/20/40)@**A1**(40) and homo-phases of SURMOF **A1** and **B**.

Speculating from the enhanced adsorption property and the morphology of hetero-SURMOFs (Figure 4.7), continuous SURMOF **A** thin film is like a "container" with closed opening that VOCs cannot penetrate directly (Figure 4.10b), while the top-deposited discrete MOF **B** particles act as "funnels"

(Figure 4.10a) to reduce the surface barrier of SURMOF **A** locally, through which section VOCs can penetrate more effectively into the "container" (Figure 4.10c). Under the synergistic effects of heterostructure, the VOCs adsorption ability of hetero-SURMOF **B@A** is enhanced greatly. Substantiating this explanation and concept of molecular funneling at hetero-structured SURMOFs, the impacts of growth parameters, including the deposited quantity of MOF components, the crystallinity of upper SURMOF **B** and the linkers used in bottom SURMOF **A**, on the VOCs sorption property of hetero-SURMOFs were systematically studied as follows.

4.2.3 The impact of deposition cycles of MOF components (the size of "funnel" and "container") on the VOCs adsorption property of hetero-SURMOFs.

Herein, hetero-SURMOF **B@A1** is selected for discussion for clarity. In order to investigate the impact of the deposited quantity of upper SURMOF **B** on the sorption property of hetero-SURMOF **B@A1**, 10, 20 and 40 cycles SURMOF **B** were deposited on 40 cycles SURMOF **A1**. Samples are denoted as **B(10/20/40)@A1(40)**. The sorption isotherms of methanol, benzene, cyclohexane and mesitylene are shown in Figure 4.11. The total storage capacity of hetero-SURMOF **B@A1** increases with more quantity of SURMOF **B** deposited on pre-formed SURMOF **A1**, and **B(40)@A1(40)** has the highest storage capacity. The morphology of **B(20/40)@A1(40)** are shown in Figure 4.12. As can be seen from this figure, more interface is created by depositing more MOF **B** through which the VOCs are easier to funnel into bottom SURMOF **A1**. Moreover, the uptake of 1,3,5-triisopropylbenzene (molecular size 9.3 Å) on **B(40)@A1(40)** was also studied as a blind test, which shows a rather low storage capacity (Figure 4.13) because of the molecule larger than the size of "funnels" (4.6 and 9 Å).

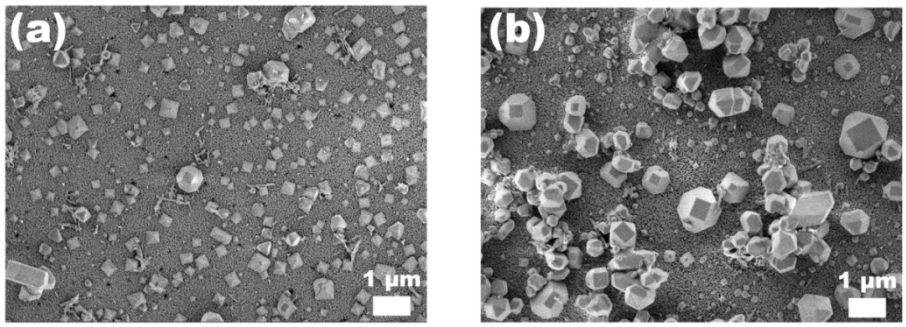

Figure 4.12. The morphology of (a) hetero-SURMOF **B(20, 20%)@A1(40, 5%)**, and (b) **B(40, 20%)@A1(40, 5%)**

Viewing from the data of hetero-SURMOF **B@A1** in Table 4.1 and Figure 4.11, it is obvious that below the threshold of funnel size, the larger the VOC is, the greater the adsorption ability of **B(40)@A1(40)** is achieved. This selective adsorption ability of a hetero-SURMOF is a promising novel concept in VOCs sensing and recognition. In turn, **B(40)@A1(40)** is also a good candidate for VOCs removal (capture). The unique selective adsorption ability of hetero-SURMOFs attribute to the synergistic effects of heterostructure interface. In the equilibrium state of the adsorption, the penetration of VOCs in and out the pores of **B@A1** should be equal. There is no doubt that VOCs can only funnel into SURMOF **A1** through the interface unblocked by top-deposited SURMOF **B** particles. However, the way for VOCs out has two possibilities: one is the unblocked interface; the other approach is to spill over into the volume of SURMOF **A1** which exhibits a still blocked surface area (absence of **B** particles). We deduce from our data that absorbed VOC molecules can obviously break through the surface barrier from inside to outside of SURMOF **A1**, and open “windows” for such VOCs spillover. Unfortunately, it is impossible to confirm the size of those “windows”, but this much is certain that the smaller the VOC is, the more likely it is to spill over. It means that large VOCs are more likely trapped in SURMOF **A1** and thus it follows the uptrend with molecular size for higher adsorption ability.

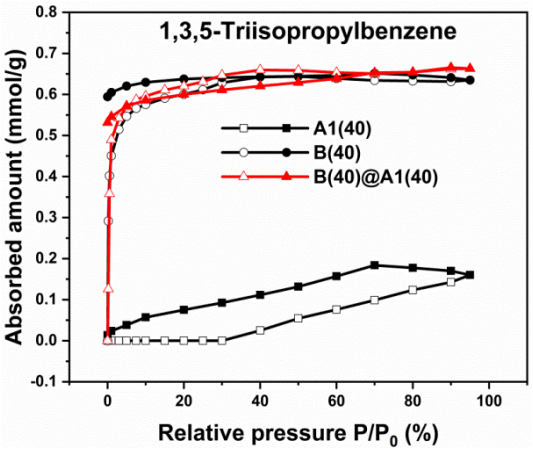

Figure 4.13. The 1,3,5-triisopropylbenzene adsorption isotherms of hetero-SURMOF **B**@**A1** and homo-phases SURMOF **A1** and **B**.

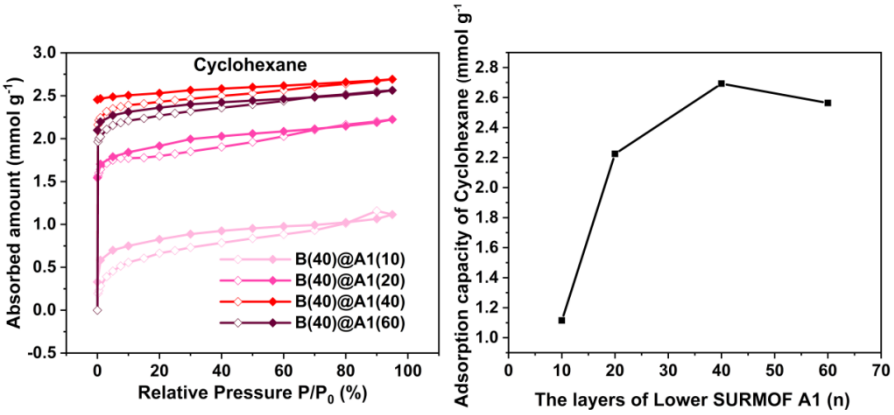

Figure 4.14. (a) The cyclohexane isotherms of hetero-SURMOF **B**@**A1** with 40 cycles SURMOF **B** on the top of 10, 20, 40 and 60 cycles of SURMOF **A1**; (b) the comparison of the cyclohexane adsorption capacity of hetero-SURMOFs **B(40)**@**A(10/20/40/60)**.

Similarly, the impact of the thickness of bottom SURMOF **A1** on the sorption property of hetero-SURMOF was studied. Hetero-SURMOFs **B(40)**@**A1(10/20/40/60)** were fabricated using stepwise LPE method. For the sake of clarity, cyclohexane was used as probe molecule to test the sorption property of hetero-SURMOFs. The sorption isotherms are shown in Figure 4.14 from which we can see that the total storage capacity of hetero-SURMOF

is rapidly enhanced from 10 to 20 cycles of SURMOF **A1**. In this range, the top-deposited MOF **B** particles are efficient to funnel VOCs into SURMOF **A1**. Afterwards, the storage capacity enhancement of hetero-SURMOF slows down and even begins to decrease by depositing more cycles SURMOF **A1**, which means that the molecular funneling via **B** particles is less efficient. This observation tells us that the thickness of SURMOF **A1** and **B** (the size of "container" and "funnel") has nonnegligible influence on the VOCs adsorption of hetero-SURMOFs. In summary, hetero-SURMOF of 40 cycles SURMOF **B** on the top of 40 cycles SURMOF **A1** is best case for studying the VOCs adsorption in this work.

4.2.4 The impact of the crystallinity of top-deposited MOF B (the quality of "funnel") on the VOCs adsorption property of hetero-SURMOF B@A1.

The crystallinity of top-deposited MOF **B** has profound impact on the interaction with bottom SURMOF **A1**, which would further affect the adsorption property of hetero-SURMOFs. Namely, well-crystalized **B** particles exhibit strong interaction with SURMOF **A1** and are efficient to remove the surface barrier at the interface, so VOCs can be easily funneled. However, the top-deposited MOF **B** with poor crystallinity is inefficient to clear the surface barrier of SURMOF **A1**, which leads to the low total storage capacity of hetero-SURMOFs. According to our previous research, the crystallinity of **B** are controlled by adjusting the amount of water in the linker solution during the fabrication process.[46] For SURMOF **A1**, integrating 5% water in H_2bdc solution is always used in this work because it is the best parameter to fabricate thin films with high quality. Hetero-SURMOFs were fabricated with various water amount (0%, 5% and 20%, and samples are denoted as **B(0%/5%/20%)@A1(5%)**) integrated in H_3btc linker solution to explore the

VOCs adsorption property. The crystallinity of obtained hetero-SURMOFs was checked by GIXRD and shown in Figure 4.15.

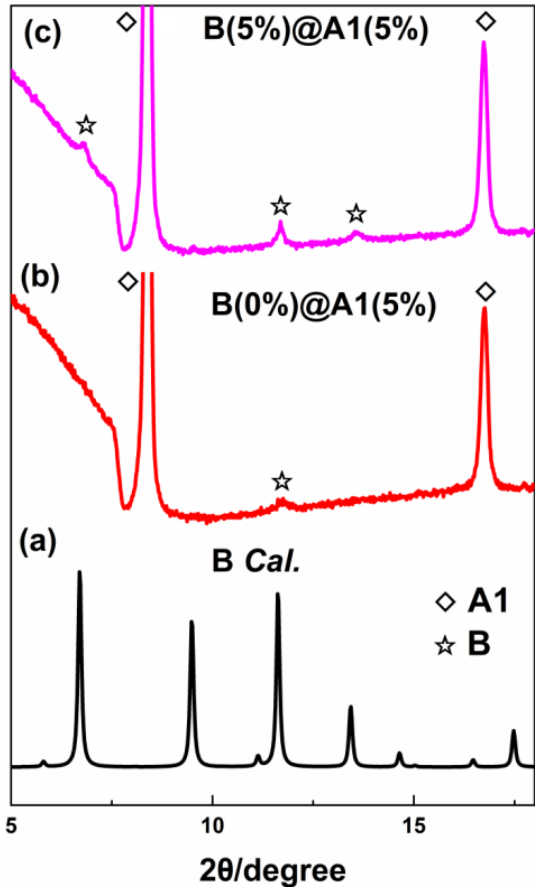

Figure 4.15. The XRD patterns of (a) calculated MOF **B**, (b) hetero-SURMOF **B(0%)@A1(5%)** and (c) hetero-SURMOF **B(5%)@A1(5%)**.

The relationship between the crystallinity of top-deposited **B** and the VOCs storage capacity of hetero-SURMOFs is presented in Figure 4.16a from which it can be seen that **B(20%)@A1(5%)** shows greatly-enhanced VOCs storage capacity compare to the other two cases. We attribute this effect to a facilitated the anchoring of H_3btc on the surface of SURMOF **A1** by increasing the water amount in linker solution. It as well as promotes the further crystal growth of **B**. By this means, the subsequently deposited **B** particles establish strong interaction with bottom SURMOF **A1**. However, with no or less additional water

in the linker solution the interfacial contact of **B** with **A1** is less. Differing from well-connected randomly-distributed **B** particles, simply mechanically-covered **B** on top of **A1** acts like a truncated “funnel” through which VOC molecules cannot penetrate into the “container” (shown in Figure 4.16a). In addition, the poor crystallinity resulted low storage capacity of **B** also attributes to the lower total VOCs storage capacity of hetero-SURMOFs **B(0%/5%)@A1(5%)**.

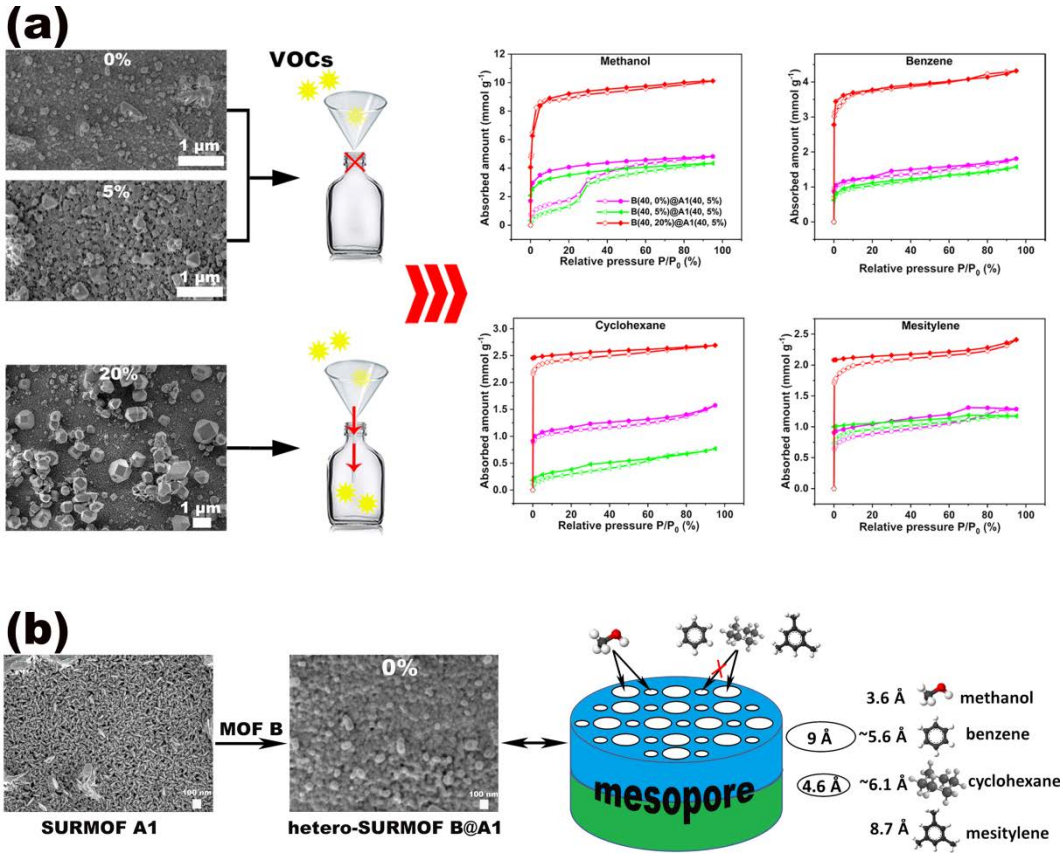

Figure 4.16. (a) The relationship between the crystallinity of MOF **B** and the VOCs adsorption capacity of hetero-SURMOF **B@A1**; (b) the schematic of mesopore in hetero-SURMOF **B@A1** which are formed by the overlay of continuous MOF **B** thin films on SURMOF **A1**, hereby the two type of windows in mesopore represents the two kind of apertures in MOF **B**. Note that, 0%, 5% or 20% means the sample was fabricated by integrating 0, 5 and 20% water in H_3btc solution of upper SURMOF **B**.

Interestingly, there is a hysteresis in the methanol sorption isotherm of hetero-SURMOFs **B(0%/5%)@A1(5%)**, which can be explained by the formation of mesopores in heterostructures (Figure 4.16b). Without (or with tiny amount) additional water integrated in the linker solution, MOF **B** is deposited on top of SURMOF **A1** as continuous film, by which the voids in SURMOF **A1** (see the SEM) are enclosed. However, the hysteresis are absent in the hydrocarbons isotherms of hetero-SURMOFs **B(0%/5%)@A1(5%)**. This may ascribe to the inefficient transportation of these enlarged hydrocarbon molecules from upper MOF **B** thin film to bottom mesopores.

4.2.5 The impact of the linkers used in SURMOF A on the adsorption property of hetero-SURMOFs B@A.

Hetero-SURMOFs **B@A** show selective adsorption ability to large VOC molecules and this selectivity is modified by adopting different linkers in bottom SURMOF **A**. The selectivity of hetero-SURMOFs **B@A1/A2/A3** to different VOCs are shown in Figure 4.17. Comparing to **B@A1**, we find that the storage capacity of small VOCs (benzene and cyclohexane) decreases more or less but that of large VOCs (mesitylene) increases by using longer H_2bpdc (**A2**) or sterically more demanding H_2TF-bdc (**A3**) as linkers to construct the bottom framework. It means that the selective adsorption ability of hetero-SURMOFs **B@A** can be tuned by employing different linkers in bottom SURMOF **A**. This tunable VOCs selective adsorption ability of hetero-SURMOFs **B@A** is attributed to the modified intralayer pore and interlayer spacing of SURMOF **A** when using functionalized or enlarged linkers (Figure 4.6). The enlarged pores reduce the energy barrier, which leads to more effective spillover of small VOCs but enhances the storage capacity of large VOCs because of the increased porosity. Thus, the tunable VOCs selective adsorption ability of **B@A** can be utilized for sensing, recognizing or even eliminating aromatics with specific size.

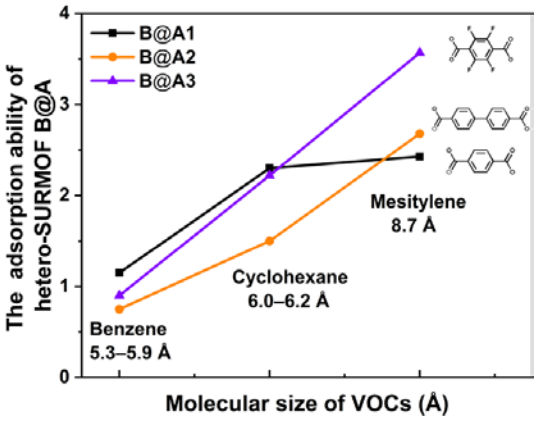

Figure 4.17 The tunable VOCs selective adsorption ability of hetero-SURMOF **B@A**. Herein, only the hydrocarbons are shown.

4.3 Conclusion

The first example of 2D-3D composite hetero-SURMOF **B@A** has been synthesized by using the liquid-phase stepwise layer-by-layer deposition approach. The characterizations of GIXRD, 2D-GIXRD, SEM and IRRAS confirmed the presence of two phases in the heterostructures. Interestingly, different linkers (bdc, bpdc and TF-bdc) adopted in bottom SURMOF **A** (**A1**, **A2** and **A3**) induce the preferred orientation of top-deposited SURMOF **B**, shown (100), (111) and no preferred orientation on top of SURMOF **A1**, **A2** and **A3**, respectively. The obtained hetero-SURMOFs **B@A** show higher VOCs storage capacity even than that of both homo-SURMOFs **A** and **B**. Importantly, we discovered a counter-intuitive uptrend of the selective absorption capacity for the hetero-SURMOF with molecular size of VOCs. We suggest “molecular funneling” to capture our findings by a metaphoric term. The impact of deposited mass of two MOF components, the crystallinity of upper SURMOF **B**, and the linkers used in bottom SURMOF **A** on the VOCs adsorption of hetero-SURMOFs were systematically studied. Eventually, we found that the hetero-SURMOF of 40 cycles SURMOF **B** fabricated with 20% water in H_3btc solution on top of 40 cycles SURMOF **A** synthesized with 5%

water in H_2bdc solution is the best case for VOCs adsorption in this work. Our work opens the door to a novel concept of materials design for VOC sensing, recognition and capture.

4.4 References

[1] R. Ghosh Chaudhuri, S. Paria, *Chem. Rev.* **2012**, *112*, 2373.

[2] N. Masoumifard, R. Guillet-Nicolas, F. Kleitz, *Adv. Mater.* **2018**, *30*, 1704439.

[3] D. Kim, G. Lee, S. Oh, M. Oh, *Chem. Commun.* **2018**, *55*, 43.

[4] Y. Mao, W. Cao, J. Li, L. Sun, X. Peng, *Chem. Eur. J.* **2013**, *19*, 11883.

[5] Z. Song, F. Qiu, E. W. Zaia, Z. Wang, M. Kunz, J. Guo, M. Brady, B. Mi, J. J. Urban, *Nano Lett.* **2017**, *17*, 6752.

[6] S. Wu, G. Zhuang, J. Wei, Z. Zhuang, Y. Yu, *J. Mater. Chem. A* **2018**, *6*, 18234.

[7] H. Furukawa, K. E. Cordova, M. O'Keeffe, O. M. Yaghi, *Science* **2013**, *341*, 1230444.

[8] V. Guillerm, L. Weselinski, Y. Belmabkhout, A. J. Cairns, V. D'Elia, L. Wojtas, K. Adil, M. Eddaoudi, *Nat. Chem.* **2014**, *6*, 673.

[9] J. R. Li, J. Sculley, H. C. Zhou, *Chem. Rev.* **2012**, *112*, 869.

[10] S. Yang, X. Lin, A. J. Blake, G. S. Walker, P. Hubberstey, N. R. Champness, M. Schroder, *Nat. Chem.* **2009**, *1*, 487.

[11] R. W. Huang, Y. S. Wei, X. Y. Dong, X. H. Wu, C. X. Du, S. Q. Zang, T. C. W. Mak, *Nat. Chem.* **2017**, *9*, 689.

[12] C. A. Trickett, T. M. Osborn Popp, J. Su, C. Yan, J. Weisberg, A. Huq, P. Urban, J. Jiang, M. J. Kalmutzki, Q. Liu, J. Baek, M. P. Head-Gordon, G. A. Somorjai, J. A. Reimer, O. M. Yaghi, *Nat. Chem.* **2019**, *11*, 170.

[13] T. Li, J. E. Sullivan, N. L. Rosi, *J. Am. Chem. Soc.* **2013**, *135*, 9984.

[14] P. Á. Szilágyi, M. Lutz, J. Gascon, J. Juan-Alcañiz, J. van Esch, F. Kapteijn, H. Geerlings, B. Dam, R. van de Krol, *CrystEngComm* **2013**, *15*, 6003.

[15] D. A. Sarigiannis, S. P. Karakitsios, A. Gotti, I. L. Liakos, A. Katsoyiannis, *Environ. Int.* **2011**, *37*, 743.

[16] J. B. DeCoste, G. W. Peterson, *Chem. Rev.* **2014**, *114*, 5695.

[17] E. Barea, C. Montoro, J. A. Navarro, *Chem. Soc. Rev.* **2014**, *43*, 5419.

[18] M. T. Luebbers, T. Wu, L. Shen, R. I. Masel, *Langmuir* **2010**, *26*, 11319.

[19] A. Planchais, S. Devautour-Vinot, S. Giret, F. Salles, P. Trens, A. Fateeva, T. Devic, P. Yot, C. Serre, N. Ramsahye, G. Maurin, *J. Phys. Chem. C* **2013**, *117*, 19393−19401.

[20] K. Vellingiri, J. E. Szulejko, P. Kumar, E. E. Kwon, K. H. Kim, A. Deep, D. W. Boukhvalov, R. J. Brown, *Sci. Rep.* **2016**, *6*, 27813.

[21] L. E. Kreno, K. Leong, O. K. Farha, M. Allendorf, R. P. Van Duyne, J. T. Hupp, *Chem. Rev.* **2012**, *112*, 1105.

[22] Z. Hu, B. J. Deibert, J. Li, *Chem. Soc. Rev.* **2014**, *43*, 5815.

[23] H. Yamagiwa, S. Sato, T. Fukawa, T. Ikehara, R. Maeda, T. Mihara, M. Kimura, *Sci. Rep.* **2014**, *4*, 6247.

[24] M. Tu, S. Wannapaiboon, K. Khaletskaya, R. A. Fischer, *Adv. Funct. Mater.* **2015**, *25*, 4470.

[25] M. Tu, R. A. Fischer, *J. Mater. Chem. A* **2014**, *2*, 2018.

[26] S. Wannapaiboon, M. Tu, R. A. Fischer, *Adv. Funct. Mater.* **2014**, *24*, 2696.

[27] K. J. Kim, P. Lu, J. T. Culp, P. R. Ohodnicki, *ACS Sens.* **2018**, *3*, 386.

[28] L. Heinke, M. Tu, S. Wannapaiboon, R. A. Fischer, C. Wöll, *Micropor. Mesopor. Mater.* **2015**, *216*, 200.

[29] X. Yang, S. Yuan, L. Zou, H. Drake, Y. Zhang, J. Qin, A. Alsalme, H.-C. Zhou, *Angew. Chem. Int. Ed.* **2018**, *57*, 3927 ; *Angew. Chem.* **2018**, *130*, 3991.

[30] S. Choi, T. Kim, H. Ji, H. J. Lee, M. Oh, *J. Am. Chem. Soc.* **2016**, *138*, 14434.

[31] Y. Gu, Y. N. Wu, L. Li, W. Chen, F. Li, S. Kitagawa, *Angew. Chem. Int. Ed.* **2017**, *56*, 15658; *Angew. Chem*. **2017**, *129*, 15864.

[32] K. Koh, A. G. Wong-Foy, A. J. Matzger, *Chem. Commun.* **2009**, *41*, 6162.

[33] W. R. Lee, D. W. Ryu, W. J. Phang, J. H. Park, C. S. Hong, *Chem. Commun.* **2012**, *48*, 10847.

[34] J. Zheng, G. Wang, M. Pan, D. Guo, Q. Zhao, B. Li, R. Li, *Micropor. Mesopor. Mater.* **2015**, *206*, 114.

[35] W. Jin, J. Ma, H. Ma, X. Li, Y. Wang, *J. Solid State Chem.* **2018**, *267*, 6.

[36] T. Rodenas, I. Luz, G. Prieto, B. Seoane, H. Miro, A. Corma, F. Kapteijn, I. X. F. X. Llabres, J. Gascon, *Nat. Mater.* **2015**, *14*, 48.

[37] C. G. Carson, K. Hardcastle, J. Schwartz, X. Liu, C. Hoffmann, R. A. Gerhardt, R. Tannenbaum, *Eur. J. Inorg. Chem.* **2009**, *2009*, 2338.

[38] O. Shekhah, H. Wang, S. Kowarik, F. Schreiber, M. Paulus, M. Tolan, C. Sternemann, F. Evers, D. Zacher, F. A. Fischer, C. Wöll, *J. Am. Chem. Soc.* **2007**, *129*, 15118.

[39] Z. Wang, S. Wannapaiboon, K. Rodewald, M. Tu, B. Rieger, R. A. Fischer, *J. Mater. Chem. A* **2018**, *6*, 21295.

[40] S. Wannapaiboon, M. Tu, K. Sumida, K. Khaletskaya, S. Furukawa, S. Kitagawa, R. A. Fischer, *J. Mater. Chem. A* **2015**, *3*, 23385.

[41] M. Tu, S. Wannapaiboon, R. A. Fischer, *Dalton Trans.* **2013**, *42*, 16029.

[42] Z. Wang, J. Liu, B. Lukose, Z. Gu, P. G. Weidler, H. Gliemann, T. Heine, C. Wöll, *Nano Lett.* **2014**, *14*, 1526.

[43] B. Liu, M. Tu, D. Zacher, R. A. Fischer, *Adv. Funct. Mater.* **2013**, *23*, 3790.

[44] J. Liu, B. Lukose, O. Shekhah, H. K. Arslan, P. Weidler, H. Gliemann, S. Brase, S. Grosjean, A. Godt, X. Feng, K. Mullen, I. B. Magdau, T. Heine, C. Wöll, *Sci. Rep.* **2012**, *2*, 921.

[45] H. K. Arslan, O. Shekhah, D. C. Wieland, M. Paulus, C. Sternemann, M. A. Schroer, S. Tiemeyer, M. Tolan, R. A. Fischer, C. Wöll, *J. Am. Chem. Soc.* **2011**, *133*, 8158.

[46] Z. Wang, K. Rodewald, R. Medishetty, B. Rieger, R. A. Fischer, *Cryst. Growth Des.* **2018**, *18*, 7451.

[47] H. Wu, Q. Gong, D. H. Olson, J. Li, *Chem. Rev.* **2012**, *112*, 836.

[48] O. Shekhah, J. Liu, R. A. Fischer, C. Wöll, *Chem. Soc. Rev.* **2011**, *40*, 1081.

[49] M. Tu, S. Wannapaiboon, R. A. Fischer, *Inorg. Chem. Front.* **2014**, *1*, 442.

[50] O. Shekhah, H. Wang, S. Kowarik, F. Schreiber, M. Paulus, M. Tolan, C. Sternemann, F. Evers, D. Zacher, R. A. Fischer, C. Wöll, *J. Am. Chem. Soc.* **2007**, *129*, 15118.

[51] O. Shekhah, H. Wang, D. Zacher, R. A. Fischer, C. Wöll, *Angew. Chem. Int. Ed.* **2009**, *48*, 5038; *Angew. Chem.* **2009**, *121*, 5138.

[52] M. Hanke, H. K. Arslan, S. Bauer, O. Zybaylo, C. Christophis, H. Gliemann, A. Rosenhahn, C. Wöll, *Langmuir* **2012**, *28*, 6877.

[53] M. Meilikhov, S. Furukawa, K. Hirai, R. A. Fischer, S. Kitagawa, *Angew. Chem. Int. Ed.* **2013**, *52*, 341; *Angew. Chem.* **2013**, *125*, 359.

Chapter 5

Defects creation in surface mounted metal-organic framework thin films

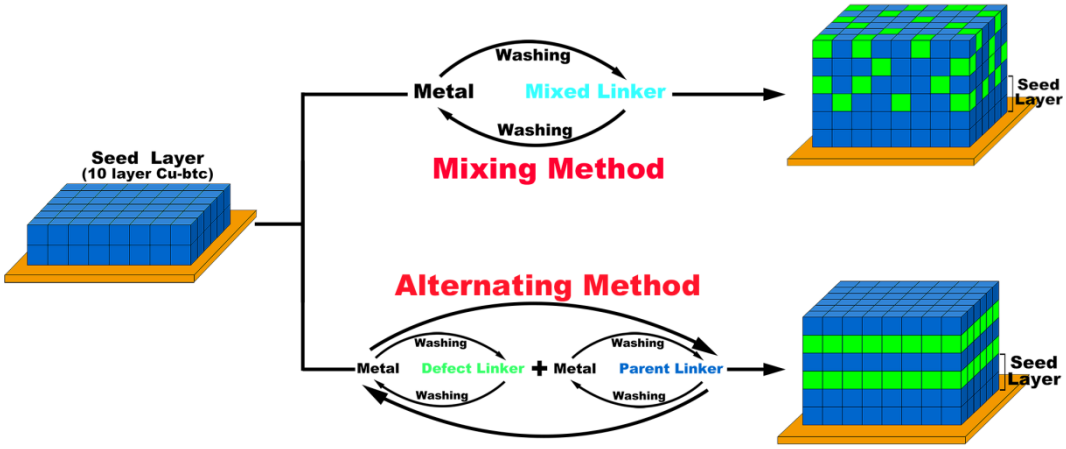

Abstract

Defect engineering is one of practical strategies for tailoring the properties of metal-organic frameworks (MOFs); however, it is still a great challenge to control the formation of defects in MOFs (e.g. quantity and distribution). This situation can be improved in MOF thin films by taking advantage of stepwise liquid-phase epitaxy (LPE). Herein, two methods based on the stepwise LPE, named mixing method and alternating method, are proposed for incorporating defects in surface mounted MOF (SURMOF) HKUST-1 by partially substituting the parent H_3btc (benzene-1,3,5-tricarboxylic acid) linker with truncated linker H_2ip (isophthalic acid), H_2OH-ip (5-hydroxyisophthalic acid) and H_2pydc (3,5-pyridinedicarboxylic acid). The phase of obtained SURMOFs were confirmed by X-ray diffraction (XRD), infrared reflection absorption spectroscopy (IRRAS) and Raman spectroscopy. The techniques of ^{1}H nuclear magnetic resonance spectroscopy (NMR), ultraviolet–visible (UV-Vis) spectroscopy, methanol adsorption and scanning electron microscope (SEM) provide the approaches for detecting defects in SURMOF HKUST-1. These two methods show enhanced controllability to the defect formation in MOF thin films.

5.1. Introduction

Metal-organic frameworks (MOFs) are a novel class of crystalline microporous materials with large internal surface area, controlled porosities, tunable properties, *etc*.,[1-3] which show great potential in many application fields like storage,[4] separation[5], catalysis[6] and chemical sensing[7]. However, there are many challenges needed to be solved before stepping into the real world technologies for MOFs. Among them, how to improve the performance or how to synthesize MOF materials with multiple functionalities is a primary one.[8] Especially under the pressure of sustainable development, this situation is more urgent. In order to endow MOFs with multifunctionalities, many synthetic strategies have been proposed.[9-16] In these strategies, defect engineering is one of the most studied one for tailoring MOFs properties, which creates metal and linker vacancies in MOFs by partially substituting the parent linker with so-called defective linker.[11] The presence of metal and linker vacancies enhances the intrinsic properties of MOFs, such as porosity,[17] catalysis[18] and magnetic properties,[19] or even creates new properties like charge transport.[20]

Defects can be formed in MOFs by artificial introducing, such as *de novo* synthesis[21] and post-synthetic treatment,[22] or even inherent formation.[23] However, it is still a great challenge to control the formation of defects in MOFs (e.g. quantity and distribution), which is important for kinetic and mechanism study in related processes. In bulk powder, defects are formed arbitrarily in MOF lattice under solvothermal conditions. Moreover, less amount defects tend to be incorporated for keeping structural integrity and lowering the lattice energy of whole system. For instance, defect-engineered HKUST-1 (also known as Cu_3btc_2, btc = benzene-1,3,5-tricarboxylate) can only incorporate the

defective linker of ip (isophthalate) at most 50% of feeding amount under solvothermal conditions.[24-25]

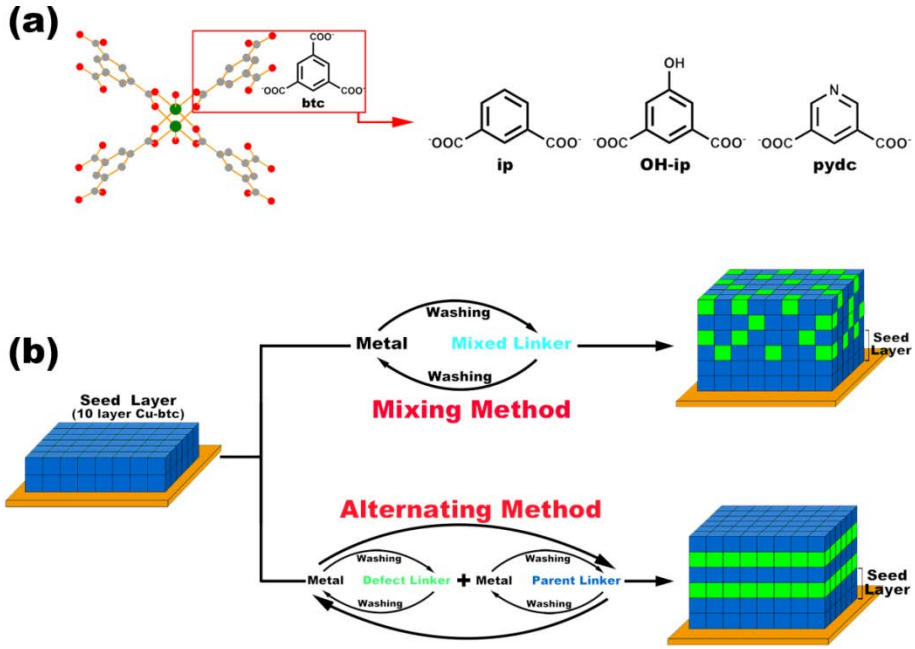

Figure 5.1. Schematic illustration of (a) DE-SURMOFs HKUST-1 formed by partially substituting parent H_3btc linker with defective linker H_2ip, H_2OH-ip or H_2pydc; and (b) the two methods for incorporating defects in SURMOF HKUST-1: the mixing method and alternating method.

Herein, we try to improve this situation in the case of MOF thin film by taking advantage of stepwise liquid-phase epitaxy (LPE, also known as Layer-by-Layer (LBL)) technique.[13, 26-27] Stepwise LPE is a promising technique for fabricating MOF thin films due to its high controllability to the growth process.[28] Typically, the metal and linker are dosed on the templating substrate in a sequential fashion with rinsing solvent after each step to remove the unreacted or physisorbed species. The obtained thin films are known as surface mounted MOFs (SURMOFs). Moreover, in combination with surface plasmon resonance (SPR) technique[27] and quartz crystal microbalance (QCM) sensor,[29] the stepwise LPE growth process can be monitored *in situ* by

recording the oscillation frequency change of the QCM sensor. Utilizing stepwise LPE, defect-engineered SURMOFs (DE-SURMOFs) could be prepared with high controllability by varying the component solution. Actually, no defect-engineered MOF thin film has been reported so far.

In this work, we attempt to synthesize DE-SURMOFs of HKUST-1 type by partially substituting parent H_3btc linker with a set of truncated H_2ip, H_2OH-ip (5-hydroxyisophthalic acid) or H_2pydc (3,5-pyridinedicarboxylic acid) using stepwise LPE technique (Figure 5.1a). Herein, we propose two methods for creating defects in SURMOF HKUST-1 (Figure 5.1b): (1) mixing method, as the name implied, the linker solution used in growth process is the mixture of parent and defective linker;[19] (2) alternating method, in which the substrate is separately exposed to parent linker solution and defective linker solution in an alternate way. The obtained DE-SURMOFs HKUST-1 were characterized by X-ray diffraction (XRD), infrared reflection absorption spectroscopy (IRRAS) and Raman spectroscopy to confirm that the structure of HKUST-1 does not change by incorporating defects. Afterwards, the measurements of ^{1}H nuclear magnetic resonance (NMR) spectroscopy, time-of-flight secondary ion mass spectroscopy (ToF-SIMS), ultraviolet–visible (UV-Vis) spectroscopy, methanol adsorption and scanning electron microscope (SEM) were performed as well to detect the defects incorporated in the lattice of HKUST-1. The advantage of two methods in the creation of defects in SURMOF HKUST-1 was compared at last.

5.2 Results and discussion

5.2.1 The growth of DE-SURMOFs HKSUT-1

The DE-SURMOFs HKUST-1 in this work were fabricated by using the stepwise LPE technique. The growth process of SURMOF can be learned from

the recorded frequency change against time (ΔF-t) curve. For clarity, the samples prepared by mixing method and alternating method are denoted as **ip_M** and **ip_A** (the cases of OH-ip and pydc are similar), respectively.

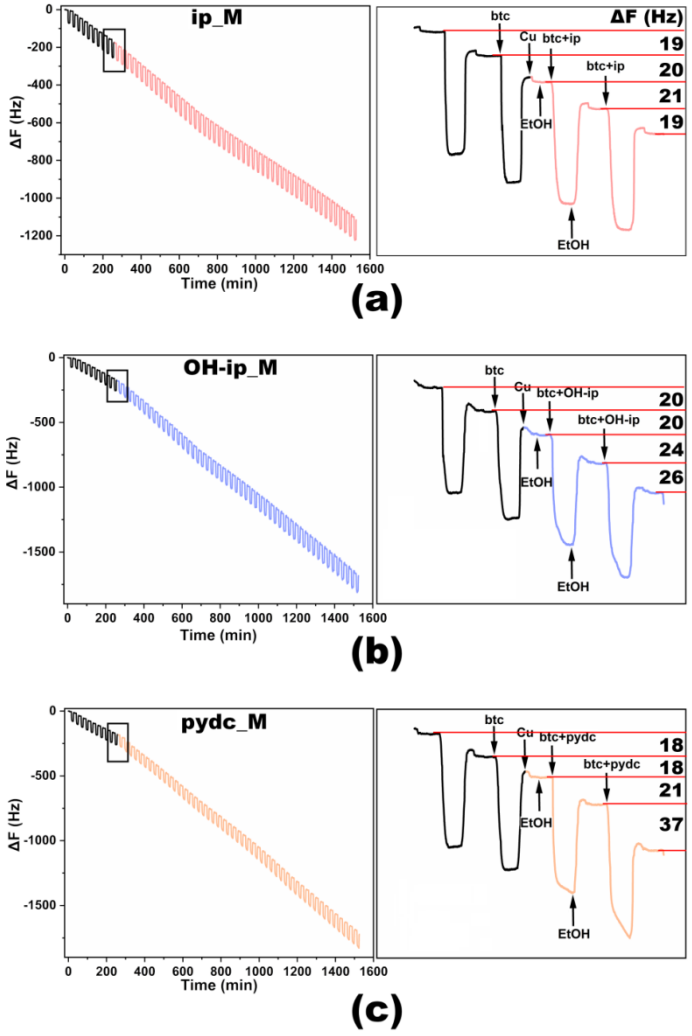

Figure 5.2. The ΔF-t growth curves of DE-SURMOFs HKUST-1 (a) **ip_M**, (b) **OH-ip_M** and (c) **pydc_M** fabricated by mixing method. The left column is the overview of thin film growth; the closer inspection of the joint of seed layer and DE-SURMOF are shown in right column in which the net ΔF of each step is indicated.

Mixing method. In this method, the parent and defective linker are integrated with 1 : 1 molar ratio as the linker solution for fabricating

DE-SURMOFs. Viewing from ΔF-t curves (left columns of shown in Figure 5.2), it is easy to know that there was mass deposited on substrate. The close observation (right columns of Figure 5.2) reveals that the defective linkers show diverse doping level (H_2ip < H_2OH-ip < H_2pydc) in SURMOF HKUST-1, which leads to the different mass deposition of the DE-SURMOF growth cycles. While the seed layer growth cycles, obviously, have similar mass deposition.

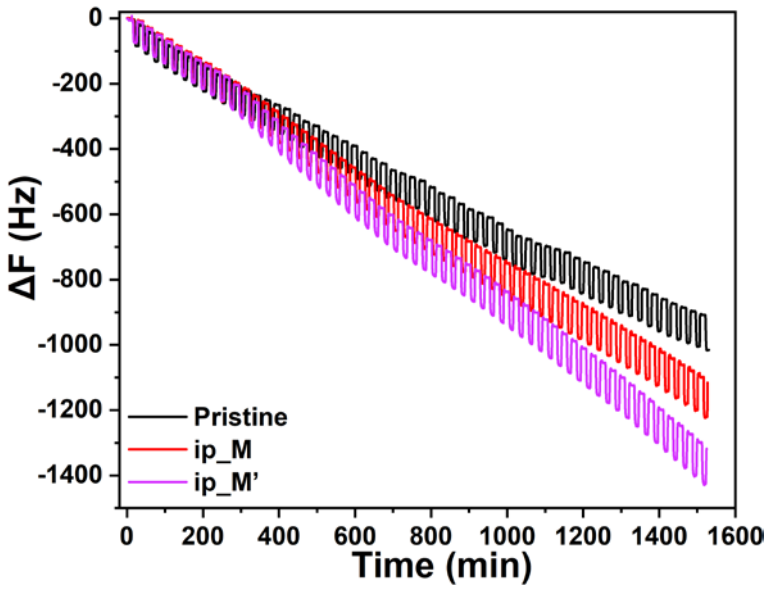

Figure 5.3. The ΔF-t growth curve of **ip_M** (red) and **ip_M'** (violet) and pristine SURMOF HKUST-1 (black). Herein, the DE-SURMOF HKUST-1 fabricated with the molar ratio of defective linker H_2ip and parent linker H_3btc 2 : 1 is named as **ip_M'**.

Moreover, DE-SURMOF HKUST-1 with higher defect density (denoted as **ip_M'**) was also fabricated by increasing the ratio of H_2ip (H_2ip : H_3btc = 2 : 1) in linker mixture solution. The ΔF-t growth curve is shown in Figure 5.3, from which we find that the mass deposited on substrate increases with raising the defect density of DE-SURMOF HKUST-1.

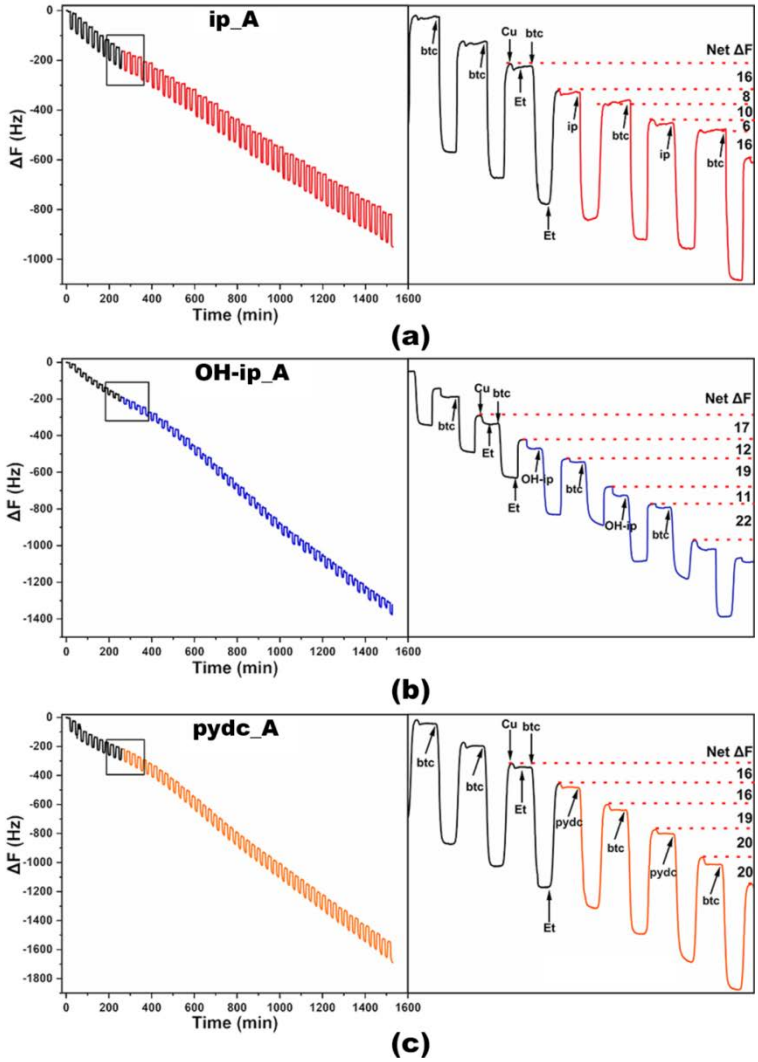

Figure 5.4. The ΔF-t growth curve of DE-SURMOFs HKUST-1 (a) **ip_A**, (b) **OH-ip_A** and (c) **pydc_A** fabricated by alternating method. The left column is the overview of thin film growth; the closer inspection of the joint of seed layer and DE-SURMOF are shown in the right column in which the net ΔF of each step is indicated.

Alternating method. In the method, the parent linker solution and defective linker solution are independently dosed on substrate in an alternate way. In a typical growth procedure, 10 cycles seed HKUST-1 were deposited firstly as seed layer, and then the loop of 1 cycle $Cu(OAc)_2$/H_3btc followed by 1 cycle $Cu(OAc)_2$/defective linker (ABAB fashion) were repeated 25 times to

obtain DE-SURMOF HKUST-1. The ΔF-t growth data shown in Figure 5.4 indicates the deposition of MOFs on substrate. Similarity, the diverse doping level of defective linkers leads to the different deposited mass of $Cu(OAc)_2$/defective linker dosing cycles (right column of Figure 5.4).

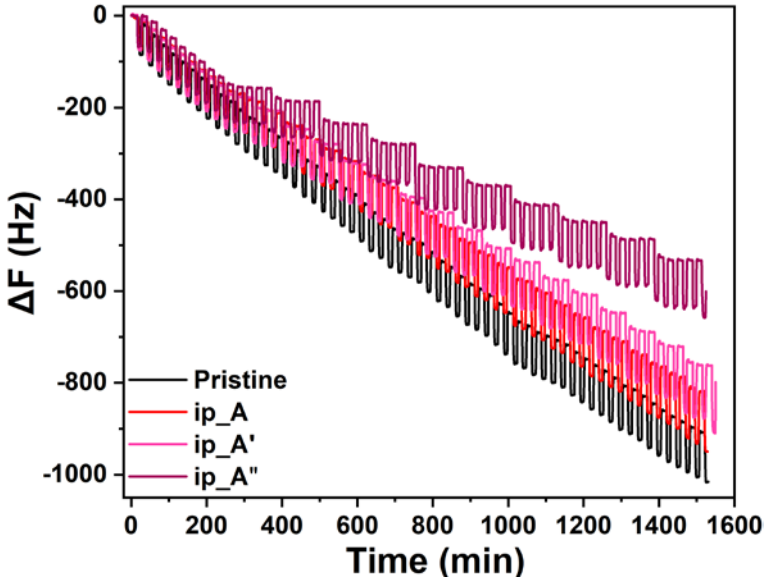

Figure 5.5. The frequency change against time (ΔF-t) growth curves of **ip_A** (red), **ip_A'** (pink) and **ip_A"** (dark red) and pristine SURMOF HKUST-1 (black).

Furthermore, DE-SURMOFs HKUST-1 with 2 and 4 cycles $Cu(OAc)_2$/ip in the repeating loop were fabricated as well (denoted as **ip_A'** and **ip_A"**, respectively), and the ΔF-t curves are shown in Figure 5.5. The mass of DE-SURMOF HKUST-1 deposited on substrate decreases with improving the $Cu(OAc)_2$/defective linker dosing cycles.

5.2.2 Phase confirmation of DE-SURMOF HKSUT-1

The purpose of synthesizing defected-engineered MOFs is modification the intrinsic properties of MOFs without changing the overall structure. Herein, the obtained DE-SURMOFs HKUST-1 was firstly characterized by XRD, IRRAS and Raman spectroscopy to confirm the structure.

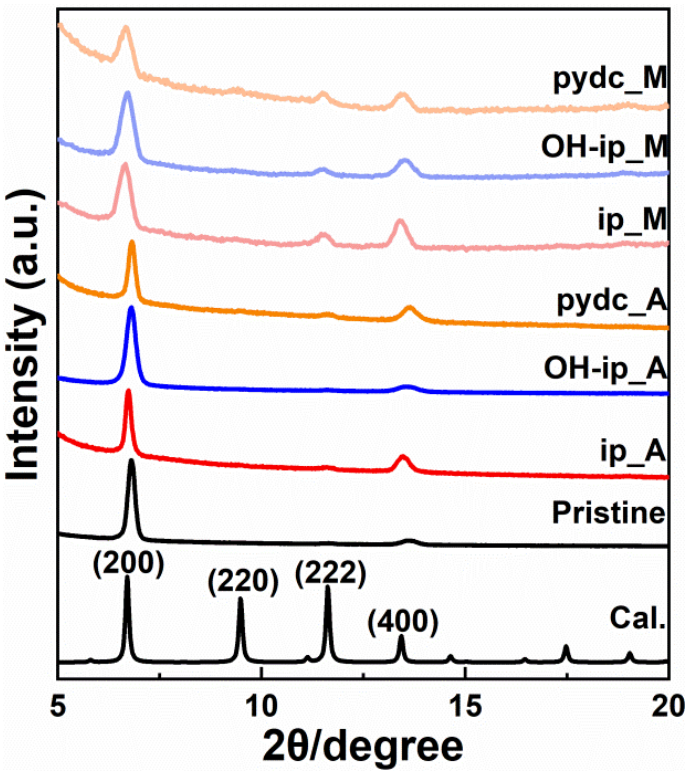

Figure 5.6. The XRD patterns of DE-SURMOFs HKUST-1 fabricated by mixing method (light color) and alternating method (dark color).

XRD patterns. The out-of-plane XRD patterns are presented in Figure 5.6, from which we can see that the peaks of DE-SURMOFs are assign to the phase of HKUST-1 and the obtained thin films show a preferred orientation of (100). By contrasting the XRD peaks, we believe that DE-SURMOFs fabricated via alternating method show higher crystallinity than those prepared via mixing method because the latter one display broader XRD peaks than the former one. The 2D-GIXRD, shown in Figure 5.7, was also performed on the thin films synthesized by alternating method as a further proof of HKUST-1 phase presence. Moreover, the crystallinity of **ip_M'**, **ip_A'** and **ip_A"** with higher defect density were checked by out-of-plane XRD as well (Figure 5.8). Viewing from this figure, it is obvious that more defects incorporating in SURMOF HKUST-1 weaken the crystallinity.

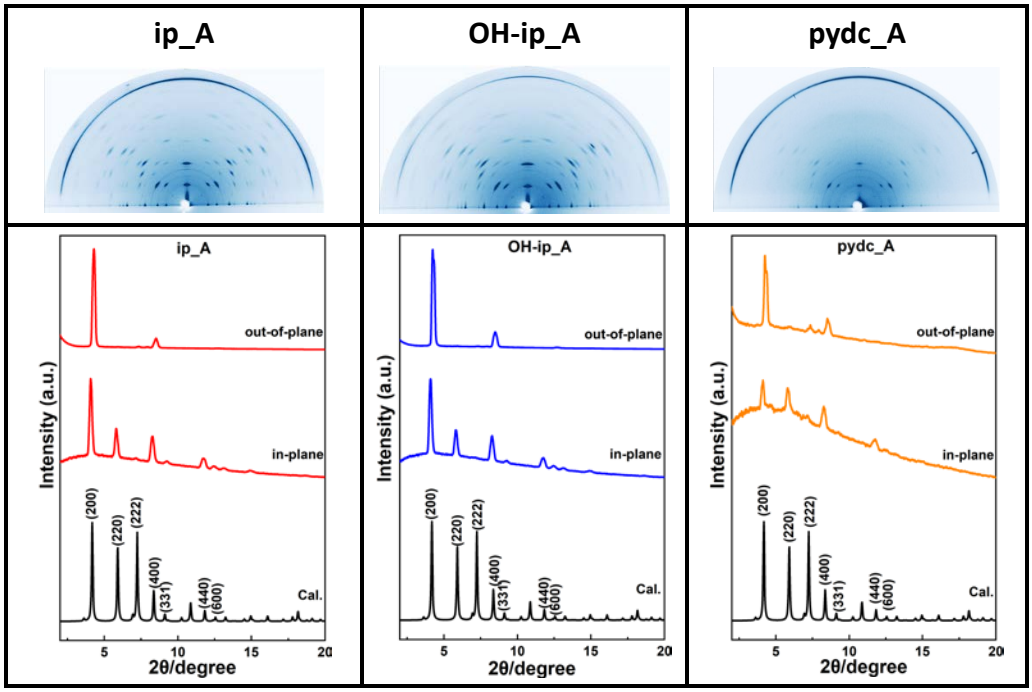

Figure 5.7. Two-dimensional grazing incidence X-ray diffraction (2D-GIXRD) patterns of DE-SURMOFs HKUST-1 fabricated by alternating method, which were performed at Beamline 9, DELTA Synchrotron under room temperature (using X-ray source energy of 13 KeV and wavelength of 0.9607 Å, refined sample-to-detector distance of 354.37 mm). The calculated pattern was obtained from Mercury by setting the wavelength as 0.9607 Å.

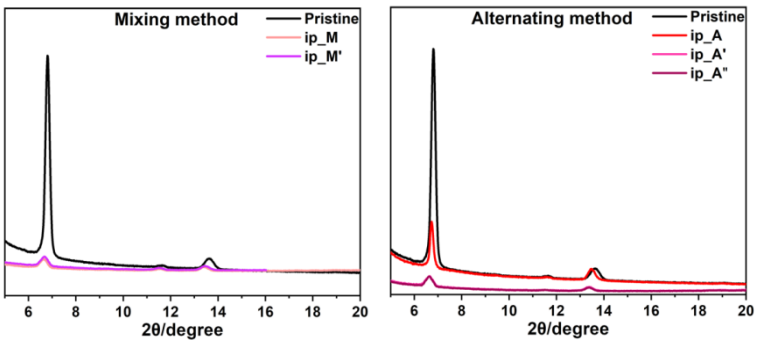

Figure 5.8. The comparation of XRD patterns of (a) **ip_M** and **ip_M'**; and (b) **ip_A, ip_A'** and **ip_A"** with pristine SURMOF HKUST-1.

Moreover, the deposition of pure HKUST-1 as seed layer has significant impact on the crystallinity of DE-SURMOFs. As we can see in Figure 5.9, the

presence of seed layer greatly promotes the crystallinity and crystallographic orientation of obtained DE-SURMOFs HKUST-1.

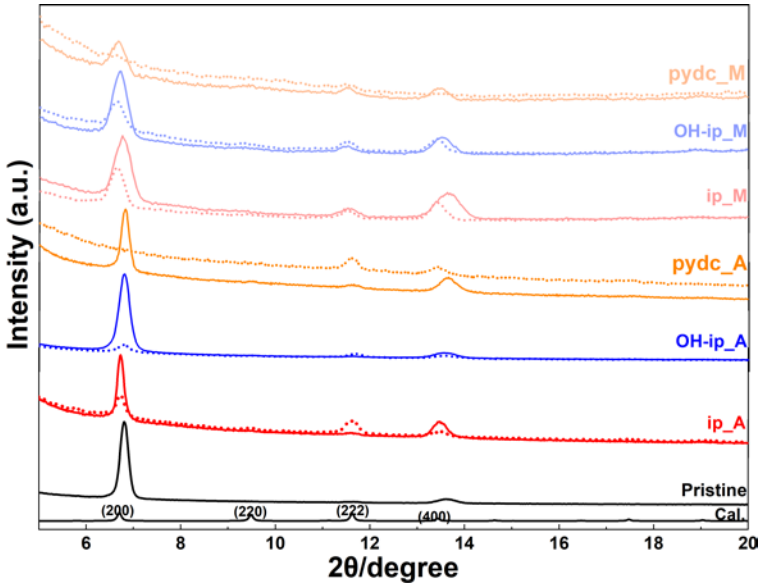

Figure 5.9. The comparation of XRD patterns of DE-SURMOFs HKUST-1 fabricated on substrate without (dashed) and with (solid) 10 cycles HKUST-1 seed layer.

IRRAS and Raman Spectra. Furthermore, the IRRAS and Raman spectroscopy were measure as well to verify the phase of DE-SURMOFs HKUST-1. The IRRAS and Raman spectra are shown in Figure 5.10 and 5.11, respectively. For the DE-SURMOFs HKUST-1 defected by ip and OH-ip, the IRRAS and Raman spectra agree well with that of pristine one. However, two additional peaks located at 1631 and 1572 cm^{-1} are observed in the IRRAS spectra of **pydc_M** and **pydc_A**, which are assigned to the COO^- vibration originating from mixed $[Cu_2(btc/pydc)_n(OAc)_{4-n}]$ paddle-wheels and $[Cu_2(OAc)_4]$ paddle-wheels.[30] The presence of mixed $[Cu_2(btc/pydc)_n(OAc)_{4-n}]$ paddle-wheels in the lattice demonstrates that acetate groups act as the counter anions in the modified paddle-wheels (Figure 5.12a).[24] Meanwhile, the attendance of $[Cu_2(OAc)_4]$ paddle-wheel peak proves that plenty of $Cu(OAc)_2$ are included in the pores of SURMOF HKUST-1 by binding with

pyridinic-N of pydc. Corresponding to the IRRAS spectra, the additional peaks originated from two types paddle-wheels are also observed in Raman spectra (Figure 5.11) at 1586 and 1034 cm^{-1}, respectively.[31]

Based on the results and discussions above, we confirm that the incorporation of defects in SURMOFs HKUST-1 does not change the overall structure. Moreover, we deduced the possible defect types in DE-SURMOFs HKUST-1, which are shown in Figure 5.12.

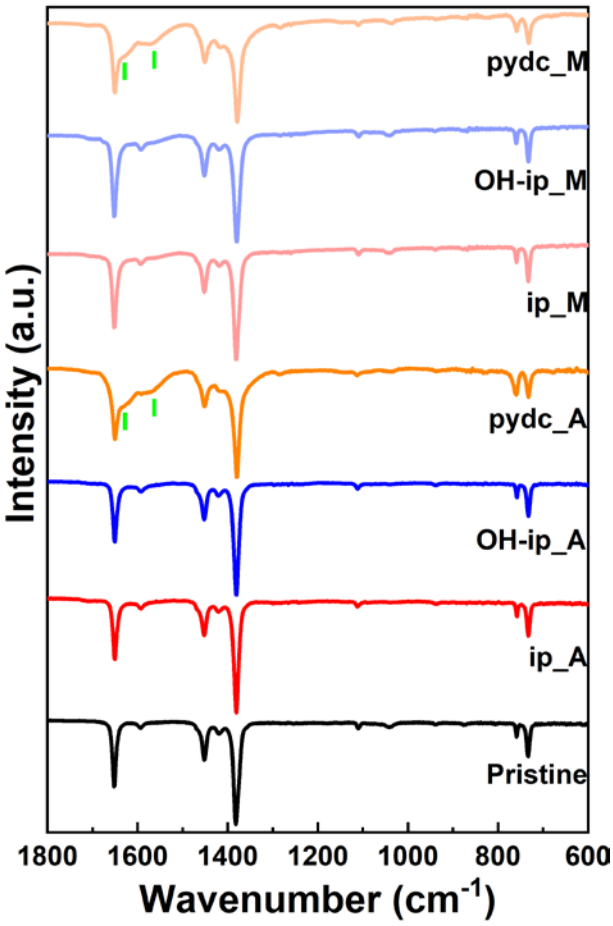

Figure 5.10. The IRRAS spectra of pristine (black) and DE-SURMOF HKUST-1 fabricated by mixing method (light color) and alternating method (dark color).

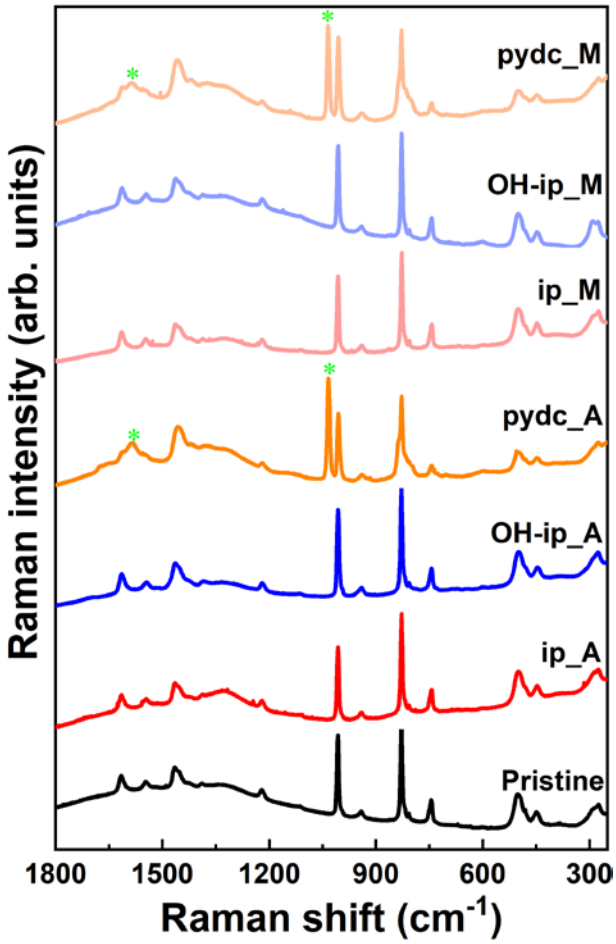

Figure 5.11. The Raman spectra of pristine (black) and DE-SURMOFs HKUST-1 fabricated by mixing method (light color) and alternating method (dark color).

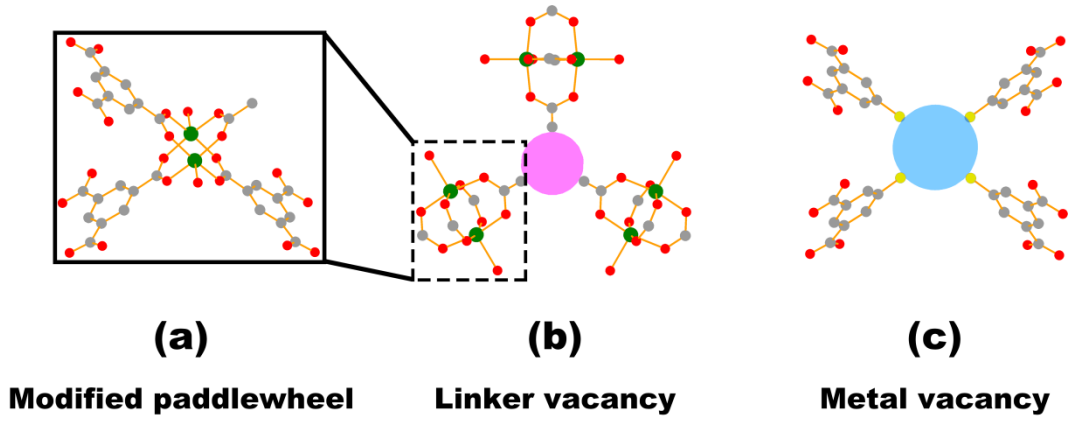

Figure 5.12. (a) The modified paddlewheel, (b) linker vacancy, and (c) metal vacancy.

5.2.3 Defects detection in defected SURMOF HKSUT-1

The incorporation of defective linkers in lattice could generate metal and linker vacancies that are important to tailor the properties of MOFs. However, it is still a challenge to detect these defects in MOFs. For bulk defect-engineered HKUST-1, a vital characterization is determining the Cu^{+} ions in the lattice.[19, 24] While limited Cu^{+} ions were formed in the growth process of SURMOF HKUST-1 due to the Cu source and mild synthetic condition. In this work, we detected the defects in DE-SURMOFs mainly focusing on the identification of defective linkers (^{1}H NMR spectroscopy, ToF-SIMS and UV-Vis spectra), and also porosity (methanol adsorption isotherms) and morphology (SEM).

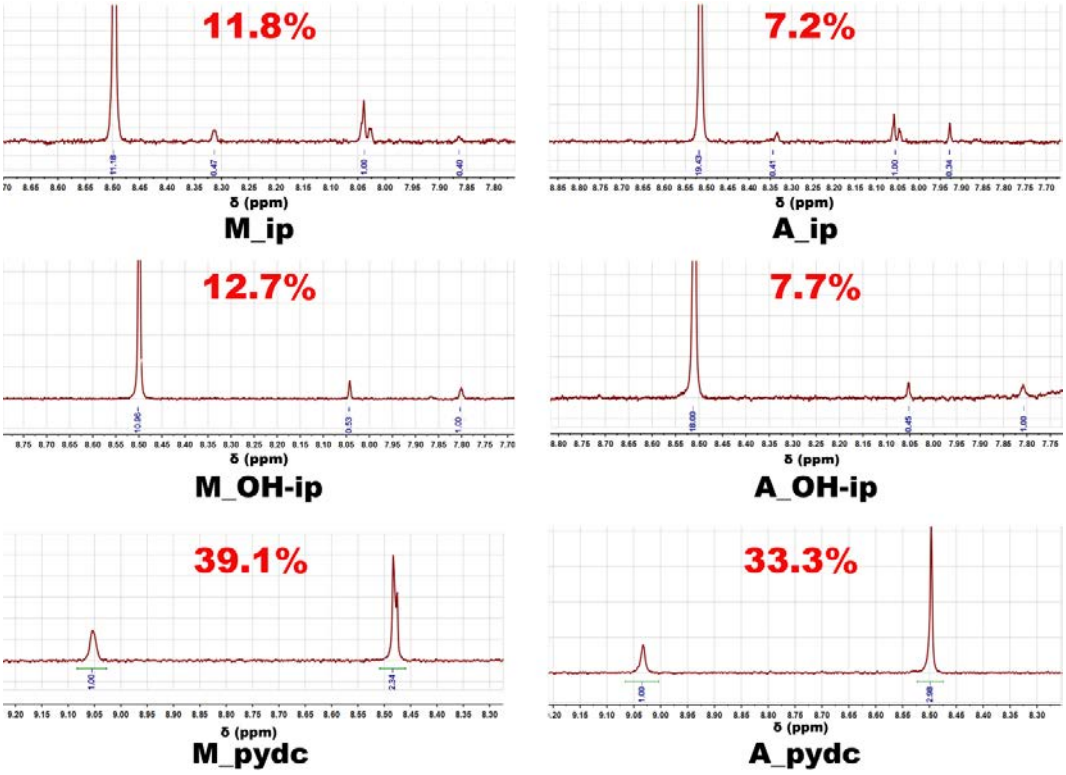

Figure 5.13. The ^{1}H NMR spectra of digested DE-SURMOFs HKUST-1 in DMSO-d_6 and DCl. The molar ratio of defective linker incorporated in the lattice is marked in red.

Quantitative detection of defective linkers in DE-SURMOF (^{1}H NMR and ToF-SIMS). The incorporated defective linkers in DE-SURMOFs HKUST-1 were quantitatively detected by ^{1}H NMR spectroscopy after digesting thin films in a mixture of DMSO-d_6 and DCl, and the results are shown in Figure 5.13. Note that, the theoretical feeding ratio of defective linkers is 41.7% (considering the seed layer). From the spectra we can see that the doping level of three defective linkers in SURMOF HKUST-1 is different (H_2ip < H_2OH-ip < H_2pydc), which is corresponding to the observation in ΔF-t growth curves. Another important information we can read from the ^{1}H NMR spectra is that more defects were incorporated in DE-SURMOFs by mixing method than by alternating method. This phenomenon could ascribe to the double rinsing steps in alternating method, by which more defective linkers were washed away. By comparing with bulk powder, we find that less amount of H_2ip was incorporated in DE-SURMOFs,[24] while more amount of H_2OH-ip and H_2pydc were integrated by mixing method.[19]

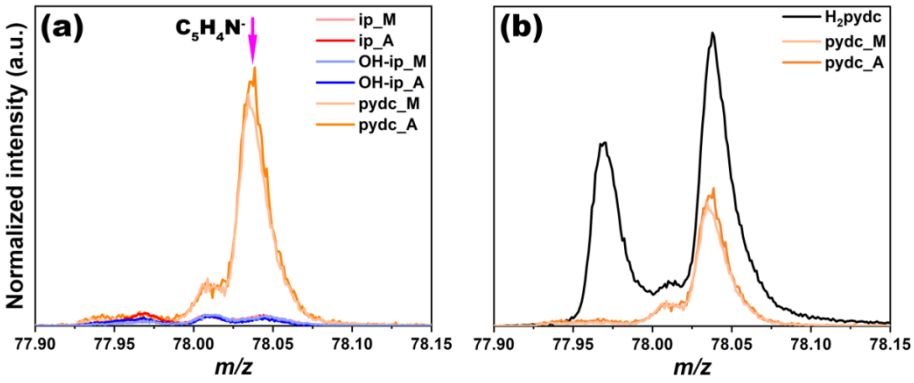

Figure 5.14. ToF-SIMS: (a) the fingerprint peak of pydc defected DE-SURMOF HKUST-1; (b) the quantification of pydc concentration in DE-SUEMOFs by referencing to precursor H_2pydc.

The measurements of ToF-SIMS were also performed to determine the amount of defective and parent linkers in DE-SURMOFs HKUST-1.[32]

Unfortunately, it is difficult to distinguish defective linker ip and OH-ip from parent linker btc in DE-SURMOFs HKUST-1 because of the close molecular structure and elemental composition. Nevertheless, the situation for pydc is different, which can be distinguished from btc (Figure 5.14a). Finally, we find that the pydc concentration of **pydc_M** is approx. 15% more than that in **pydc_A** (Figure 5.14b) by referencing to precursor H_2pydc, which agrees with the results of NMR analysis.

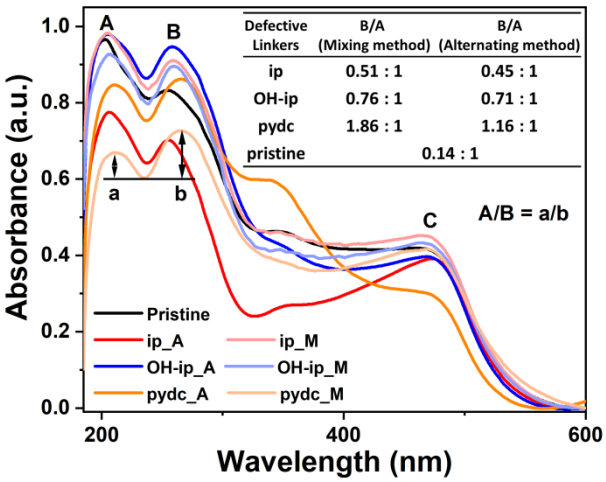

Figure 5.15. The UV-Vis spectra of pristine (black) and DE-SURMOFs (color) HKUST-1. The insert table is the net absorption intensity ratio **B**/**A** of each spectrum.

UV-Vis spectra. Since defects in the MOF lattice may affect the electronic and optical properties of the material,[33-34] the UV-Vis spectroscopy, shown in Figure 5.15, was employed to investigate the defects in DE-SURMOFs HKSUT-1. The UV-Vis spectra of obtained SURMOFs show two characteristic absorption bands for HKUST-1, which are assigned to π–π*-transition of benzene ring at about 205 nm (band **A**)[35-36] and ligand-to-metal-charge-transfer (LMCT) at about 260 nm (band **B**)[37]. Moreover, absorption of d–d-transitions in Cu-paddle-wheels can be observed in the visible range (around 460 nm, band **C**) as well. As we can see in the

spectra, with incorporating defective linkers in SURMOFs, the intensity of band **B** increases relative to that of band **A** by comparing to the pristine sample. In order to show how much the intensity of band **B** was enhanced more clearly, the ratio of absorption intensity of band **B** and **A** (**B**/**A** = b/a, shown in the insert table of Figure 5.15) is proposed. The **B**/**A** ratio reflects the defect density in DE-SURMOF HKUST-1. Interestingly, the **B**/**A** ratio shows an uptrend in following sample order: defect-free, ip defected, OH-ip defected and pydc defected, which could ascribe to the diverse doping level of defective linkers and more important the diverse electron enrichment of functional groups of defective linkers (COO^- < H < OH < pyridinic-N).[38] Furthermore, the DE-SURMOFs fabricated by mixing method have larger **B**/**A** ratios than those synthesized by alternating method. It means that more defects were incorporated in lattice by mixing method, which is corresponding to the results of NMR analysis.

Methanol adsorption. The presence of metal and linker vacancies influences the porosity of DE-SURMOF HKUST-1. Herein, methanol vapor adsorption, presented in Figure 5.16, was performed on SURMOFs to investigate the impact of defects on sorption properties. The DE-SURMOFs HKUST-1 defected by H_2ip and H_2OH-ip exhibit enhanced adsorption capacity more or less in comparison with the parent one. Notably, **ip_M** shows the highest methanol adsorption capacity (14.69 mmol g^{-1}) among all thin films. This result indicates that the porosity of DE-SURMOF HKUST-1 is improved. However, the adsorption capacity of **pydc_M** and **pydc_A** is drastically reduced, which is probably due to the inclusion of large amount of $Cu(OAc)_2$ in the pores of HKUST-1 through bonding with the pyridinic-N of pydc. Note that, the adsorption and desorption branches are separated in all of isotherms, which could ascribe to the interaction between methanol molecules and MOFs. This interaction slows down the desorption of methanol molecules from the

pores, so the desorption branch is higher than the adsorption branch, especially at the low relative pressure range.

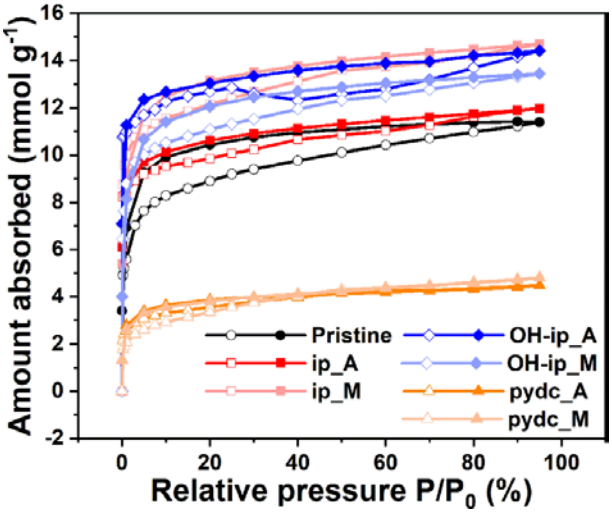

Figure 5.16. The methanol adsorption isotherms of pristine (black) and DE-SURMOFs HKUST-1 fabricated by mixing method (light color) and alternating method (dark color).

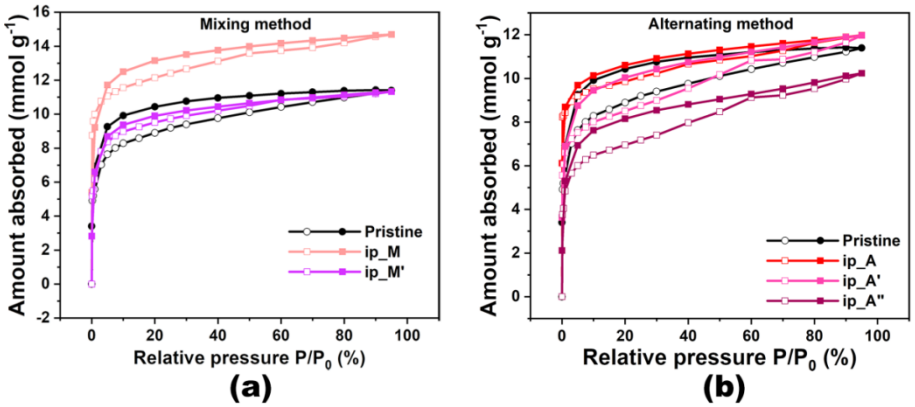

Figure 5.17. The comparation of methanol adsorption isotherms of (a) **ip_M** and **ip_M'**; and (b) **ip_A, ip_A'** and **ip_A"** with pristine SURMOF HKUST-1.

The methanol adsorption isotherms of **ip_M**', and **ip_A**' and **ip_A**" were also measured, which are shown in Figure 5.17. It is noticeable that the methanol adsorption capacity of DE-SURMOF HKUST-1 tends to decrease

with raising defect density, which is because that more defects integrated in the lattice leads to the structure degradation.

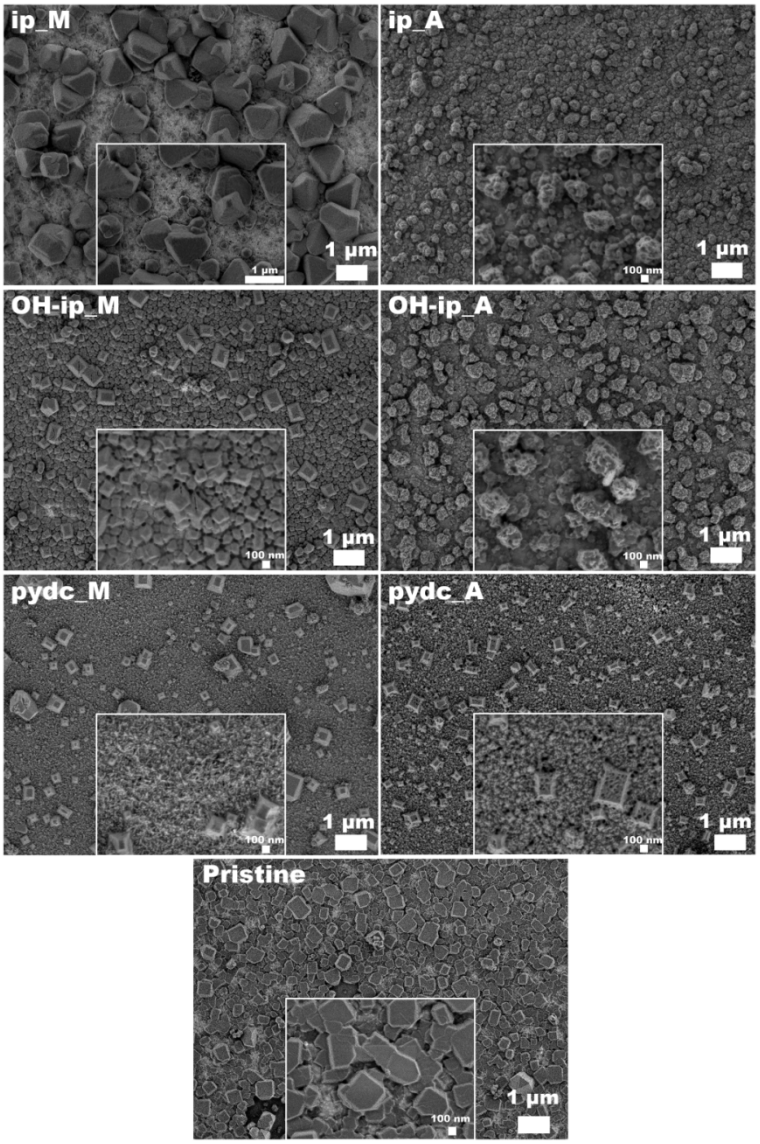

Figure 5.18. The morphology of pristine and DE-SURMOFs HKUST-1.

SEM. The morphology of SURMOFs were recorded by SEM, which are presented in Figure 5.18. With the addition of different defective linker, the obtained DE-SURMOFs HKUST-1 show a diverse morphology compare with the pristine one. Moreover, the fabrication method influences the morphology as well. For DE-SURMOFs defected by ip and OH-ip, the samples fabricated

by mixing method are assembled by regular-shaped and smooth octahedra or cubes, while those samples prepared by alternating method constitute by plenty of grotesque MOF particles. However, the morphology of pydc defected DE-SURMOFs HKUST-1 seem independent from the synthetic method, which the SEM of **pydc_M** and **pydc_A** are similar.

5.2.4 Comparison of two methods

As discussed above, it is clear that mixing method is more efficient to incorporate defective linkers in SURMOF HKUST-1 than alternating method. Moreover, DE-SURMOFs HKUST-1 defected by OH-ip and pydc via mixing method have higher defect density even than bulk powder.

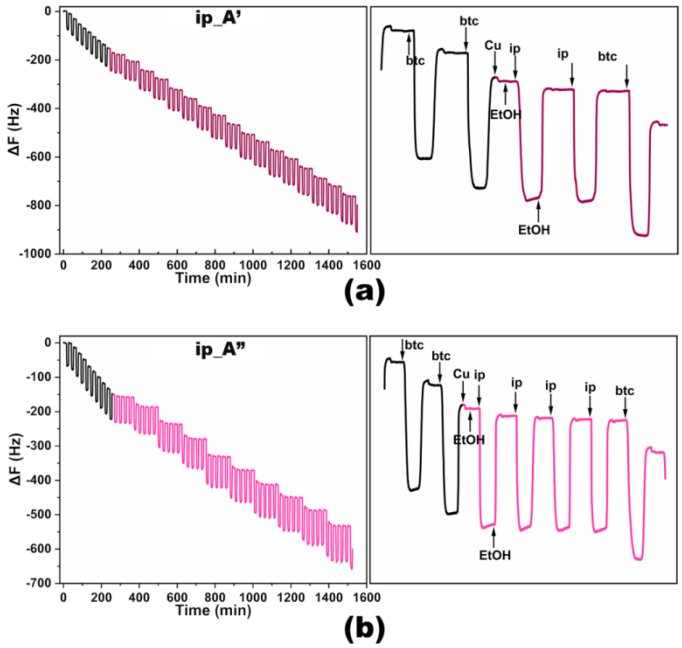

Figure 5.19. The frequency change against time growth curves of DE-SURMOF HKUST-1 (a) **ip_A'** and (b) **ip_A"**. The left column is the overall graph; the closer inspection of the joint of seed layer and DE-SURMOF are shown in the right column.

Alternating method shows a higher controllability in the distribution of defects in DE-SURMOFs HKUST-1 (Figure 5.1b), which can be viewed from

the ΔF-t growth curves of **ip_A'** and **ip_A"**. As shown in Figure 5.19, a flat stage appears during the $Cu(OAc)_2$/H_2ip dosing steps, which means that the surface of SURMOF is terminated by H_2ip and the growth of thin film is interrupted.[13] But the growth can continue when alternate to dosing $Cu(OAc)_2$/H_3btc. Speculating from this truth, the parent and defective linkers are distributed in a "ABAB" fashion in DE-SURMOFs.

5.3 Conclusion

In conclusion, two synthetic methods, mixing method and alternating method, are employed to fabricate DE-SURMOFs HKUST-1 by partially substituting the parent H_3btc linker with truncated defective linker H_2ip, H_2OH-ip and H_2pydc. The frequency change against time growth curves indicates the growth of DE-SURMOFs HKUST-1. The measurements of XRD, IRRAS and Raman spectroscopy confirm that the lattice of HKUST-1 remains with integrating defective linkers. The defects of DE-SURMOFs HKUST-1 were characterized by ^{1}H NMR, ToF-SIMS, UV-Vis, methanol vapor adsorption and SEM. At last, we compared the advantages of two methods for incorporating defects in SURMOF HKUST-1: mixing method is more efficient to incorporate defects in MOF lattice; while alternating method shows a higher controllability in the distribution of defects in DE-SURMOFs HKUST-1. These two methods supply a possible way to control over the defect formation in MOF thin films.

5.4 Reference

[1] H. Furukawa, K. E. Cordova, M. O'Keeffe, O. M. Yaghi, *Science* **2013**, *341*, 1230444.

[2] H. Li, M. Eddaoudi, M. O'Keeffe, O. M. Yaghi, *Nature* **1999**, *402*, 276.

[3] H. C. Zhou, S. Kitagawa, *Chem. Soc. Rev.* **2014**, *43*, 5415.

[4] L. J. Murray, M. Dinca, J. R. Long, *Chem. Soc. Rev.* **2009**, *38*, 1294.

[5] J. R. Li, J. Sculley, H. C. Zhou, *Chem. Rev.* **2012**, *112*, 869.

[6] A. H. Chughtai, N. Ahmad, H. A. Younus, A. Laypkov, F. Verpoort, *Chem. Soc. Rev.* **2015**, *44*, 6804.

[7] L. E. Kreno, K. Leong, O. K. Farha, M. Allendorf, R. P. Van Duyne, J. T. Hupp, *Chem. Rev.* **2012**, *112*, 1105.

[8] A. U. Czaja, N. Trukhan, U. Muller, *Chem. Soc. Rev.* **2009**, *38*, 1284.

[9] Q. L. Zhu, Q. Xu, *Chem. Soc. Rev.* **2014**, *43*, 5468.

[10] K. K. Tanabe, S. M. Cohen, *Chem. Soc. Rev.* **2011**, *40*, 498.

[11] S. Dissegna, K. Epp, W. R. Heinz, G. Kieslich, R. A. Fischer, *Adv. Mater.* **2018**, *30*, e1704501.

[12] Z. Fang, B. Bueken, D. E. De Vos, R. A. Fischer, *Angew. Chem. Int. Ed.* **2015**, *54*, 7234.

[13] Z. Wang, S. Wannapaiboon, K. Rodewald, M. Tu, B. Rieger, R. A. Fischer, *J. Mater. Chem. A* **2018**, *6*, 21295.

[14] S. Wannapaiboon, M. Tu, R. A. Fischer, *Adv. Funct. Mater.* **2014**, *24*, 2696.

[15] A. Betard, R. A. Fischer, *Chem. Rev.* **2012**, *112*, 1055.

[16] Z. Zhang, Y. Chen, X. Xu, J. Zhang, G. Xiang, W. He, X. Wang, *Angew. Chem. Int. Ed. Engl.* **2014**, *53*, 429.

[17] K. Behrens, S. S. Mondal, R. Noske, I. A. Baburin, S. Leoni, C. Gunter, J. Weber, H. J. Holdt, *Inorg. Chem.* **2015**, *54*, 10073.

[18] Y. Liu, R. C. Klet, J. T. Hupp, O. Farha, *Chem. Commun.* **2016**, *52*, 7806.

[19] Z. Fang, J. P. Durholt, M. Kauer, W. Zhang, C. Lochenie, B. Jee, B. Albada, N. Metzler-Nolte, A. Poppl, B. Weber, M. Muhler, Y. Wang, R. Schmid, R. A. Fischer, *J. Am. Chem. Soc.* **2014**, *136*, 9627.

[20] I. Stassen, N. Burtch, A. Talin, P. Falcaro, M. Allendorf, R. Ameloot, *Chem. Soc. Rev.* **2017**, *46*, 3185.

[21] F. Vermoortele, B. Bueken, G. Le Bars, B. Van de Voorde, M. Vandichel, K. Houthoofd, A. Vimont, M. Daturi, M. Waroquier, V. Van Speybroeck, C. Kirschhock, D. E. De Vos, *J. Am. Chem. Soc.* **2013**, *135*, 11465.

[22] F. Vermoortele, R. Ameloot, L. Alaerts, R. Matthessen, B. Carlier, E. V. R. Fernandez, J. Gascon, F. Kapteijn, D. E. De Vos, *J. Mater. Chem.* **2012**, *22*, 10313.

[23] P. St Petkov, G. N. Vayssilov, J. Liu, O. Shekhah, Y. Wang, C. Wöll, T. Heine, *Chemphyschem* **2012**, *13*, 2025.

[24] W. Zhang, M. Kauer, P. Guo, S. Kunze, S. Cwik, M. Muhler, Y. Wang, K. Epp, G. Kieslich, R. A. Fischer, *Eur. J. Inorg. Chem.* **2017**, *2017*, 925.

[25] G. Barin, V. Krungleviciute, O. Gutov, J. T. Hupp, T. Yildirim, O. K. Farha, *Inorg. Chem.* **2014**, *53*, 6914.

[26] O. Shekhah, H. Wang, S. Kowarik, F. Schreiber, M. Paulus, M. Tolan, C. Sternemann, F. Evers, D. Zacher, R. A. Fischer, C. Wöll, *J. Am. Chem. Soc.* **2007**, *129*, 15118.

[27] O. Shekhah, H. Wang, D. Zacher, R. A. Fischer, C. Wöll, *Angew. Chem. Int. Ed.* **2009**, *48*, 5038; *Angew. Chem.* **2009**, *121*, 5138.

[28] M. Tu, S. Wannapaiboon, R. A. Fischer, *Inorg. Chem. Front.* **2014**, *1*, 442.

[29] V. Stavila, J. Volponi, A. M. Katzenmeyer, M. C. Dixon, M. D. Allendorf, *Chem. Sci.* **2012**, *3*, 1531.

[30] G. Delen, Z. Ristanovic, L. D. B. Mandemaker, B. M. Weckhuysen, *Chem. Eur. J.* **2018**, *24*, 187.

[31] M. Todaro, A. Alessi, L. Sciortino, S. Agnello, M. Cannas, F. M. Gelardi, G. Buscarino, *J. Spectrosc.* **2016**, *2016*, 1.

[32] Tatjana Ladnorg, Alexander Welle, Stefan Heißler, Christof Wöll, H. Gliemann, *Beilstein J. Nanotechnol.* **2013**, *4*, 638.

[33] K. Muller, K. Fink, L. Schottner, M. Koenig, L. Heinke, C. Wöll, *ACS Appl. Mater. Inter.* **2017**, *9*, 37463.

[34] K. Muller, J. Singh Malhi, J. Wohlgemuth, R. A. Fischer, C. Wöll, H. Gliemann, L. Heinke, *Dalton Trans.* **2018**, *47*, 16474.

[35] G. Mahalakshmi, V. Balachandran, *Spectrochim. Acta A Mol. Biomol. Spectrosc.* **2014**, *124*, 535.

[36] R. Kania, J. K. E. Malongwe, D. Nachtigallová, J. Krausko, I. Gladich, M. Roeselová, D. Heger, P. Klán, *J. Phys. Chem. A* **2014**, *118*, 7535.

[37] Z.-G. Gu, L. Heinke, C. Wöll, T. Neumann, W. Wenzel, Q. Li, K. Fink, O. D. Gordan, D. R. T. Zahn, *Appl. Phys. Lett.* **2015**, *107*, 183301.

[38] M. K. Nazeeruddin, S. M. Zakeeruddin, K. Kalyanasundaram, *J. Phys. Chem.* **1993**, *97*, 9607.

Chapter 6

Experimental and analytical details

In this chapter, the experimental and analytical procedures of Chapter 2-5 are included. The general characterization methods are introduced at the beginning. Then, the sample preparation details of Chapter 2-5 are described separately. Except the functional isophthalate (fu-ip) ligands used in Chapter 3, other chemicals are commercial available (Sigma-Aldrich, Alfa Aesar, Acros Organics, abcr and TCI) and used without further purification.

6.1 General characterization methods

6.1.1 X-ray diffraction

Powder X-ray diffraction (PXRD) measurements on bulky MOFs were performed by the PANalytical Empyrean series 2 instrument. The MOF powder samples were placed on a zero background silicon wafer. The samples were measured in Bragg-Brentano geometry with a PIXcel position sensitive detector and a Cu Kα radiation source (λ = 1.54178 Å voltage and intensity were 45 kV and 40 mA, respectively) at room temperature. The measurements were conducted under continuous mode within the typical range of 2θ = 5-50° at a step of 0.01313°, with accumulation time 1.5s per step. Kβ radiation was removed by a Ni-filter.

Grazing incidence XRD (GIXRD) measurements on MOF thin films were collected on the same instrument but under grazing incidence mode and within the range of 2θ = 5-20°.

2-Dimensional GIXRD (2D-GIXRD) measurements were performed on DELTA synchrotron,[1] Dortmund, Germany under room temperature with X-ray source energy of 13 keV and wavelength of 0.9607 Å, and refined sample-to-detector distance of 354.37 mm. Calibration was done with a capillary measurement of LaB_6 powder. Calibration and data processing was performed with the DAWN software package.[2-3]

6.1.2 Infrared spectroscopy

The infrared (IR) spectra of powder samples were recorded on a Bruker Alpha-P FTIR instrument (in glovebox) in the ATR geometry with a diamond ATR unit. Infrared reflection absorption spectroscopy (IRRAS) measurements on flat samples were conducted on a Biorad Excalibur FTIR spectrometer (FTS 3000) with 2 cm^{-1} resolution at an angle of incidence of 80° relative to the surface normal and further processed by using boxcar apodization.

6.1.3 Scanning electron microscopy (SEM)

Scanning electron microscopy (SEM) images were taken by a JEOL JSM-7500F field emission scanning electron microscope. The samples were measured at 0.5-1 kV under Gentle Beam (GB) mode. Note that, it is not necessary to sputter conducting materials on the surface of samples under GB mode.

6.1.4 Volatile organic chemicals sorption isotherm

Volatile organic chemicals (VOCs) sorption properties of MOF thin films fabricated on quartz crystal microbalance (QCM) sensors were measured by environmental-controlled BEL-QCM instrument, BEL Japan. The schematic illustration of BEL-QCM is presented in Figure 6.1. Prior to sorption measurements, the MOF thin films were activated by soaking in pure CH_2Cl_2 for 2 days with several exchanges at room temperature and then subsequently dried in a pure N_2 stream. Afterwards, samples were placed into the BEL-QCM instrument cells and heated at 50 °C under a He stream (99.999%, 100 sccm) for a few hours. After the activation process, the QCM frequency was recorded when the frequency change was stable within ±5 Hz over 30 min. Afterward, VOCs sorption isotherms were collected in a range of relative vapor pressures (P/P_0) of saturated vapor in a He gas flow at 25 °C from 0 to 95.0%. The mass of SURMOFs and adsorption amounts were calculated from the difference of

the read QCM frequency and the fundamental frequency of the bare QCM substrate according to Sauerbrey's equation.

Herein, the Sauerbrey's equation is shown below.

$$\Delta M = -\frac{A\sqrt{\mu \times \rho}}{2F_0^2}\Delta F$$

F_0: Fundamental frequency,

ΔM: Mass change,

A: Surface area of electrode,

μ: Shear stress of quartz (2.947×1010 kg/(m×s^2)),

ρ: Density of quartz (2648 kg/m^3),

ΔF: Frequency change.

The fundamental frequency of QCM sensors in this dissertation is around ca. 4.95 MHz, hence depositing about 3.5 ng mass on the QCM sensor results in a 1 Hz decrease of the frequency.

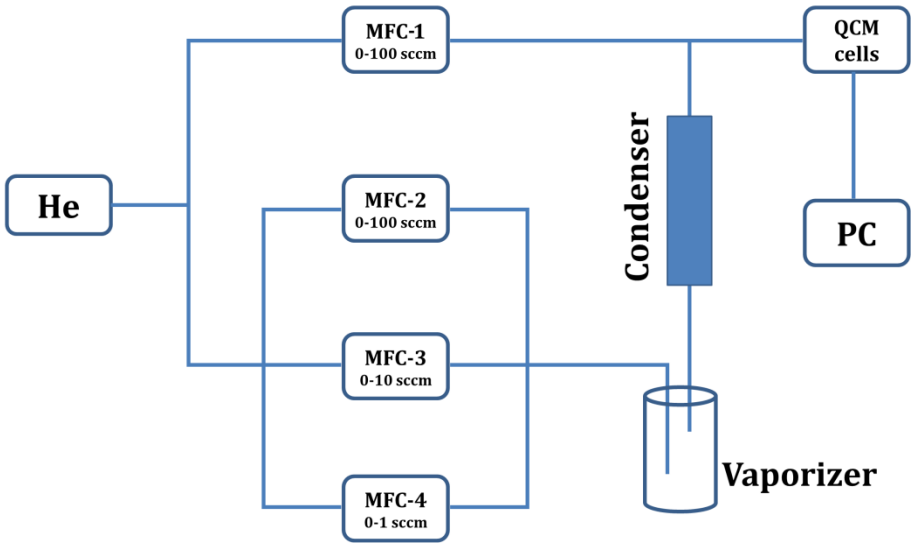

Figure 6.1. Schematic experimental setup of an environmental-controlled

QCM instrument used for organic vapour adsorption of MOF thin-films. The total gas flow to the QCM cell was kept constantly to be 100 sccm. Herein, the MFC means mass flow controller.

6.1.5 Water contact angle

Contact angle measurements of water drops (WCA) on the surface of MOF thin films were measured on a KRÜSS EasyDrop instrument. Prior to the measurements, samples were activated in pure CH_2Cl_2 for 24 hours and subsequently dried in a pure N_2 stream. Afterwards, the WCA was measured by recording the shape of water drop at 30 seconds counting from the drop fell on the sample surface.

6.1.6 Nuclear magnetic resonance

Nuclear magnetic resonance (NMR) spectra of fu-ipH_2 in Chapter 3 were recorded on a Bruker AV400 spectrometer at room temperature. ^{1}H and ^{13}C NMR spectra were referenced to the signals of DMSO-d_6.

The ^{1}H NMR spectra of digesting thin films in a mixture of DMSO-d_6 and DCl in Chapter 5 were also recorded on a Bruker AV400 spectrometer at room temperature. ^{1}H NMR spectra were referenced to the signals of DMSO-d_6.

6.1.7 Time-of-flight secondary ion mass spectroscopy

Time-of-flight secondary ion mass spectroscopy (ToF-SIMS) was performed on a TOF.SIMS 5 instrument (ION-TOF GmbH, Münster, Germany). For all experiments a short pulse width (2 ns) 20 keV Bi^{3+} ion beam was applied as analysis beam. Three individual area of 500×500 μm^2 were selected to measure for each sample.

6.1.8 Ultraviolet-visible (UV-Vis) spectroscopy

UV-Vis spectroscopy measurements were done on a SHIMADZU UV-3600 Plus UV-Vis-NIR spectrophotometer in a range of 180-600 nm.

6.1.9 Raman spectroscopy

Raman spectra were recorded using a Renishaw Raman Microscope spectrometer with an Ar^+ laser emitting at 785 nm, output power limited to 10% (100% power) under room temperature.

6.2 Experimental details of Chapter 2

6.2.1 Pretreatment of QCM substrates

In a standard pretreatment procedure, the Au-coated QCM substrates (AT cut type, Au electrode, diameter 14 mm, thickness 0.3 mm, and fundamental frequency ca. 4.95 MHz) were used for surface mounted MOF (SURMOF) thin films growth. Prior to fabrication processes, QCM substrates were cleaned by soaking them in the mixed solution of water/H_2O_2/ammonia with a volumetric ratio of 5/1/1 at 75 °C for 15 min. Afterwards, the surface-cleaned QCM substrates were functionalized by soaking them in a 20 μM solution of 16-mercaptohexadecanoic acid (MHDA) in acetic acid/ethanol (9/1) for 24 hours at room temperature followed by rinsing with pure ethanol to remove the physisorbed MHDA. The fundamental frequency of MHDA-functionalized QCM substrates were then read on the BEL-QCM.

6.2.2 The growth of Cu-paddlewheel-based SURMOFs: Cu_3btc_2, Cubdc and Cu_2bdc_2dabco on Q-Sense

The SURMOFs of Cu_3btc_2 were fabricated by using the stepwise liquid-phase epitaxy (LPE) method with integrating a different amount of water in H_3btc linker solution. The amount of water ranging from environmental humidity (EH) to 100% was integrated in the growth processes to study the influence of humidity on the quality of obtained Cu_3btc_2 SURMOFs (shown in Table 6.1). The MHDA-functionalized QCM substrates were placed in an automated QCM instrument Q-Sense E4 Auto which was operating at 40 °C at

a flow rate of 100 µL/min in the open air. In each deposition cycle, the QCM substrate was first exposed to the 0.5 mM $Cu(OAc)_2$ solution for 5 min and then 0.2 mM H_3btc linker solution for 10 min. Each subsequent step of dosing components was separated by a rinsing step of 5 min absolute ethanol to remove unreacted or physisorbed species. This procedure was repeated 60 times, which means that 60 cycles Cu_3btc_2 SURMOFs were deposited on the QCM substrate.

Table 6.1. The water content in the linker solution of H_3btc for Cu_3btc_2 SURMOF, H_2bdc for Cubdc SURMOF and H_2bdc/dabco for Cu_2bdc_2dabco SURMOF.

Trial No.	Water content in H_3btc solution (v/v %)	Water content in H_2bdc solution (v/v %)	Water content in H_2bdc/dabco solution (v/v %)
1	Environmental humidity (EH)	EH	EH
2	EH +1%	EH +1%	EH +1%
3	EH + 3%	EH + 3%	EH + 3%
4	EH + 5%	EH + 5%	EH + 5%
5	EH + 10%	EH + 10%	EH + 10%
6	EH + 20%	EH + 20%	EH + 20%
7	EH + 30%	EH + 30%	EH + 30%
8	EH + 50%	/	/
9	EH + 70%	/	/
10	EH + 80%	/	/
11	EH + 90%	/	/
12	EH + 100%	/	/

2-Dimensional (2D) Cubdc SURMOFs (60 cycles) were prepared using the same conditions as above, except the H_2bdc linker solution. Unlike Cu_3btc_2 SURMOFs, the water content in linker solution ranging from EH to EH + 30%

was selected to study the impact of humidity on the quality of Cubdc SURMOFs.

60 cycles Cu_2bdc_2dabco SURMOFs were synthesized by using the same conditions to that of Cu_3btc_2 SURMOFs except the linker solution which is the mixture of H_2bdc and dabco here. The amount of water integrated in the linker solution was from EH to EH + 30%.

6.2.3 The growth of SURMOF Cu_3btc_2 by using dipping robot setup

The SURMOFs of Cu_3btc_2 were fabricated with additional water in H_3btc solution by using dipping robot setup as well. The setup is mounted in glovebox, so the inner humidity can be controlled, which herein the relative humidity was set to 7%. More details of dipping robot are presented in literature.[4] The amount of water integrated in the linker H_3btc solution was from 0 to 20%. The functionalized substrate was dipped successively in $Cu(OAc)_2$ (1 mM) and H_3btc (0.2 mM) ethanolic solution for 10 and 15 min respectively, after each step the substrate was immersed in pure ethanol for 2 min. The recycling procedure was repeated for 20 cycles.

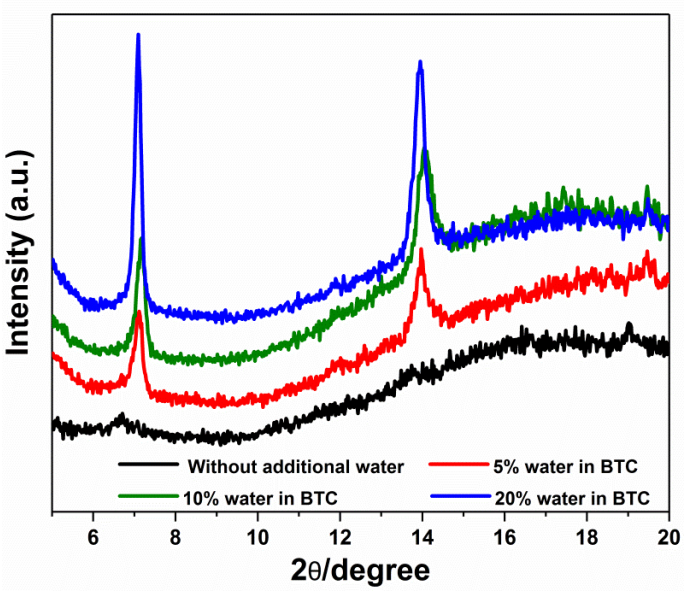

Figure 6.2. Out-of-plane XRD patterns of SURMOFs Cu_3btc_2 fabricated by using dipping robot with various amount of water in H_3btc solution.

The obtained SURMOFs Cu_3btc_2 were characterized by out-of-plane XRD and SEM, which are shown in Figure 6.2 and 6.3. From the results we can find that the thin films fabricated by integrating 20% water in the linker solution show better quality than other cases.

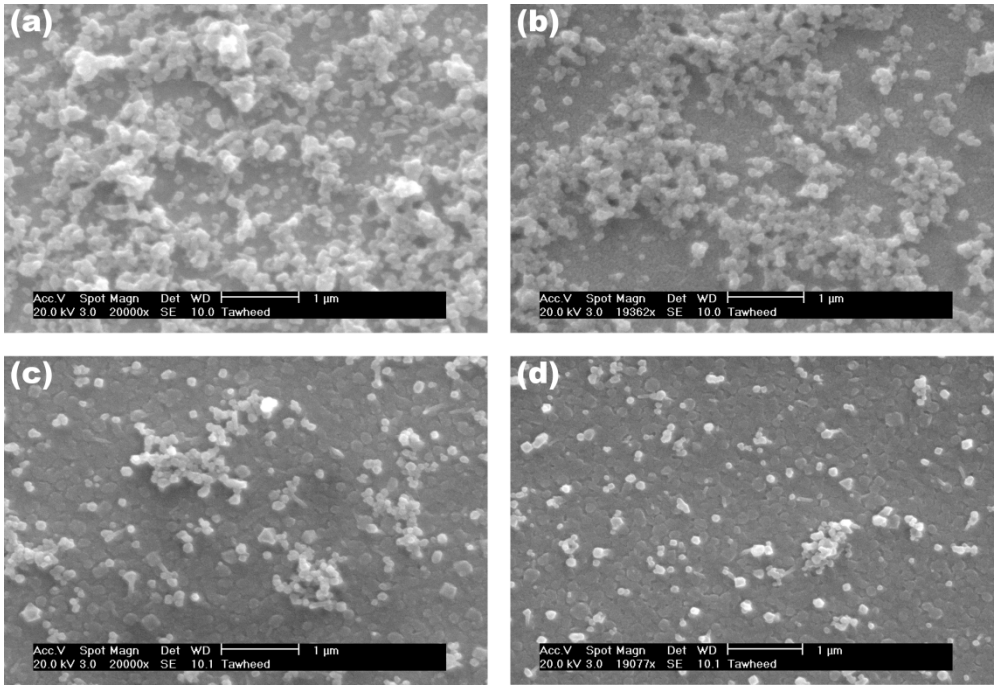

Figure 6.3. SEM images of SURMOFs Cu_3btc_2 fabricated by using dipping robot with various amount of water in H_3btc solution.

6.2.4 The growth of SURMOF Cubdc by using hand-spray system

The SURMOFs of 2D Cubdc were also fabricated with additional water in H_3btc solution by using hand-spray system.[5] Herein, the growth process was performed in the open air. The amount of water integrated in the linker H_3btc solution was from 0 to 20%. The MHDA-functionalized substrates were fixed on a sample holder and a 1 mM of $Cu(OAc)_2$ ethanol solution for 10 seconds and a 0.2 mM of H_3btc solution were subsequently sprayed at room temperature for 10 and 20 seconds, respectively. Between each step the substrates were sprayed with ethanol for 3-5 seconds. The XRD patterns of

obtained SURMOF Cubdc are shown in Figure 6.4. Basically, the crystallinity of SURMOF Cubdc enhances with increasing the water content in linker solution.

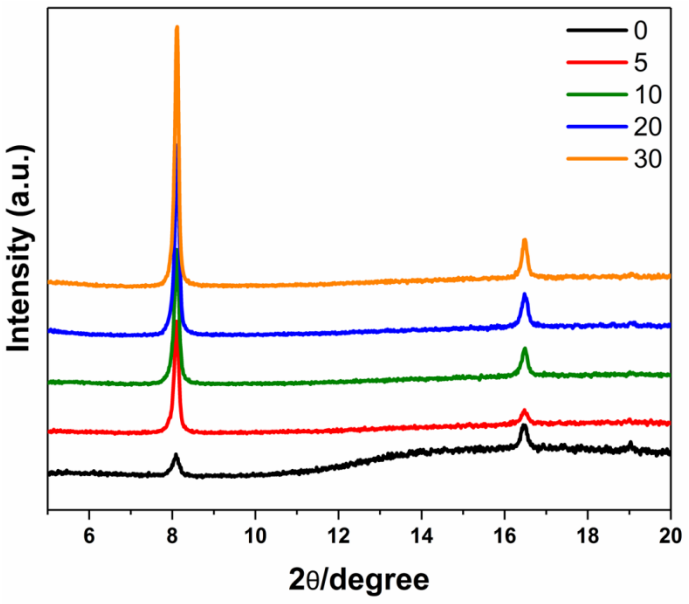

Figure 6.4. Out-of-plane XRD of SURMOFs Cubdc fabricated by using hand-spray system with various amount of water in H_2bdc solution.

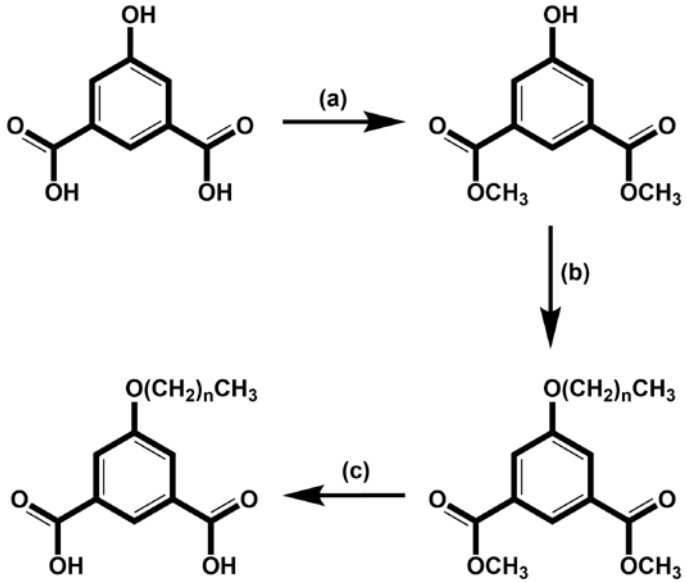

(a) methanol, H_2SO_4, reflux 18h; (b) $CH_3(CH_2)_nBr$, acetone or acetonitrile or N,N-dimethylmethanamide reflux 16h, n = 0, 1, 2, 3, 5, 9, 17; (c) KOH; methanol; reflux 18h

Scheme 6.1. Synthesis of fu-ipH_2 lingands.

6.3 Experimental details of Chapter 3

6.3.1 Synthesis of fu-ip ligands

The fu-ipH_2 ligands used in Chapter 3 were synthesized according to Scheme 6.1.[6]

Dimethyl 5-hydroxy isophthalate. 5-hydroxy isophthalic acid (33.05 g, 181 mmol) was suspended in methanol (500 mL) followed by adding concentrated sulfuric acid (10 mL) and the mixture was heated to reflux for overnight. After cooling to room temperature, the solution was neutralized with saturated aqueous $NaHCO_3$. Afterwards, the methanol was removed in vacuo, and the residue was extracted with dichloromethane. The organic phase was dried over anhydrous Mg_2SO_4 and the solvent removed by rotary evaporation to afford dimethyl 5-hydroxy isophthalate as a colorless solid (32.87 g, 156 mmol, 86% yield).

5-Methoxyisophthalic acid (Me-ipH_2). Dimethyl 5-hydroxy isophthalate (11.44g, 54.4 mmol), potassium carbonate (13.69 g, excess) and acetone (260 mL) were charged in a 500 mL flask, and the mixture was heated to reflux for 2 hours. After this time, iodomethane (8.87 g, 62.5 mmol) was added to the mixture, which was allowed to reflux overnight. After that, the solvent was removed in vacuo, and the solid residue was suspended in dichloromethane (300 mL) and water (300 mL). This mixture was extracted with dichloromethane three times, the obtained organic layer was collected, washed with brine, dried over Mg_2SO_4 and finally the solvent removed under reduced pressure. This afforded dimethyl 5-methoxy isophthalate as a colorless solid (10.99 g, 51.2 mmol, 90% yield).

The obtained dimethyl 5-methoxy isophthalate (9.46 g, 42.2 mmol) was hydrolyzed in the mixture of potassium hydroxide (11.99 g, 213.7 mmol) and

methanol (250 mL) under refluxing for approximately 18 hours. Then the cooled solution was acidified by concentrated HCl. Afterwards, the precipitate was collected by vacuum filtration, and washed copiously with water. The obtained Me-ipH_2 (8 g, 41.1 mmol, 97% yield) was dried at ambient temperature and pressure for a few days.

5-Ethoxyisophthalic acid (Et-ipH_2), 5-Propoxyisophthalic acid (Pr-ipH_2), and 5-Butoxyisophthalic acid (Bu-ipH_2). Et-, Pr- and Bu-ipH_2 were synthesized using the same conditions as that of Me-ipH_2, except the iodomethane was replaced by bromoethane, 1-bromopropane and 1-bromobutane, respectively.

5-Hexyloxyisophthalic acid (He-ipH_2), 5-Decyloxyisophthalic acid (De-ipH_2), 5-Octadecyloxyisophthalic acid (Od-ipH_2). He-, De- and Od-ipH_2 were synthesized based on the same method as Me-ipH_2 as well, except the different *n*-alkyl bromides and solvent (DMF) were used.

4-bromo-1-butanol. In order to synthesize 5-(4-Hydroxybutoxy)isophthalic acid (BuOH-ipH_2), 4-bromo-1-butanol was firstly synthesized by adding concentrated H_2SO_4 (1 mL) and HBr (16 mL of 48% w/w) dropwisely to THF (10 g) at 0 °C with stirring and then refluxing for 90 min. After cooling in ice water, the resulted solution was neutralized with $NaHCO_3$ following by the addition of 50 mL water. Afterwards, the product was extracted by diethyl ether, washed by brine, dried over anhydrous Mg_2SO_4. Finally the product was collect by removing the solvent under vacuum.

BuOH-ipH_2. The obtained 4-bromo-1-butanol was reacted with dimethyl 5-hydroxyisophthaliate to form dimethyl 5-(4-hydroxybutoxy)isophthalate. After that, the obtained chemical was hydrolyzed and acidified to form the desired organic linker BuOH-ipH_2.

NMR characterization of fu-ip ligands:

Me-ip: ^{1}H NMR (400 MHz, DMSO-d_6) δ 13.31 (bs, 2H, -CO_2H), 8.08 (t, 1H, Ar-H, *J* = 3 Hz), 7.65 (d, 2H, Ar-H, *J* = 1.44 Hz), 3.87 (s, 3H, -CH_3). ^{13}C NMR (101 MHz, DMSO-d_6) δ 166.87 (-CO_2H), 159.85 (C-OMe), 133.07 (C-CO_2H), 122.67 (Ar), 119.00 (Ar), 56.12 (-CH_3) ppm.

Et-ip: ^{1}H (400 MHz, DMSO-d_6) δ 13.29 (bs, 2H, -CO_2H), 8.07 (t, 1H, Ar-H, *J* = 2.93 Hz), 7.63 (d, 2H, Ar-H, *J* = 1.47 Hz), 4.13 (q, 2H, -CH_2CH_3, *J* = 20.8 Hz). 1.36 (t, 3H, -CH_3, *J* = 13.8 Hz). ^{13}C NMR (101 MHz, DMSO-d_6) δ 166.89 (-CO_2H), 159.11 (C-OEt), 133.06 (C-CO_2H), 122.56 (Ar), 119.44 (Ar), 64.22 (-CH_2CH_3), 14.95 (-CH_3) ppm.

Pr-ip: ^{1}H (400 MHz, DMSO-d_6) δ 13.28 (bs, 2H, -CO_2H), 8.07 (t, 1H, Ar-H, *J* = 5.28 Hz), 7.63 (d, 2H, Ar-H, *J* = 1.32 Hz), 4.04 (t, 2H, -OCH_2-, *J* = 35.2 Hz), 1.75 (m, 2H, - CH_2CH_3), 1.00 (t, 3H, -CH_3, *J* = 14.8 Hz). ^{13}C NMR (101 MHz, DMSO-d_6) δ 166.89 (-CO_2H), 159.27 (C-OPr), 133.05 (C-CO_2H), 122.56 (Ar), 119.47 (Ar), 70.01 (-OCH_2-), 22.37 (-CH_2CH_3), 10.76 (-CH_3) ppm.

Bu-ip: ^{1}H NMR (400 MHz, DMSO-d_6) δ 13.28 (bs, 2H, -CO_2H), 8.07 (t, 1H, Ar-H, *J* = 2.96 Hz), 7.63 (d, 2H, Ar-H, *J* = 1.44 Hz), 4.07 (m, 2H, -OCH_2-), 1.72 (m, 2H, -$CH_2CH_2CH_3$), 1.44 (m, 2H, -CH_2CH_3), 0.94(t, 3H, -CH_3, *J* = 18.7 Hz). ^{13}C NMR (101 MHz, DMSO-d_6) δ 166.89 (-CO_2H), 159.26 (C-OBu), 133.03 (C-CO_2H), 122.57 (Ar), 119.45 (Ar), 68.25(-OCH_2-), 31.03 (-$CH_2CH_2CH_3$), 19.10 (-CH_2CH_3), 14.12 (-CH_3) ppm.

He-ip: ^{1}H NMR (400 MHz, DMSO-d_6) δ 13.27 (bs, 2H, -CO_2H), 8.07 (t, 1H, Ar-H, *J* = 2.92 Hz), 7.63 (d, 2H, Ar-H, *J* = 1.85 Hz), 4.06 (t, 2H, -OCH_2-, *J* = 12.8 Hz), 1.73 (m, 2H, -$CH_2(CH_2)_3CH_3$), 1.42 (m, 2H, -$CH_2(CH_2)_2CH_3$), 1.31(m, 4H, -$(CH_2)_2CH_3$), 0.87 (q, 3H, -CH_3, *J* = 13.8 Hz). ^{13}C NMR (101 MHz, DMSO-d_6) δ 166.88 (-CO_2H), 159.26 (C-OHe), 133.04 (C-CO_2H), 122.56 (Ar),

119.45 (Ar), 68.53 (-OCH_2-), 31.42 (-$CH_2(CH_2)_3CH_3$), 28.93 (-$CH_2(CH_2)_2CH_3$), 25.53 (-$CH_2CH_2CH_3$) 22.52 (-CH_2CH_3), 14.34 (-CH_3) ppm.

De-ip: ^{1}H NMR (400 MHz, DMSO-d_6) δ 13.27 (bs, 2H, -CO_2H), 8.07 (t, 1H, Ar-H, *J* = 3.16 Hz), 7.62 (d, 2H, Ar-H, *J* = 1.48 Hz), 4.06 (t, 2H, -OCH_2-, *J* = 12 Hz), 1.72 (m, 2H, -$CH_2(CH_2)_7CH_3$), 1.41 (m, 2H, -$CH_2(CH_2)_6CH_3$), 1.23 (m, 12H, -$(CH_2)_6CH_3$), 0.84 (t, 3H, -CH_3, *J* = 13.4 Hz). ^{13}C NMR (101 MHz, DMSO-d_6) δ 166.89 (-CO_2H), 159.24 (C-ODe), 133.07 (C-CO_2H), 122.57 (Ar), 119.43 (Ar), 68.51 (-OCH_2-), 31.76 (-$CH_2(CH_2)_7CH_3$), 29.45-28.95 (5C, -$(CH_2)_5(CH_2)_2CH_3$), 25.84 (-$CH_2CH_2CH_3$) 22.56 (-CH_2CH_3), 14.39 (-CH_3) ppm.

Od-ip: ^{1}H NMR (400 MHz, DMSO-d_6) δ 13.27 (bs, 2H, -CO_2H), 8.07 (t, 1H, Ar-H, *J* = 3.08 Hz), 7.63 (d, 2H, Ar-H, *J* = 1.84 Hz), 4.06 (t, 2H, -OCH_2-, *J* = 12.8 Hz), 1.73 (m, 2H, -$CH_2(CH_2)_{15}CH_3$), 1.42 (t, 2H, -$CH_2(CH_2)_{14}CH_3$, *J* = 15.2 Hz), 1.23 (m, 28H, -$(CH_2)_{14}CH_3$), 0.85 (t, 3H, -CH_3, *J* = 49.2 Hz). ^{13}C NMR (101 MHz, DMSO-d_6) δ 166.88 (-CO_2H), 159.25 (C-OOd), 133.05 (C-CO_2H), 122.57 (Ar), 119.44 (Ar), 68.51 (-OCH_2-), 31.77 (-$CH_2(CH_2)_{15}CH_3$), 29.51-28.96 (13C, -$(CH_2)_{13}(CH_2)_2CH_3$), 25.83 (-$CH_2CH_2CH_3$) 22.56 (-CH_2CH_3), 14.40 (-CH_3) ppm.

BuOH-ip: ^{1}H NMR (400 MHz, DMSO-d_6) δ 13.28 (bs, 2H, -CO_2H), 8.07 (m, 1H, Ar-H), 7.65 (q, 2H, Ar-H, *J* = 7.6 Hz), 4.17 (m, 2H, -OCH_2-, *J* = 7.6 Hz), 3.44 (m, 2H, -CH_2OH), 1.93(m, 2H, -$CH_2CH_2CH_2OH$), 1.51-1.79 (m, 2H, -CH_2CH_2OH). ^{13}C NMR (101 MHz, DMSO-d_6) δ 166.89 (-CO_2H), 159.22 (C-OBuOH), 133.07 (C-CO_2H), 122.63 (Ar), 119.50 (Ar), 70.07 (-OCH_2-), 68.17 (-CH_2OH), 26.03 (-$CH_2CH_2CH_2OH$), 25.62 (-CH_2CH_2OH) ppm.

6.3.2 Fabrication of homo-SURMOF Cu_3btc_2 (B) and Cu_2ndc_2dabco (A)

Homo-SURMOF **A** and **B** were fabricated using a same conditions in Section 6.2. Note that, 5% and no additional water was integrated in H_3btc

solution for SURMOF **B** and H_2ndc/dabco solution for SURMOF **A**, respectively. 40 cycles of SURMOFs were deposited on the QCM substrates.

6.3.3 Implementation of the fu-ip ligands on the external surface of SURMOF B.

First of all, SURMOF **B** (60 cycles) was synthesized by stepwise LPE, and then was characterized to check the phase. Afterwards, SURMOF **B** was returned to the Q-Sense cells for growing another 5 cycles of SURMOF **B**. Then, the precursors were changed to $Cu(OAc)_2$/ethanol/fu-ipH_2/ethanol for another 5 cycles to implement the fu-ip ligands on the external surface of SURMOF **B**. As a reference, one of the samples was continued to dose H_3btc at the second stage. Note that, the solvent used to prepare the linker solutions for the second stages (the last 5 cycles) is absolute ethanol without additional water.

6.3.4 Fabrication of hetero-SURMOF A@B

Hetero-SURMOF **A@B** was prepared as follows: SURMOF **B** was firstly grown on the Au-coated QCM substrate for a total of 40 cycles and then taken out for characterization. Afterwards, the sample was returned to the Q-Sense fabrication cell and then rinsed with absolute ethanol for 1 hour. After that, the QCM substrate was further dosed with one cycle of the $Cu(OAc)_2$/ethanol/fu-ipH_2/ethanol interlayer ($Cu(OAc)_2$: 10 min, ethanol: 10 min, fu-ipH_2 (in ethanol with 5% H_2O): 10 min and finally ethanol: 10 min) prior to the fabrication of the outer layer SURMOF **A**. The procedure for preparing SURMOF **A** (40 cycles) was the same as SURMOF **B** except for using 0.2 mM H_2ndc/dabco as the linker solution. Note that the absolute ethanol without additional water was used as a solvent to dissolve H_2ndc/dabco.

6.4 Experimental details of Chapter 4

Firstly, the QCM substrates were treated by the standard procedure stated in Section 6.2.

In this chapter, all of SURMOFs were fabricated by stepwise LPE for certain cycles using the automated QCM instrument Q-Sense E4 Auto at 40 °C with a flow rate of 100 µL/min. In each deposition cycle, the functionalized QCM substrate was first exposing to 0.5 mM $Cu(OAc)_2$ solution for 5 min and then 0.2 mM linker (H_2bdc or H_3btc) solution for 10 min. Each subsequent step of dosing components was separated by a washing step with absolute ethanol for 5 min. Note that, the solution of linker was prepared using mixed solvent of water and ethanol (5% H_2O for H_2bdc and 20% H_2O for H_3btc). For the hetero-SURMOFs, a certain cycles SURMOF Cubdc was firstly fabricated on the QCM substrate, and then the other SURMOF Cu_3btc_2 sequentially dosed on top of that.

6.5 Experimental details of Chapter 5

Firstly, the QCM substrates were treated by the standard procedure stated in Section 6.2.

6.5.1 Thin films grown by mixing method

In this method, 0.2 mM linker solution was obtained by dissolving parent and defect-generating linkers (molar ratio 1 : 1) in water/ethanol (v/v 2 : 8) solvent. No additional water was integrated in $Cu(OAc)_2$ solution. SURMOFs were fabricated by stepwise LPE using the automated QCM instrument Q-Sense E4 Auto at 40 °C with a flow rate of 100 µL/min. Firstly 10 cycles HKUST-1 thin films were deposited on SAM-functionalized QCM substrate as seed layer, then another 50 cycles $Cu(OAc)_2$/mixed linker were subsequently deposited. In each deposition cycle, the QCM substrate was first exposing to

0.5 mM $Cu(OAc)_2$ solution for 5 min and then 0.2 mM linker solution for 10 min. Each subsequent step of dosing components was separated by a washing step with absolute ethanol for 5 min.

6.5.2 Thin films grown by alternating method

Herein, SURMOFs were synthesized by following procedure: (1) 10 cycles HKUST-1; (2) $Cu(OAc)_2$/ethanol/defective linker/ethanol; (3) $Cu(OAc)_2$/ethanol/parent linker/ethanol. The time of each cycle is the same as Section 6.5.2. The last two steps are repeated 25 times for obtaining thick films. The concentration of $Cu(OAc)_2$, parent linker and defect linker are 0.5, 0.2, 0.2 mM, respectively. The same mixed solvent (water/ethanol = 2/8) was used to dissolve linkers.

6.6 Reference

[1] C. Krywka, C. Sternemann, M. Paulus, N. Javid, R. Winter, A. Al-Sawalmih, S. Yi, D. Raabe, M. Tolan, *J. Synchrotron Radiat.* **2007**, *14*, 244.

[2] M. Basham, J. Filik, M. T. Wharmby, P. C. Chang, B. El Kassaby, M. Gerring, J. Aishima, K. Levik, B. C. Pulford, I. Sikharulidze, D. Sneddon, M. Webber, S. S. Dhesi, F. Maccherozzi, O. Svensson, S. Brockhauser, G. Naray, A. W. Ashton, *J. Synchrotron Radiat.* **2015**, *22*, 853.

[3] J. Filik, A. W. Ashton, P. C. Y. Chang, P. A. Chater, S. J. Day, M. Drakopoulos, M. W. Gerring, M. L. Hart, O. V. Magdysyuk, S. Michalik, A. Smith, C. C. Tang, N. J. Terrill, M. T. Wharmby, H. Wilhelm, *J. Appl. Crystallogr.* **2017**, *50*, 959.

[4] Z.-G. Gu, A. Pfriem, S. Hamsch, H. Breitwieser, J. Wohlgemuth, L. Heinke, H. Gliemann, C. Wöll, *Micropor. Mesopor. Mater.* **2015**, *211*, 82.

[5] H. K. Arslan, O. Shekhah, J. Wohlgemuth, M. Franzreb, R. A. Fischer, C. Wöll, *Adv. Funct. Mater.* **2011**, *21*, 4228.

[6] L. J. McCormick, S. A. Morris, A. M. Z. Slawin, S. J. Teat, R. E. Morris, *Cryst. Growth Des.* **2016**, *16*, 5771.

Chapter 7

General conclusion and outlook

Chapter 7

Metal-organic framework (MOF) thin film based devices show great potential in many applications of sensing, separation, optics and electronics. However, there are a lot of challenges needed to be overcome before applying them in real-world technologies. A primary challenge is how to fabricate MOF thin films with high quality/performance. Hence, feasible thin film fabrication techniques are required for fabricating MOF thin films with high quality to meet the demands of desired applications. Over the past decades, numerous techniques have been developed for growing MOF thin films on various substrates. In this dissertation, we have comprehensively studied the so-called stepwise liquid-phase epitaxial (LPE) growth technique, which offers, in principle, a high control of the quality (crystallographic orientation, crystallinity, morphology, *etc*.) of obtained surface-mounted MOF thin films (SURMOFs). Moreover, in order to fulfill the rapid growing demands of practical applications, lots of MOF thin film based new materials with novel properties and functionalities are developed as well, such as heterostructured SURMOFs and MOF thin film composites loaded with functional spices in the pores. The goals of this dissertation are understanding the fundamental principle of MOF thin film fabrication and further exploring novel MOF thin film based materials for practical applications by establishing heterostructures and incorporating defects.

Firstly, the impact of humidity on the growth of Cu-paddlewheel-based SURMOFs (Cu_3btc_2, Cubdc and Cu_2bdc_2dabco) was systematically studied. The SURMOFs are synthesized using stepwise LPE method, and the humidity was controlled by integrating different amount of water in linker solution. After characterizing the obtained SURMOFs with XRD, SEM, IRRAS and methanol sorption isotherm, it is easy to find that the SURMOFs of Cu_3btc_2 and Cubdc fabricated by integrating 5% water in linker solution show better quality (high crystallinity, preferred orientation, dense and homogenous morphology, lower

defect density, and high adsorption capacity) than other cases. However, the SURMOF of Cu_2bdc_2dabco cannot grow with additional water in fabrication process. In combination of the results and the pK_α of related carboxylic acid containing linkers, we speculate that water molecules significantly enhance the proton transfer from carboxyl groups of linker to acetate groups of $Cu(OAc)_2$ to form deprotonated linkers and AcOH, which promotes the nucleation and crystal growth of SURMOFs. On the other hand, water molecules and generated AcOH can also interact with the formed framework, which leads to the etching of misoriented MOF particles from film. Under the synergistic effect of water molecules, the quality of Cu-paddlewheel-based SURMOFs is rationally controlled.

Secondly, we try to solve the synthetic problem of lattice-mismatched hetero-SURMOF $Cu_2ndc_2dabco@Cu_3btc_2$ by employing various functionalized isophthalate (fu-ip) ligands to modify the interface between two SURMOFs. As reported in literature, hetero-SURMOF $Cu_3btc_2@Cu_2ndc_2dabco$ can be fabricated by stepwise LPE technique, while the heterostructure with reversed order cannot be obtained under the same condition. Starting from this problem, we firstly studied how the fu-ip ligands (fu = alkoxyl chains) bind on the surface of SURMOF Cu_3btc_2, in which only with the functional groups binding in the “head-on” fashion with proper exposure of the nucleation-directing terminal functional groups validly acts as a template for the subsequently hetero-growth of SURMOF Cu_2ndc_2dabco. The QCM frequency change profiles, IRRAS and the water contact angle measurements prove the right binding status of fu-ip ligands on the external of SURMOF Cu_3btc_2. Moreover, the surface modification does not change the intrinsic properties of SURMOF Cu_3btc_2, including crystallinity, crystallographic orientation, surface morphology, and sorption isotherms. Afterwards, a second series of fu-ip ligands are used to modify the external surface of SURMOF Cu_3btc_2 for the deposition of

SURMOF Cu_2ndc_2dabco on the top. The characterizations of XRD and SEM suggest that hetero-SURMOF $Cu_2ndc_2dabco@Cu_3btc_2$ can only be fabricated by modifying the interface with fu-ip ligands containing long flexible aliphatic spacers and coordination-active functional terminal groups. This strategy is expected to be generally efficient for the growth of hetero-SURMOF, especially the lattice-mismatched ones, which could benefit the further development of the MOF-based synergistic unit for targeted applications such as selective sorption, sensing and catalysis.

Further, a novel 2D-3D hybrid hetero-SURMOF Cu_3btc_2@SURMOF-2 (herein, three kinds of SURMOF-2 Cubdc/bpdc/TF-bdc were studied) was developed for volatile organic compounds (VOCs) sensing, recognition and adsorption. In this hetero-SURMOF, bottom SURMOF-2 shows a quite lower VOCs storage capacity, which is probably because of the surface barrier prevented VOC molecules penetrating into the pores. However, this surface barrier can be removed by depositing Cu_3btc_2 on the top, which leads to a higher total storage capacity of resulted hetero-SURMOF even than that of homo-SURMOF Cu_3btc_2. Interestingly, the top-deposited Cu_3btc_2 was obtained as discrete particles instead of continuous film randomly scattered on the surface of SURMOF-2 and their orientation are determined by the linker used in bottom SURMOF-2, namely, showing (100), (111) and no preferred orientation on Cubdc/bpdc/TF-bdc, respectively. Moreover, we also studied the impact of the thickness of upper SURMOF Cu_3btc_2 (10, 20 and 40 layers) and bottom SURMOF-2 (10, 20, 40 and 60 layers), the crystallinity of Cu_3btc_2 particles (which is controlled by involving water in the H_3btc linker solution during the fabrication process), and the linkers adopted in bottom SURMOF-2 on the VOCs sorption behaviors of hetero-SURMOFs Cu_3btc_2@SURMOF-2. Eventually, we found that the hetero-SURMOF of SURMOF Cu_3btc_2 (40 cycles) fabricated with 20% water in H_3btc solution on top of SURMOF-2 (40 cycles)

synthesized with 5% water in H_2bdc solution is the best case for VOCs adsorption. In addition, the hetero-SURMOFs Cu_3btc_2@SURMOF-2 show selective adsorption ability (normalized storage capacity by that of homo-SYRMOF Cu_3btc_2) to large VOCs, and this selectivity can be tuned by employing different linkers in bottom SURMOF-2. This work opens a door to a novel concept of materials design for VOCs sensing, recognition and removal.

At last, defect-engineered (DE) SURMOFs HKUST-1 were prepared by two methods based on stepwise LPE, namely mixing method and alternating method. Three kinds of so-called defective linkers H_2ip, H_2OH-ip and H_2pydc were employed to create defects in SURMOF HKUST-1. The obtained DE-SURMOFs HKUST-1 were characterized by XRD, IRRAS and Raman spectroscopy to prove that the incorporation of defects does not change the overall structure of HKUST-1. The defects in DE-SURMOFs HKUST-1 were detected by ^{1}H NMR, ToF-SIMS, UV-Vis, methanol vapor adsorption and SEM. At last, we find that mixing method is more efficient to incorporate defects in MOF lattice; while alternating method shows a higher controllability in the distribution of defects in DE-SURMOFs HKUST-1. These two methods supply a possible way to control over the defect formation in MOF thin films.

Appendix

List of scientific publications

1) **Zheng Wang**, Suttipong Wannapaiboon, Katia Rodewald, Min Tu, Bernhard Rieger and Roland A. Fischer, “Directing the Hetero-growth of Lattice-mismatched Surface-mounted Metal–organic Frameworks by Functionalizing the Interface”, *J. Mater. Chem. A*, 2018, **6**, 21295–21303.

2) **Zheng Wang**, Katia Rodewald, Raghavender Medishetty, Bernhard Rieger, and Roland A. Fischer, “Control of Water Content for Enhancing the Quality of Copper Paddle-Wheel-Based Metal−Organic Framework Thin Films Grown by Layer-by-Layer Liquid-Phase Epitaxy”, *Cryst. Growth Des.*, 2018, **18**, 7451−7459.

3) **Zheng Wang**, Suttipong Wannapaiboon, Katia Rodewald, Bernhard Rieger, and Roland A. Fischer, “Molecular Funneling: Synergistic Effect of Heterostructured Dissimilar Metal-Organic Framework Thin Films”, 2019, manuscript in preparation.

4) **Zheng Wang**, Sebastian Henke, Matthias Opel, Katia Rodewald, Bernhard Rieger, Roland A. Fischer, “Defects Creation in Surface Mounted Metal-Organic Framework Thin Films”, 2019, manuscript in preparation.

Scientific poster presentation

“Surface Termination of HKUST-1 Surface-mounted Metal-organic Framework Thin Films (SURMOFs)”, The 5th International Conference on Metal-Organic Frameworks & Open Framework Compounds (MOF2016), Long Beach, California, USA (September 11 - 15, 2016)

Curriculum Vitae

Personal Information

Name	Zheng Wang
Gender	Male
Date of birth	Otcober 28, 1988
Place of birth	Laian, China
Citizenship	Chinese
Marital Status	Married
E-mail	hengwangfocus@gmail.com

Educational Background

09/15-10/19	PhD student at the Chair of Inorganic and Metal-Organic Chemistry, Technical University of Munich, Germany *Supervisor*: Prof. Dr. Roland A. Fischer *Thesis*: Copper-Paddlewheel-Based Surface Mounted Metal-Organic Framework Thin Films
09/11-06/14	Master of Engineering in materials engineering, Key Laboratory of Functional Materials and Devices for Special Environments of CAS & Xinjiang Key Laboratory of Electronic Information Materials and Devices, Xinjiang Technical Institute of Physics & Chemistry, Chinese Academy of Sciences, Urumqi, China *Supervisor*: Prof. Dr. Shilie Pan *Thesis*: The Design, Synthesis and Properties of Alkalis-magnesium Mixed Borates with Isolated B-O Groups
09/07-06/11	Bachelor in materials science and engineering, School of Materials Science and Engineering, Zhengzhou University, Zhengzhou, China

Fellowships and Awards

10/2015-09/2019	PhD fellowship funded by Chinese Scholarship Council (CSC)
11-15/09/2014	Conference participation (California, MOF2016) funded by Graduate School of Technical University of Munich
2011-2014	Scholarship of graduate school, Chinese Academy of Sciences
05/2009	First prize in “Challenge Cup” National Science and Technology College of Extra-curricular Academic Competition Works of Henan Province in 2009
2007-2011	Second-Class Scholarship for Excellent Students of Zhengzhou University (three times)

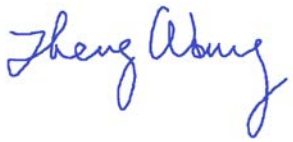

(Mr. Zheng Wang)

Date of record: 04.07.2019

Munich, Germany